STUDY ON THE SOLID PARTICLE EROSION AND EROSION-CORROSION BEHAVIOR OF ALUMINUM AND STEELS

BY

JAHANZAIB MALIK

A Thesis Presented to the
DEANSHIP OF GRADUATE STUDIES

KING FAHD UNIVERSITY OF PETROLEUM & MINERALS

DHAHRAN, SAUDI ARABIA

In Partial Fulfillment of the
Requirements for the Degree of

MASTER OF SCIENCE

In

MATERIALS SCIENCE AND ENGINEERING

APRIL, 2014

KING FAHD UNIVERSITY OF PETROLEUM & MINERALS

DHAHRAN- 31261, SAUDI ARABIA

DEANSHIP OF GRADUATE STUDIES

This thesis, written by **Jahanzaib Malik** under the direction of his thesis advisor and approved by his thesis committee, has been presented and accepted by the Dean of Graduate Studies, in partial fulfillment of the requirements for the degree of

MASTER OF SCIENCE IN MATERIALS SCIENCE AND ENGINEERING

Dr. Ihsan-ul-Haq Toor
(Advisor)

Dr. Zuhair Mattoug Gasem
Department Chairman

Dr. Wael Hasan Ahmed
(Member)

Dr. Salam A. Zummo
Dean of Graduate Studies

Dr. Zuhair Mattoug Gasem
(Member)

15/5/14
Date

عمادة الدراسات العليا
DEANSHIP OF GRADUATE STUDIES

Dedicated to my beloved parents.

ACKNOWLEDGEMENTS

I would like to take this opportunity to thank my advisor Dr. Ihsan-ul-Haq Toor, Assistant Professor, Mechanical Engineering Department, for his tremendous support and effective supervision throughout the course of my study at KFUPM. Efficient planning, detailed discussions, active correspondence and regular meetings with Dr. Ihsan, were some of the key factors that helped me achieve this task.

I would especially like to thank Dr. Hassan Badr, Professor, Mechanical Engineering Department, for providing me with an opportunity to work in his project. He has been very helpful and supportive, and always acknowledged my work with kind remarks.

I am also very thankful to Dr. Wael Hasan Ahmed, Associate Professor, Mechanical Engineering Department, for his thorough guidance and his pivotal role in planning and orienting this research work.

I am very grateful to Dr. Zuhair Mattoug Gasem, Associate Professor, Chairman Mechanical Engineering Department, for reviewing and analyzing my work and for providing important technical suggestions and improvements in this research.

I thank Mr. Lateef Hashmi (Lab Engineer), Mr. Sadaqat Ali (Lab Engineer), and Mr. Nestor Ankah (Graduate Student) for providing technical assistance in the lab.

Financial support and resources for this research work provided by National Science, Technology and Innovation Plan (Project No. 11-ADV1619-04), Mechanical Engineering Dept. and Deanship of Scientific Research, are highly acknowledged.

Most importantly, I would like to express my deepest gratitude to my family for supporting and motivating me at each and every step. My father’s advices and my mother’s love and prayers has always kept me on the right path and helped me achieve my goals.

TABLE OF CONTENTS

LIST OF TABLES

LIST OF FIGURES

ABSTRACT (ENGLISH)

Full Name : Jahanzaib Malik

Thesis Title : Study on the Solid Particle Erosion and Erosion-Corrosion Behavior of Aluminum and Steels

Major Field : Materials Science and Engineering

Date of Degree : April 2014

Solid particle erosion (SPE) is a mechanical degradation process in which the material gradually wears away through subsequent impact by abrasive particles while erosion-corrosion (EC) combines both: electrochemical degradation by electrolyte and mechanical wear by solid particles entrained in a flow. The mechanism of erosion-corrosion depends on whether erosion precedes corrosion and/or corrosion precedes erosion. The latter is known as corrosion-enhanced erosion**.** In the present work, solid particle erosion comparison of two stainless steels (AISI 316 and AISI 310S), one carbon steel 1020 and aluminum 6060-T4 (solution heat-treated and naturally aged) was carried out and the effect of hardness on their erosion resistance was evaluated. All erosion experiments were performed according to ASTM G76-95 standard. In the second part of the thesis, corrosion-enhanced erosion behavior of carbon steel AISI 1020 and stainless steel AISI 316 was investigated. Specimens were immersed in low pH chloride bearing environments for different immersion times. The corroded specimens were then subjected to SPE in order to evaluate the effect of pre-corroded specimens on their erosion rates (corrosion enhanced erosion).

Aluminum 6060-T4 showed maximum erosion resistance at all conditions. Scanning electron microscopy (SEM) of the eroded surfaces revealed ductile erosion mechanism on all the alloys. Results from the corrosion-enhanced erosion experiments indicated significant increase in erosion rates of corroded carbon steel 1020, while the erosion rates of stainless steel 316 were found to be less affected by the corrosion. In addition, the erosion rates for carbon steel specimens immersed for 24h were found to be higher than those immersed for other times. This was attributed to the increase in hardness and surface roughness for 24h immersed specimens relative to all other immersion times. Scanning Electron Microscopy revealed evidence of material cutting, shredding and localized fractures in eroded-corroded AISI 1020. Extensive plastic deformation by extrusion and forging is observed in AISI 316 but without any evidence of fracture marks. In relation to the bulk hardness of the test materials, it was found that the erosion rates for both corroded and un-corroded specimens increase with the increase in bulk hardness of the alloys.

ABSTRACT (ARABIC)

ملخص الرسالة

الاسم الكامل : جهانزيب مالك

عنوان الرسالة : دراسة التاكل بالجسيمات الصلبة والتاكل الكهروميكانيكى لسبائك الالومنيوم والصلب المقاوم للصدا

التخصص : **علوم وهندسة المواد**

تاريخ الدرجة العلمية : **ابريل ٢٠١٤**

تآكل الجسيمات الصلبة هو عملية تدهور ميكانيكية والتى تتاكل فيها المادة تدريجيا من خلال الصدم بجزيئات كاشطة بينما EC يجمع بين التدهور الكهروكيميائي والتاكل الميكانيكى من خلال وضع جزيئات صلبة فى السائل المتدفق. آلية التآكل تعتمد على ما إذا كان التآكل الميكانيكى يسبق التآكل الكهروكيميائى او ان التآكل الكهروكيميائى يسبق التآكل الميكانيكى. و النوع الاخير معروف بانه تاكل كهروكيميائى محسن بالتاكل الميكانيكى. في العمل الحالي تم مقارنة تاكل الجسيمات الصلبة لنوعين من الصلب المقاوم للصدأ (AISI ٣١٦ and AISI ٣١٠S) واحدة من الصلب الكربونى ١٠٢٠والالومنيوم T4-6060 (معالج حراريا ومعتق طبيعيا) وتم دراسة وتقييم تاثير الصلادة على مقاومة هذه المواد للتاكل الميكانيكى .تم اجراء جميع تجارب التاكل طبقا للمواصفات ASTM G76-95. فى الجزء الثانى من الرسالة تم دراسة سلوك التاكل الكهروكيميائى المحسن بالتاكل لسبائك الصلب ١٠٢٠ AISI والصلب المقاوم للصدأ ٣١٦ AISI. تم غمر العينات فى وسط من كلوريد منخفض pH لاوقات مختلفة. وتم تعريض العينات المتاكلة ل SPE لتقييم تاثير التاكل الكهروكيمائى الاولى للعينة على معدل التاكل .

اظهرت سبائك الالومنيوم 6060-T4 مقاومة للتاكل فى كل ظروف الاختبار. واظهرت نتائج المجهر الالكترونى لسطح العينات المتاكلة ان الية التاكل مطيلة لكل السبائك. واظهرت النتائج لتجارب التاكل المحسن زيادة فى معدل التاكل للصلب الكربونى ١٠٢٠ بينما كان معدل التاكل للصلب المقاوم للصدأ ٣١٦ قليل التاثر بالتاكل

الكهروكيميائى.بالاضافة الى ذلك فان معدل التاكل للصلب الكربونى المغمور ٢٤ ساعة كان اعلى من التى غمرت لاوقات الاخرى. ويرجع ذلك الى زيادة الصلادة وخشونة للسطح للعينات التى غمرت لمدة ٢٤ ساعة مقارنة بالعينات الاخرى.اظهرت نتائج المجهر الالكترونى وجود قطع وكسر جزئى فى عينات الصلب الكربونى ٢٠١٠ المتاكلة. كما اظهرت النتائج وجود تشكل دائم بالبثق والحدادة فى عينات الصلب المقاوم للصدأ ٣١٦ ولم يتضح اى دليل علو وجود علامات كسر. وتم التوصل الى ان معدل التاكل لكل من العينات المتأكله والغير متاكلة يزيد مع زيادة صلادة السبائك.

CHAPTER 1

INTRODUCTION

All classes of materials whether engineering materials, construction materials or biomaterials undergo degradation during their service life. These degradation processes can be broadly classified into mechanical, thermal and electrochemical. When it comes to metals, electrochemical degradation becomes a severe problem. Billions of dollars are spent annually due to damages incurred by corrosion and erosion in oil & gas, petrochemical and power generation industries. Extensive experimental study of erosion and corrosion can help us evaluate high performance materials and identify properties that may contribute to their erosion and corrosion resistance. Hence, the scope of this thesis is to experimentally study two types of materials degradation processes:

1) Solid Particle Erosion

2) Erosion-Corrosion.

1.1 Solid Particle Erosion

Erosion is derived from the Latin verb "*rodene*" which means to wear away gradually [1]. It is different from abrasion, where material removal occurs by unidirectional sliding of two bodies. During erosion, particles entrained in high velocity air jet are repeatedly impacted on the metal resulting in material removal from the surface. Solid particles of

various sizes impact on the surface of the metal leading to material removal by micromechanical deformation and fracture processes. The main factors that influence the erosion rate of metals are: properties of metals, particle size, particle shape, impact velocity and impact angle.

In case of ductile materials, the impact of solid particles cause localized plastic deformation and eventually leads to failure, whereas in case of brittle materials, high velocity impact of solid particles result in cracking and chipping-off of the small chunks. Erosion mechanism in more detail will be discussed in the literature review section. Solid particle type and morphology is also important. It is generally known that particles having sufficiently higher hardness such as SiC, are detrimental in the erosion process, whereas, particles such as calcite which have lower hardness cause less erosion damage. The particles size can be in the range of 10 μm to 10 mm. The velocities of solid particles largely depend on the application. The angle of incidence or impact angle of the particles also plays a vital role in the material loss. Hence, all these factors together define the erosion rate of the metals and alloys. Therefore, correlations need to be developed by generating experimental data in order to gain better understanding of the erosion behavior and effect of individual factors on the erosion rates.

1.2 Erosion-Corrosion

Erosion-corrosion is another form of material degradation process which is caused and accelerated by relative motion of the environment and metal surface. Mass loss is due to combined effect of erosion and corrosion processes. Hence, metal loss occurs partly due

to mechanical wear by solid particles (abrasive media) entrained in the solution and partly due to electrochemical reactions between the electrolyte and the metal surface.

1.2.1 Factors Affecting Erosion-Corrosion

There are various parameters that effect erosion-corrosion such as: environment effect, material effect, flow velocity and solid particle loading.

1) **Environment effect:**

One of the most important factors in erosion-corrosion is the environment. It includes pH, temperature, oxygen content and fluid chemistry. It is generally known that high pH solutions prevent corrosion. Therefore, also contribute in reducing the erosion-corrosion effect. Dissolved oxygen can create an oxidizing environment and hence, enhance the erosion-corrosion. Oxygen content can also help repair the passive film and protect the metal under stagnant conditions. However, during fluid flow oxygen promotes rapid passivation and de-passivation, hence increases erosion-corrosion. Elevated temperatures accelerate the electrochemical reactions and therefore increase erosion-corrosion. Electrolyte chemistry is also a contributing factor in erosion-corrosion. High chloride content is damaging for the protective layer. In seawater environment, rate of erosion-corrosion is higher than that in fresh water [2].

2) **Material effect:**

Soft materials such as copper alloys, aluminum alloys and zinc are more susceptible to erosion-corrosion. Apart from that, passive alloys such as stainless steels, Ti alloys and Ni-based alloys are more resistant to erosion-corrosion. The type of passive layer also

plays a vital role: thick and porous layers are vulnerable to erosion-corrosion while uniform and compact passive layers are more protective. Alloy additions can also reduce to effect of erosion-corrosion, Mo and Cr additions in stainless steels and Ni-based alloys improve the pitting corrosion resistance and hence resist erosion-corrosion [2].

3) Fluid velocity:

Fluid velocity affects the flow regime within a pipe section. At low velocities, flow is mainly laminar but, at high velocities, the flow becomes turbulent and enhances erosion-corrosion. Protective film is initially broken down by particle impacts and the turbulent flow prevents the repassivation on the surface of the metal. This results in accelerated mass loss from the surface of the material.

4) Solid particle loading:

There are many types of solid particles entrained in the flow: magnetite in oil pipelines, silica in water pipelines, suspended solids in sewage lines, etc. Concentrations and physical properties of these particles affect the rate of erosion-corrosion. As we increase the particle concentration in liquid flow, inter-particle collision takes place and flow regimes are disturbed. Flow direction becomes more damaging when particles are of larger size [3]. Apart from the concentration and physical property, third factor which affects the erosion-corrosion rate is the shape of the particles. The particles with angular shape tend to cause more damage than spherical ones.

CHAPTER 2

LITERATURE REVIEW

2.1 Review of Literature on Solid Particle Erosion

Solid Particle Erosion in metals caused by abrasive particles entrained in high velocity air stream has been studied extensively by various researchers in the past few decades. Erosion has been a critical problem in metals and alloys undergoing high velocity impacts by solid particles during the service time. For instance, gas turbine blades, helicopter rotor blades, gas pipelines and valves are subjected to solid particle erosion and degrade with time. It is important to understand the erosion mechanism occurring in these metals and alloys, and the how the particle impact angle and velocity effect the erosion behavior of these metals. Erosion rate is defined as mass loss of material per gram of abrasive particles causing the erosion and generally reported as a dimensionless unit (g/g).

2.1.1 Erosion Mechanism

As mentioned earlier, erosion mechanism depends on the ductility and brittleness of the material. The first theory in this regard was given by Finnie in 1960 [4]. He developed analytical models to predict erosion rates, which were based on the assumption that ductile material were eroding by microcutting mechanism. Lack of physical observation at that time limited the understanding of erosion mechanism. However, in late 70s, by

utilizing high depth of field of Scanning Electron Microscope, erosion behavior was studied and it was found that microcutting mechanism could not completely described what was actually happening. All erosion mechanisms consisted of sequential plastic deformation processes leading to material degradation [1].

1) Erosion Mechanism of Ductile Materials

Alan Levy [5], described the platelet mechanism of erosion which is applicable to the ductile metals. SEM images of aluminum eroded with steel shots (Figure 2.1) revealed that platelets were formed by combined action of extrusion and forging. Once these platelets are formed they are forged into distressed condition and become vulnerable to be knocked off. Figure 2.2 illustrates the proposed stages of erosion by Alan [5]. It shows that the first impact on the surface is causing the material to be extruded in the shape of a lip, third impact on this extruded lip is forging it into a platelet morphology which is then knocked out in further impacts. Platelet mechanism is the prime mechanism by which ductile materials erode and has been extensively reported by many authors.

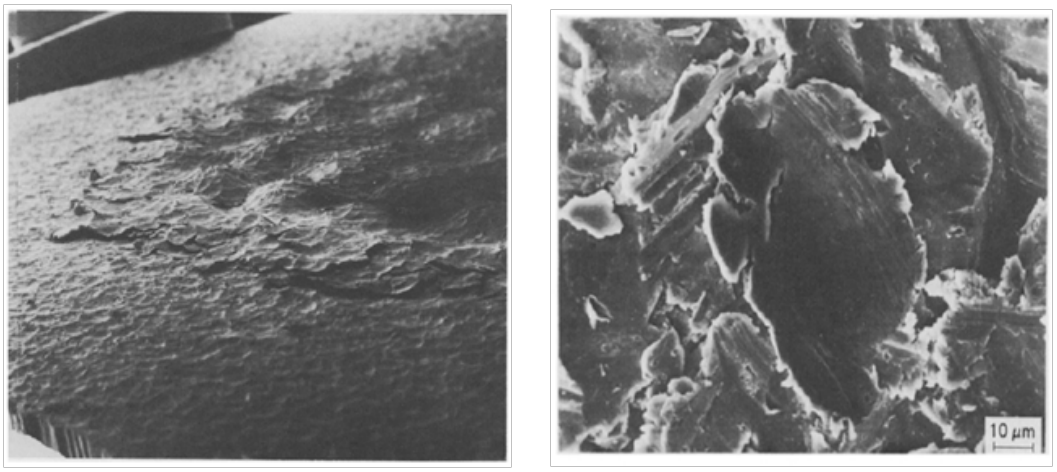

Figure 2.1 a) SEM image of Aluminum eroded with steel shots, b) Platelet morphology on Aluminum surface [5].

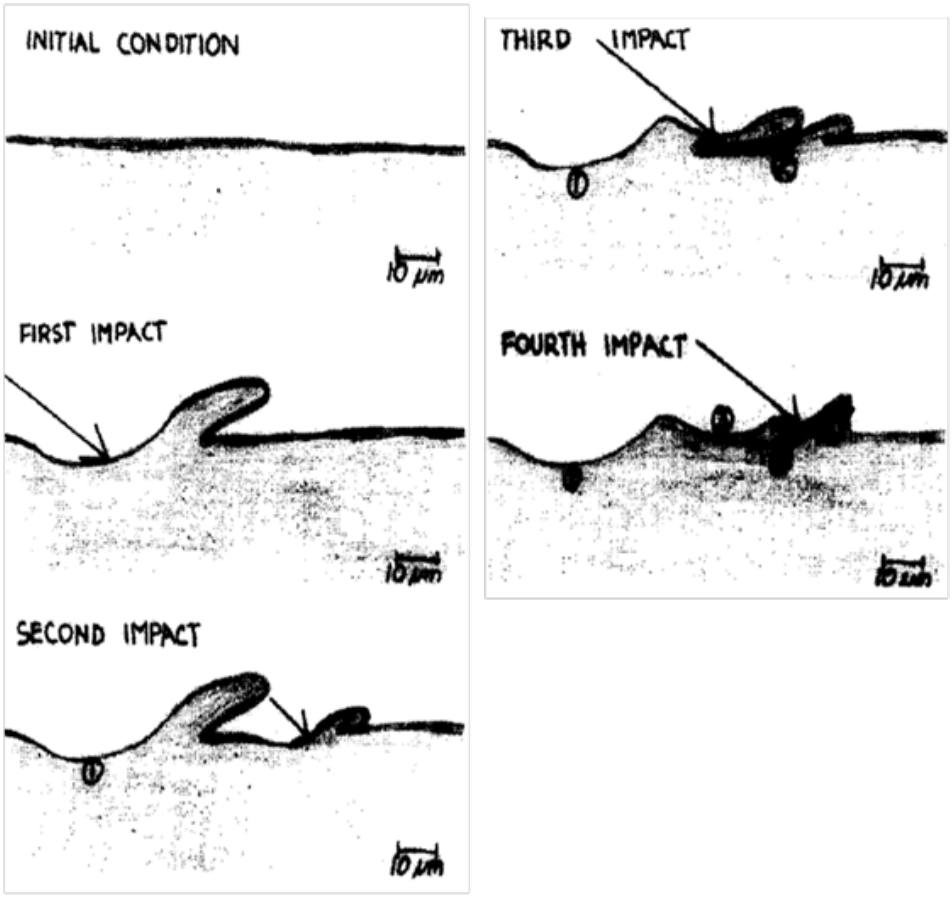

Figure 2.2 Schematic of erosion sequence proposed on Cu-plated sample [5].

G. L. Sheldon and Ashok Kanhere [6] studied the erosion mechanism by impinging aluminum alloys with large single particles. They observed material displacement in form of plastic deformation, which eventualy led to fracture. It was also reported that both multiple impacts and single impacts showed similar erosion mechnisn of material flow and fracture rather than cutting and chipping off. Similarly, J.R. Laguna-Camachoa et al. [7] in their erosion study on stainless steels, also observed plastic deformation leading to lip, pits and craters formation.

Hence, it can be deduced that the general erosion mechanism by which ductile materials erodes is plastic deformation chracterized by extursion/plouging action with various mophological features such as lip formation, craters and pitting.

2) Erosion Mechanism of Brittle Materials

This erosion of brittle materials occurs mostly by cutting and chipping mechanism. G. Zambelli and A. V. Levy [8] studied this behavior by forming scales on metal surface under oxidation conditions. Thick scale of nickel oxide was formed on pure nickel and eroded using 250 µm SiC at the velocity of 30 and 100 m/s, and impact angle of 90°. SEM images given in Figure 2.3 shows the morphology of cracks and craters formed after erosion of brittle NiO scale. It was further explained by schematic shown in Figure 2.4, that when the particle impinges, planar cracks form along the interface between the two scales. After the particle is bounced off, radial and lateral cracks breaks the surface, illustrating a cracking and chipping off mechanism in brittle materials/scales, which is different from ductile metals where extrusion and forging takes place.

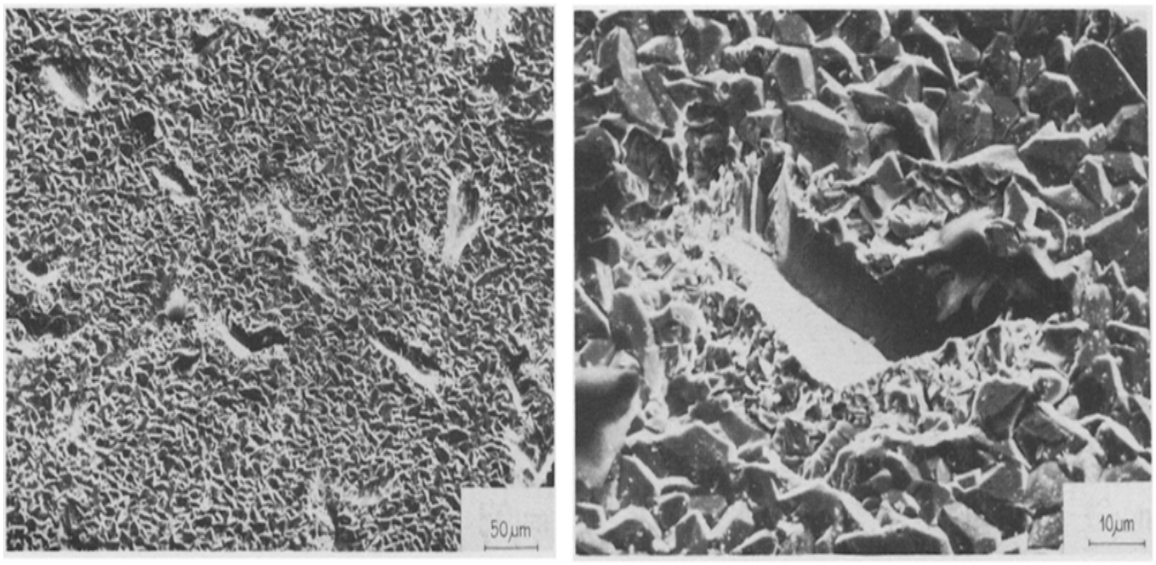

Figure 2.3 a) Crater on NiO scale by SiC erosion b) High magnification image of the crater formed, (Veclocity = 100 m/s and Impact angle = 90°) [8].

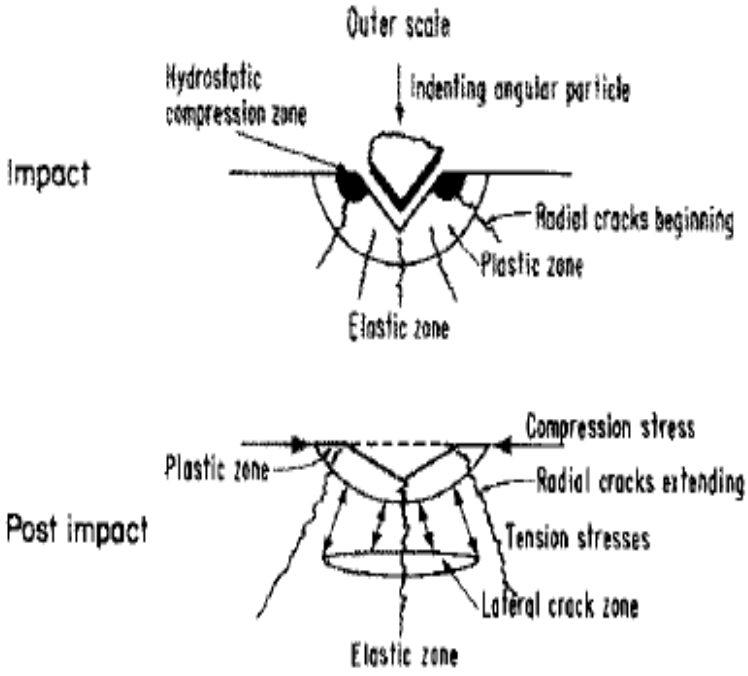

Figure 2.4 Schematic of stress field and crack propagation during erosion of brittle scale [8].

2.1.2 Surface Heating during Erosion

Surface heating during erosion of metals by solid particles has been studied by many researcher [9][10]. Unlike abrasion which is a non-adiabatic wear process, surface heating in solid particle erosion is adiabatic. Frictional heating occurs on the surface during the erosion process having the thickness in the range of 5-15 µm [5]. Some authors also saw evidence of melting particularly in soft alloys (lower melting temperature), when they were eroded using high velocities [1] [11].

2.1.3 Work hardening of the Substrate

Extensive plastic deformation causes work hardening of the surface region just below the impact zone. This is because the kinetic energy of the incident solid particles is greater than that required for platelet formation. The excess kinetic energy leads to work hardening of the surface below the eroded region [5]. Microhardness measurements of the cross sections showed increased hardness zone below the eroded surface [12].

Work hardening plays an important role in determining the erosion behavior of the material. Initially the erosion rates are lower and increase in subsequent impacts as the material is being work hardened. When the sub-surface layer is fully work-hardened the rate of material loss reaches a steady state, known as steady-state erosion rate (units: mm^3/g). Mass of erodent required to reach steady state erosion depends on the type of erodent used and the strain hardening coefficient of the target material. Materials with higher stain hardening coefficient quickly forms a work hardened layer and erode at steady state, while lower strain hardening coefficient materials require more erodent mass before reaching steady-state erosion rate [1] [5].

2.1.4 Effect of Mechanical Properties

Erosion resistance of metals is related to its mechanical properties such as ductility, hardness, toughness and strength. I. Finnie [4] in 1960's, carried out erosion tests on pure metals and showed that their erosion resistance is directly proportional to their hardness. Iron being harder than aluminum has higher erosion resistance than aluminum. However, within an alloy, the increase in hardness has not much effect on their erosion resistance. For example, when steel is quenched and tempered, its hardness increases but the erosion resistance remains unchanged or even decreases slightly in some cases [13].

Similar phenomenon was shown by McCabe et. al [14], Finnie [4] and A. V Levy [15] when erosion tests were carried out on steels of varying hardness and are summarized in Figure 2.5. It can be seen from the figure that irrespective of velocity, angle, erodent type and steel grade, the erosion resistance slightly decreases with increase in hardness. Sundararajan [13] studied the effect of metal hardness on their erosion and abrasion resistance. He postulated that the reason why erosion resistance remains unchanged (or decreases) with increasing hardness of an alloy is due to the adiabatic heating during the erosion of metal. Under adiabatic condition the increase in hardness of alloy by heat treatment or work hardening causes a decrease in critical strain for localization. Secondly adiabatic heating normalizes the immediate eroding area thus mitigating any increase in hardness by heat treatment or work-hardening.

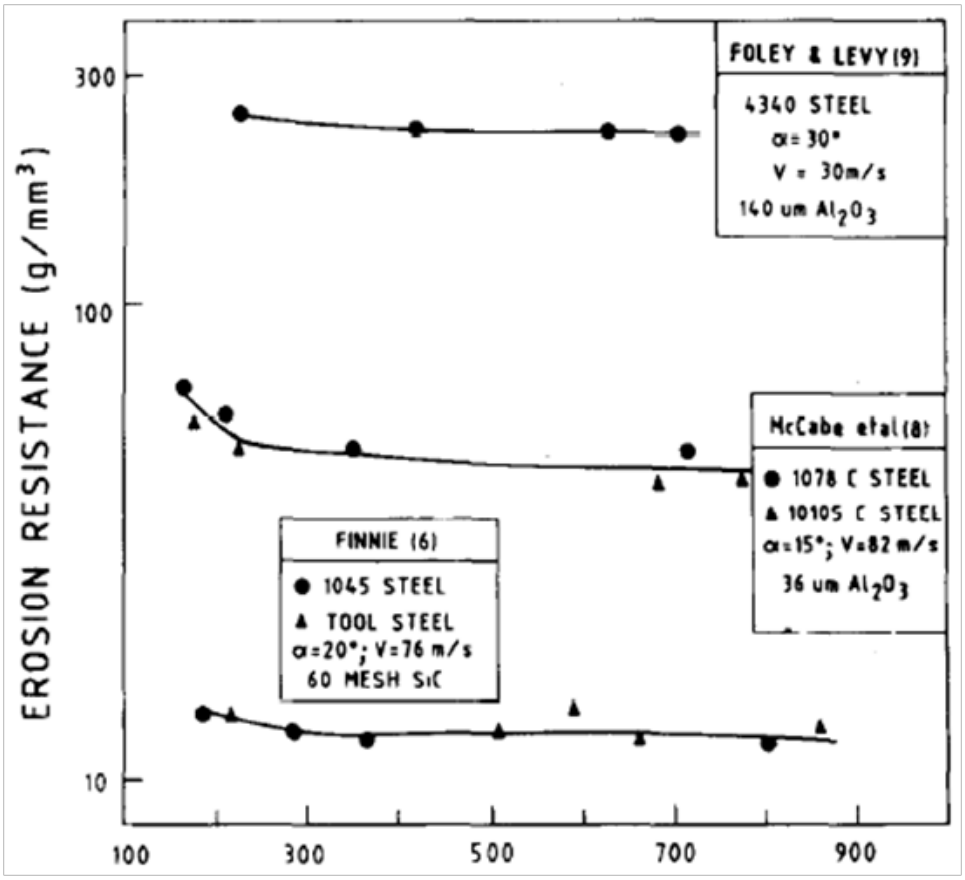

Figure 2.5 Erosion Resistance of steels vs hardness (x-axis) [13].

AV Levy [16] related the erosion resistance of metals to their ductility and strength. He studied erosion behavior of a carbon steel AISI 1020, stainless steel AISI 304 and a low alloy steel AISI 4340. It was seen that the increase in hardness and strength both led to decrease in erosion resistance, however materials having similar strength but different percentage elongation (ductility) eroded quite differently. From Figure 2.6, it can be seen that 1100-0 aluminium with higher ductility of 35% and lower strength has lower erosion rate compared to much stronger 7075-T6 aluminium with 11% elongation. In another experiment, erosion behaviour of as-wrought and annealed stainless steels was studied (Figure 2.7), it was seen that the erosion rate decreased when as-wrought steel was annealed to improve its ductility. Higher ductility yield in higher erosion resistance, due to dissipation of kinetic energy of the impinging particles causing plastic deformation in the local region so that the local fracture strains of the platelets formed are not exceeded. But there is a limiting value of ductility beyond which the erosion rate start to increase considerably because the fracture strength of the material is not enough to bear the force of incoming particles.

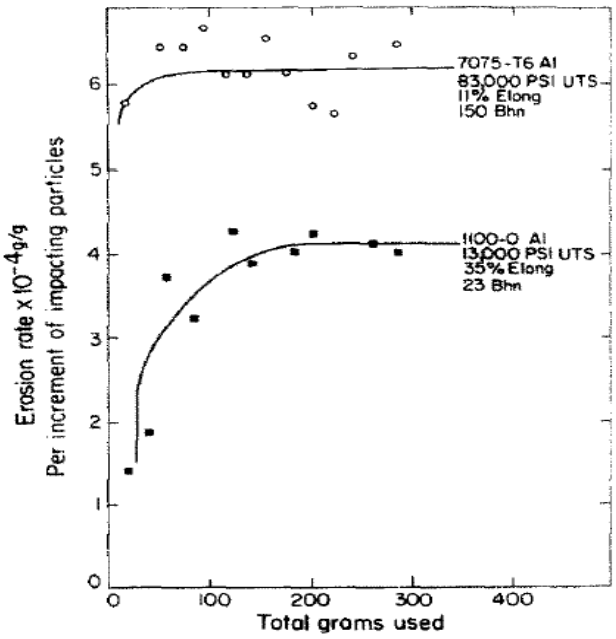

Figure 2.6 Comparison of mass loss (erosion) between 1100-O and 7075-T6 aluminum alloys. Velocity = 30 m/s, SiC particles [16].

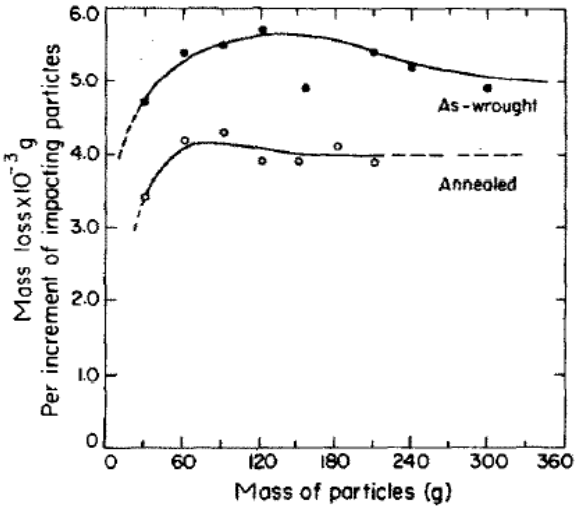

Figure 2.7 Comparison of mass loss (erosion) between as-wrought and annealed stainless steel AISI 304. Impact angle = 30°; Velocity = 60 m/s, using alumina [16].

Shewmon et al. [17] studied the erosion behavior as-received (12 HRC) and hardened (45 and 60 HRC) AISI 1060 steel by single WC impacts. At low angles, higher material loss was reported for ductile materials but at higher angles steel with high hardness was less erosion resistant compared to ductile steel. Furthermore, he studied the reason for this shift of erosion rates in hardened steels at higher impact angles. A mode of material strain called adiabatic shear bands (ASB) were seen to be formed in hardened steels. No ASBs were seen in 12 HRC steel. The formation of ASBs at oblique angles in 45 HRC occurred but was less pronounced. Whereas, in 60 HRC steel ABSs formation increased with increase in impact angles causing higher material loss. Hence, material loss mechanism for 12, 45 and 60 HRC is classified as: i) Lip extrusion and separation, ii) Lip extrusion along with fracture and iii) ASB induced material removal, respectively. Shewmon's work explains the underlying mechanism by which hardened steels erode compared to that of more ductile steels, however, from his study, correlation of erosion resistance to hardness cannot be made as the steady-state erosion rate was not reached.

In an another study, Salik et al. [12] studied the effect of mechanical properties and heat treatment on erosion behavior of 6061 aluminum alloy. Single crystal aluminum alloys with three different crystal orientation were tested and it was found out that the erosion rate is independent of the crystal orientation as erodent interacts with the work-hardened layer which is same of the three orientations. Further in their study, annealed, heat treated and precipitation treated aluminum alloy was tested. It was seen that with an increase in hardness by solution annealing, the erosion resistance also increased, however, further increase in hardness with precipitation treatment led to the decrease in erosion resistance.

M Green et al. [18] studied the influence of carbon content, thermal hardening and tempering of various plain carbon steel grades on their erosion resistance. Similar phenomenon was seen: in case of ductile steels the kinetic energy of incoming particles is dissipated in the plastic deformation whereas in case of hardened and brittle materials the kinetic energy of the incoming particles is dissipated in the form of material removal resulting in higher erosion rates.

Trilok Singh, S. N. Tiwarib and G. Sundararajan [19] investigated the solid particle erosion behavior of three austenitic stainless steels (304, 316, 410). They used three impact angles with two velocities at each angle. It was found that initial erosion rates increase gradually before reaching a steady state value, which is independent of the angle. The authors also characterized the subsurface deformation due to erosion and found that the thickness of the damaged layer increases with an increase in impact angle and impact velocity. Moreover, it was found that the SS 410 has higher erosion resistance as compared to SS 316 and SS 310. This was attributed to its tempered martensitic microstructure causing significantly lower subsurface deformation depth and also the presence of a soft zone (subsurface zone with lower hardness).

Recent study on the erosion behavior of stainless steels has been investigated by J.R. Laguna-Camacho et al. [7]. They used SS 316, SS 304 and SS 420 as their test specimens. SS 420 exhibited higher erosion resistance compared to other test specimens. This was related to the type of erosion damage observed on all the three materials. AISI 316 and AISI 304 exhibited the brittle type damage whereas, AISI 420 showed ductile erosion behavior and hence higher erosion resistance.

So far it has been observed that the solid particle erosion is strongly influenced by the hardness and ductility of the eroding material. Sundararajan [20] further investigated different hardening mechanisms and their effect on erosion resistance. It was reported that both, grain size refinement and dislocation strengthening, increases the bulk hardness but does affect the erosion resistance. While, increasing the hardness via solid solution strengthening can degrade the erosion performance of the alloys. It has also been observed that the transformational hardness (quenching austenitic stainless steel to form martensite) is also ineffective in improving the erosion resistance. In addition, Andrew Ninham [21] reported the effect of mechanical properties of various alloys. Extensive experimental study on annealed, aged and cold rolled samples revealed the change in erosion rates with changes in elongation and hardness. It was also reported that hardness and elongation are inversely related to one another. The slight change in erosion rate with hardness and ductility was due to their inverse relationship.

It is clear from the above review that the solid particle erosion is a complex phenomenon. It not only involves material deformation but also fracture at very high strain rates. In addition, the adiabatic heating during the erosion process also affects the localized properties and in turn makes the erosion process more complex. Hence, it is necessary to correlate erosion rates with a combination of material properties (hardness, strength and ductility) and erosion mechanism.

2.1.5 Effect of Erodent Characteristics

Apart from material properties and process parameter, abrasive particles (erodent) are another important variable in solid particle erosion. Particle hardness, mass, shape and size considerable affect the erosion rates of the substrate. Morphology of the particles is also important when characterizing the solid particle erosion. Particles can be of various shapes which include: spherical, semi-angular and angular. Angular particles cause more damage than the spherical ones. It is generally known that the ratio of substrate hardness to erodent hardness affects the erosion rates. Softer erodent leads to lesser mass loss while erodent with higher hardness constitutes greater damage on the material being eroded. Hence, hardness of the erodents can be used as measure of their strength and integrity. Table 2.1 below summarizes various types of erodents and their Vicker's hardness:

Table 2.1 Different types of erodent [22]

Erodent Type	Density (g/cm^3)	Vickers Hardness
$CaCO_3$ (calcite)	…	115
$Ca_5(PO_4)_3$ (apatite)	…	300
Coal Ash	0.64	500
Black Powder (Magnetite)	…	600
Steel grit	7.9	800
Quarts	2.7	1100
Al_2O_3 (alumina)	4.0	1900
SiC (Silicon carbide)	3.2	3000

According to this table calcite is the softer erodent with a hardness of HV 115, while alumina and silicon carbide are considerably harder with HV of 1900 and 3000, respectively. Hence, alumina and silicon carbide will cause higher erosion rates as compared to softer particles.

Sreeram Srinivasan et al. [23] investigated the effect of erodent hardness on erosion rates of brittle materials. They used alumina and SiC erodent of the same diameter but different hardness, to study this behavior. The reason of lower erosion rates with softer particles was attributed to the fragmentation and crushing of particles after impacting the substrate. This reveals that softer particles cannot transfer all of the stored kinetic energy in eroding the substrate; some of the energy is consumed by fragmentation of the particle itself. The detailed effect of erodent composition and hardness was studied by Alan V. Levy and Pauline Chik [22]. They used six different erodents in the erosion testing of carbon steel 1020. The range of HV hardness for the erodent used was from 115 for calcite to 3000 for SiC. It was found that the erosion rate of the carbon steel increases with the hardness of the erodent, upto HV 700 (SiO_2), after which it remains almost constant. The erosivity difference between alumina and SiC was attributed to the sharp angularity of SiC particles. Furthermore, it was observed that the softer particles (calcite, apatite) were fragmented after the impact whereas no breakage was seen in alumina and SiC. In addition to the fracture of the softer particles, evidence of particle embedment was also observed.

M. Vite-Torres et al. [24] used angular silicon carbide (SiC) and round steel grit to study the erosion behavior of stainless steel AISI 410. Scanning electron microscopy of both shapes is shown in Figure 2.8.

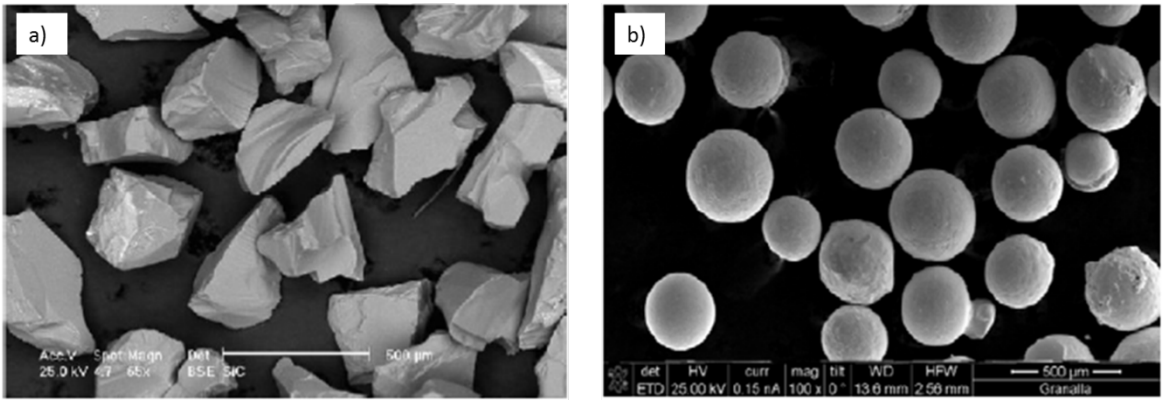

Figure 2.8 a) Angular silicon carbide, b) Round shape steel grit [24]

The erosion rate caused by angular SiC was two times greater than that by steel grit. This difference in erosion rates is mainly due to the sharp cutting edges of SiC, resulting in efficient material cutting. Whereas, round steel grit mainly caused materials displacement but less detachment [24].

In another study, Z. Feng and A. Ball [25] used seven different erodents which include, glass beads, steel shot, diamond, silicon carbide, silica, alumina and tungsten carbide erodent particles. The erodents were used to study the erosion behavior of stainless steel 304 and WC – 7% Co. It was found that SS 304 exhibited better erosion resistance when harder particles were used. However, this resistance relative to WC - 7% Co was diminished when softer particles were used.

2.1.6 Erosion Models

Previous sections have shown that solid particle erosion is a complex phenomenon involving high strain rates, adiabatic heating, extensive plastic deformation and fracture. The development of a universal erosion model which can incorporate all the important parameters is undoubtedly a challenging task. This is the reason that till date we don't have any universal predictive model for solid particle. However, this section will review some of the most popular erosion models which have already been developed. Furthermore, the practicability and applicability of these models will be discussed.

Sundararajan [26], [27] and Hutchings [28], [29] models are few of the earliest models developed by researchers to study and predict erosion phenomenon. The theoretical erosion model was proposed by Sundarajan and Shewmon [26], and is valid for normal impacts (90° angle). The major consideration in this model is the critical plastic strain which is defined as the strain required to plastically deform the target material leading to lip formation. The model considers the distance of plastic zone L after the particle impact and also assumes that the maximum strain increment occurs at the point of impact and decreases as the distance from point of impact increases. First expression of erosion rate is developed by considering the number of impacts N_c causing the removal of material volume L:

$$E = \frac{L\, p_t}{N_c \left(\frac{4}{3}\right) \pi r^3 p_b} \qquad (1)$$

Where, p_t and p_b are target density and particle density, respectively and r is the radius of the particle. Now the parameter N_c is given by:

$$N_c = \frac{\varepsilon_c}{2\pi L^2 \Delta\epsilon_m \left\{1-\frac{(t+1)}{(t+2)}\right\} F(t)} \quad (2)$$

The substitution of N_c in to the earlier equation of E gives the form:

$$E = \frac{2V_d p_t \Delta\epsilon_m \{1-((t+1))/((t+2))\} F(t)}{\frac{4}{3}\pi r^3 p_b \varepsilon_c} \quad (3)$$

The above model suggests that the erosion rate is inversely proportional to the critical strain ε_c and directly proportional to the volume displaced during the particle impacts.

Later, Sundararajan [27] developed a comprehensive model for erosion of ductile materials which is valid for all impact angles. Again, the assumption made in this model is the localization of the plastic zone under the particle impact so that there is no net flow hardening. Furthermore, the critical coefficient of friction between the eroding particle and the target material, μ_c is discussed. First, the erosion rate at normal angles E_n is given by:

$$E_n = ((2\text{^}n\ C)/nC_p) F(t) V^2 sin^2(1-e^2) \quad (4)$$

Now, the expression for oblique angles is given by:

$$E_o = V_{lip}\frac{p}{m} = \left\{C(n+1)\frac{V^2}{2^{2-n}} nC_p(1+\lambda)\right\}\left(\frac{\mu}{\mu_c}\right)\left(2-\frac{\mu}{\mu_c}\right) cos^2\boldsymbol{\alpha} \quad (5)$$

Then the overall erosion rate was obtained by adding the oblique E_o and normal E_n erosion rates:

$$E = (2^n CV^2 \sin^2 \alpha F(t)/nC_p)[1 + \{(n+1)(\mu/\mu_c)(2 - \mu/\mu_c)/4(1+\lambda)\ \tan^2 \alpha F(t)\} - e^2] \qquad (6)$$

The model is applicable to all impact angles and suggests that the peak erosion rate at any particular angle is strongly dependent of the coefficient of friction μ. The peak erosion rates move towards lower angles for increasing values of μ.

Another famous model for the erosion of metals is given by Hutchings [28]. This model implies a similar criterion of critical plastic strain. However, this model is applicable for spherical particles impacting the targeting metal at normal incidence angles.

Development of the erosion model involves the consideration of spherical eroding particle mass: $m = 4\pi r^3 \rho/3$ and kinetic energy $mv^2/2P$. Where P is the constant pressure exerted by the substrate to resist the indentation. Figure 2.9 illustrates the distribution of the kinetic energy during the particle impact:

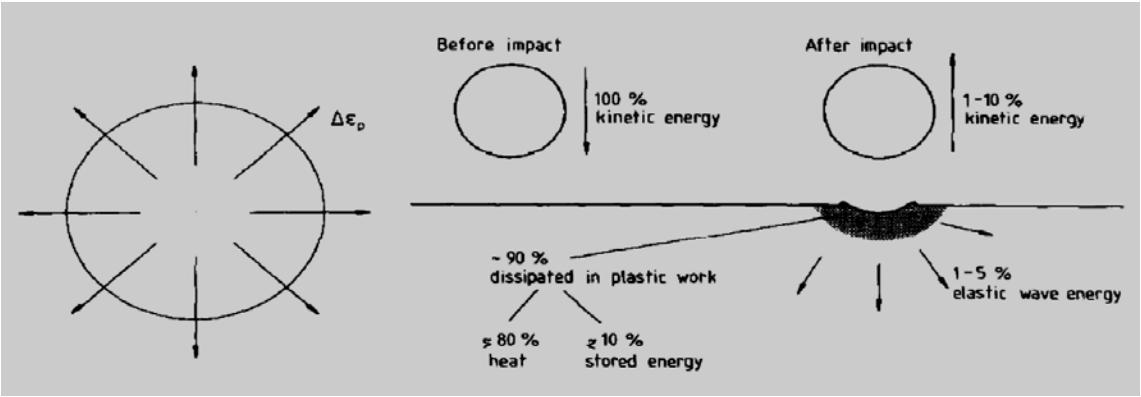

Figure 2.9 Radial plastic strains due to particle impact. The distribution of energies before and after the particle impact at normal incidence angle [28].

The elementary (caused by single impact) volume of material loss is given by: $\alpha mv^2/2P$. For mean number of particle impacts N_f the volume loss becomes: $\alpha mv^2/2PN_f$. After incorporating the density ρ, the erosion rate E which is defined as the target mass loss per unit mass of erodent is given by:

$$E = \frac{\alpha \rho v^2}{2PN_f} \qquad (7)$$

The model incorporates two important material properties: dynamic hardness and ductility. And according to this model the high erosion resistance is obtained in materials with high hardness and high ductility. However, the author recommends further investigations into the effect of these properties on the erosion rate.

A recently developed model which can be applied to all metals and alloys is given by Oka et. al [30]. As discussed earlier, the mechanical properties of the material are the key parameters which affect the erosion phenomenon. It was found that the material hardness is an important parameter in predicting solid particle erosion and hence, must be incorporated in the predictive model. For the impact angle dependence of erosion rate at any arbitrary angle, the following equation is proposed:

$$E_{(\alpha)} = g(\alpha)E_{90} \qquad (8)$$

$$g(\alpha) = (\sin \alpha)^{n1} (1+Hv(1-\sin \alpha))^{n2} \qquad (9)$$

$$E_{90} = Cv^n \qquad (10)$$

Gives,

$$E = (\sin \alpha)^{n1} (1+Hv(1-\sin \alpha))^{n2}[Cv^n] \qquad (11)$$

Where g(α) is defined as normalized erosion rate i.e., ratio of erosion rate at a given angle α to erosion rate at normal angle. Combining eq. 1-3 gives E (mm^3Kg^{-1}) as a function of Vickers hardness Hv, impact angle α, impact velocity v and velocity exponent n with C, n_1, n_2 as constants. Equation (4) is the final correlation between erosion rate, impact angle, Vicker's hardness and impact velocity. Using this equation one can correlate their experimental data and determine the value of constants with the help of regression analysis.

2.1.7 Discrepancy between Erosion Rates of Steels and Aluminum Alloys

Direct comparison of erosion behavior between steels and aluminum under standard testing conditions has been rarely investigated. Fang and Chuang [31] studied erosion behavior of AISI 430 and 304 stainless steels, ARC-TEN weathering steel, brass, and 6063 aluminum alloy and concluded that stainless steels had lowest volume loss while Al 6063 showed considerably high volume loss. In aluminum, they observed that initial particle impacts led to piling up of material in the form of ridges which were removed by subsequent particle impacts. Similarly, Oka et al. [32] carried out erosion tests on several materials which included metallic materials, plastics and ceramic materials using silica sand at a velocity of 130 m/s. Their study showed that the softer the material the higher the erosion rates at oblique angles. Hence, lead and aluminum indicated higher erosion rates compared to steels.

Contrary to the above findings, Harsha et al. [33] reported in their recent study on various ferrous and non-ferrous alloys that the erosion rate for aluminum was minimum compared to other alloys which included steels, cast iron and brass. High erosion resistance of aluminum was attributed to its high ductility and the rapid work hardening

ability thus resisting mass loss. In another recent study carried out by Juan et al.[34], solid particle erosion behavior of carbon steels, stainless steels, aluminum, brass and copper was analyzed using SiC erodent. Their findings showed that stainless steels had minimum erosion resistance while aluminum exhibited maximum erosion resistance, considering this behavior as unexpected; they assumed that room temperature may have altered the behavior of these alloys.

Based on the above review, previous studies have shown some contradiction between the erosion characteristics of aluminum and steels. Hence, the objective of this study is to compare erosion behavior of commonly used stainless steels (AISI 310S and AISI 316), carbon steel (AISI 1020) with aluminum 6060-T4 alloy under standard testing conditions, in order to better understand the disparity between the erosion rates of aluminum and steels. Comparison was done by evaluating the effect of bulk hardness of the alloys. Furthermore, the effect of erosion rates with respect to solid particle velocity and impact angle was analyzed, followed by scanning electron microscopy study to understand the erosion mechanism involved.

2.2 Review of Literature on Erosion-Corrosion

Erosion-Corrosion problem in materials involve flow-induced degradation. This form of damage occurs in all types of flow and generally begins with the electrolytic dissolution and/or mechanical abrasion of the passive layer. Erosion-Corrosion is broadly classified into two groups: single phase flow and multiphase flow. Single phase flow refers to only one phase (liquid, solid or gas) flow through an enclosed section. While, multiphase refers to the type of flow which contains two or more phases such as: oil and water, vapor

and liquid or solid and liquid. The underlying mechanism in erosion-corrosion depends on whether erosion precedes corrosion and/or corrosion precedes erosion. The latter is known as corrosion-enhanced erosion. Matsumura [35] explains the effect of corrosion on erosion and attributes the enhancement of erosion to the removal of work hardened layer which is caused or accelerated by corrosion attack. Other mechanisms include: i) selective corrosion attack at grain boundaries resulting in increased susceptibility of grain removal by erosion [36], and ii) increase in the number of surface defects due to micropitting [37]. A combined attack on the material by erosion and corrosion is referred to as synergism. During synergism mass loss of the material is accelerated by erosion-enhanced corrosion and corrosion-enhanced erosion [38].

Previously, many researchers have investigated the erosion-corrosion behavior of steels using various systems, such as rotating electrode systems [39]–[42], flow loop systems [43]–[47] and jet impingement systems [48]–[52]. In addition, Md. Aminul Islam et al. [53] recently studied the erosion-corrosion behavior of API X-70 steel. They carried out cyclic erosion and corrosion tests on the steel surface and hence, determined the erosion-enhanced corrosion and corrosion-enhanced erosion of their test specimen. It was found that the corrosion attack removes the work hardened layer and exposes stress-free surface to the erosion as a result the erosion of corroded surface is greatly enhanced. C. F. Dong et al. [54] investigated the erosion-accelerated corrosion of a carbon steel 1020 and stainless steel 316L in a galvanic couple. The results indicated that as the flow velocity increases, erosion becomes a dominating variable in the synergism of the galvanic couple. Hence, the pure erosion and corrosion-enhanced erosion components dominated the overall erosion-corrosion process.

Mechanical and electrochemical interactions during the erosion-corrosion of carbon steel A1045 were reported by H.X. Guo et al. [41]. The corrosion-enhanced erosion increased with an increase in anodic current density due to corrosion induced damage in the surface layer of the alloys. In contrast, A. Neville and X.Hu [55] in their study of erosion-corrosion behavior of high-alloy stainless steels highlighted that resistance to weight loss does not increase with an increase in the hardness. Moreover, J. G. Chacon Nava, F. H. Stott and M. M. Stack [56] investigated the effect of harness on erosion-corrosion resistance of various materials. It was concluded that the erosion-corrosion damage increases with increasing hardness at high temperatures. This was attributed to the non-adherent and less protective oxide scale formation.

2.2.1 Erosion-Corrosion Mechanism

The actual mechanism by which film damage occurs is still not clearly understood. This is because a large number of factors are involved during erosion-corrosion which includes surface shear stress, flow regimes, velocity gradients and mechanical forces due to bubbles impingement and/or suspended solid particles. Figure 2.10 illustrates various forces acting on the surface of metal during erosion-corrosion (Reproduced by R. J. K Wood [38], original by [57]). Following mechanisms are illustrated in the figure:

1) Single phase flow:
    a. Mass transfer, fluctuating pressures and fluctuating shear stresses
2) Multiphase flow:
    a. Liquid/solid, gas/liquid and liquid/air interactions with the surface.
    b. Imploding vapor bubbles on the metal surface.

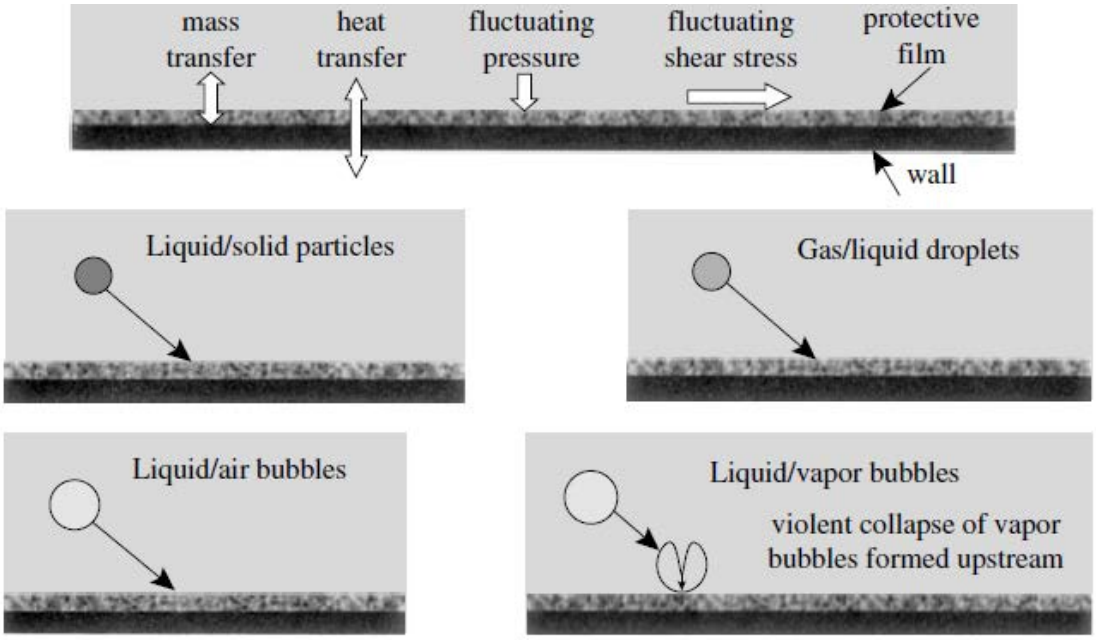

Figure 2.10 Flowing media interaction with metal surface resulting in erosion-corrosion [57]

2.2.2 Effect of Flow Velocity on Erosion-Corrosion

Like erosion, flow enhanced degradation also increases with an increase in flow velocity. At lower velocities the flow is laminar with lower velocity gradient and mass loss is prevented by protective layer on the metal surface. However, as the velocity is increased up to a certain point known as breakaway velocity, there is a sharp increase in erosion-corrosion rate which is primarily due to the turbulent flow causing breakdown in the protective layer. Further increase in velocity leads to disturbed turbulent flow where the protective layer is completely removed and subsequent removal of material occurs by high shear stresses [58]. Hence, erosion-corrosion problem is more serious when the flow is turbulent.

U. Lotz et al. [59] studies erosion-corrosion in disturbed two phase flow. Tests were carried out in flow loop having a sudden decrease in pipe diameter and the flowing media used was CO_2 saturated 3 wt %. NaCl. They observed maximum erosion-corrosion in the constriction and downstream of the constriction. Moreover, solid particles accelerated the erosion-corrosion rate by removing the corrosion products from the metal surface.

E.A.M. Hussain et al. [52] investigated the erosion-corrosion 2205 duplex stainless steel using jet impingement apparatus. A range of hydrodynamic conditions were studied and their effect on the mass loss was analyzed. Potentiodynamic polarizations scans were carried out to measure corrosion. The maximum erosion-corrosion rate was observed directly below the impinging flow due to particle impacts at higher kinetic energy in this region. At greater radial distances from the impingement flow, erosion-corrosion was less severe although the flow was turbulent this was due to lower angle of particle impacts.

2.2.3 Corrosion-Enhanced Erosion Problem in Industry

The mechanism of Erosion-Corrosion depends on whether erosion precedes corrosion and/or corrosion precedes erosion. The latter is known as corrosion-enhanced erosion. Stagnant solution which remains in the gas pipelines after hydrostatic testing can initiate corrosion on the pipe wall. When these pipelines are brought into operation, the solid particles entrained in the gas/liquid flow can further aggravate mass loss at the corrosion sites. Previous studies have focused on understanding erosion-corrosion phenomenon as a whole. However, in the present study, our prime focus within erosion-corrosion is to study the mechanism in which corrosion preceded erosion. Therefore, a different approach is used to study the corrosion-enhanced erosion behavior of two most commonly used steels (carbon steel AISI 1020 and stainless steel AISI 316). The test specimens were corroded by immersing in low pH chloride bearing environments. The corroded specimens were then subjected to solid particle erosion. Hence the effect of corrosion on the increase in erosion rate is investigated and compared with the pure erosion data for the same materials. Furthermore, the corrosion-enhanced erosion behavior is correlated with the material hardness and surface roughness. Finally, the samples are analyzed using scanning electron microscopy (SEM) in order to evaluate the material degradation mechanism involved in erosion/corrosion process.

2.3 Motivation and Objectives

2.3.1 Motivation

Erosion-Corrosion is a serious problem in industry. Billions of dollars are spent annually due to damages incurred by corrosion and erosion in oil & gas, petrochemical and power generation industries. Solid Particle Erosion (SPE) and erosion-corrosion experimental data can be useful in order to evaluate material performance and service life in various industrial equipment and systems.

Stainless steels AISI 316, AISI 310S, carbon steels AISI 1020 and aluminum 6060-T4 are most commonly and extensively used in industries where erosion and erosion-corrosion is a critical problem. Hence, these alloys have been selected for in-depth SPE and erosion-corrosion investigations. Previously there has been extensive research carried out to evaluate their individual erosion and corrosion behavior. However, direct erosion comparison between steels and aluminum ally has been rarely investigated. Literature review indicates some contradiction between erosion resistances of two classes of materials. Furthermore, there is a need to develop quantitative erosion correlations to assist in computational fluid dynamics in order to better predict and extrapolate erosion problems.

2.3.2 Objectives

1. Comparison of solid particle erosion behavior between Stainless Steels (AISI 316, AISI 310), Carbon Steel 1020 and Aluminum 6060-T4 by evaluating:
    a. Effect of hardness on their erosion behavior.
    b. Eroded surface morphology (SEM analysis).
2. Develop correlations using erosion model to provide useful data for computational fluid dynamics which will help predict SPE at desired conditions.
3. Simulating erosion-corrosion tests for stainless steel AISI 316 and carbon steel 1020. Hence, investigate pure erosion and corrosion-enhanced erosion.
4. Compare pure erosion rates (SPE on polished specimens) with corrosion-enhanced erosion rates.

CHAPTER 3

MATERIALS AND METHODS

3.1 Erosion Test Apparatus

In this study, room temperature Air Jet Erosion Tester manufactured by KOEHLER Instrument Company, Inc. (Model # K93700) was utilized for solid particle erosion testing. Figure 3.1 (a) and (b) shows the image and schematic of the erosion apparatus, respectively. The nozzle diameter, length and other specifications of the equipment conforms to the ASTM-G76-95 [60] standard. Particle flow rate is precisely controlled by the rotation frequency of the discharge wheel, located at the outlet of the erodent hopper, shown in Figure 3.1(b). Flow rate was calculated by collecting and measuring the erodent mass flowing through the nozzle for 10 min at a specified wheel frequency. Hence, a graph relating frequency of the discharge wheel and erodent flow rate was constructed, shown in Figure 3.2. Particle velocity was measured using double disc rotating method, described elsewhere [61]. Velocity was measured with an accuracy of ± 2m/s and was correlated with air pressure as shown in Figure 3.3. Both particle flow rate and velocity calibrations were checked after every 20 experiments.

Figure 3.1 (a) Air Jet Erosion Tester KOEHLER Instrument Company, Inc. (Model # K93700), inset image: Mixing chamber and sample holder

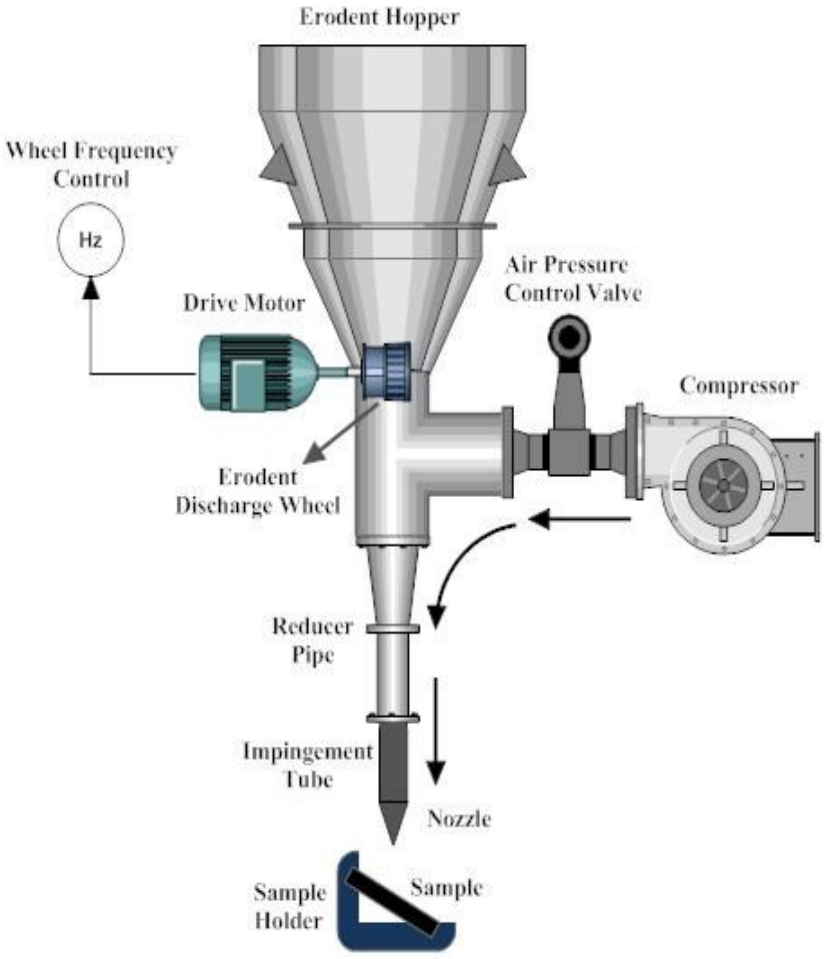

Figure 3.1 (b) Schematic of air jet erosion tester (not drawn to scale)

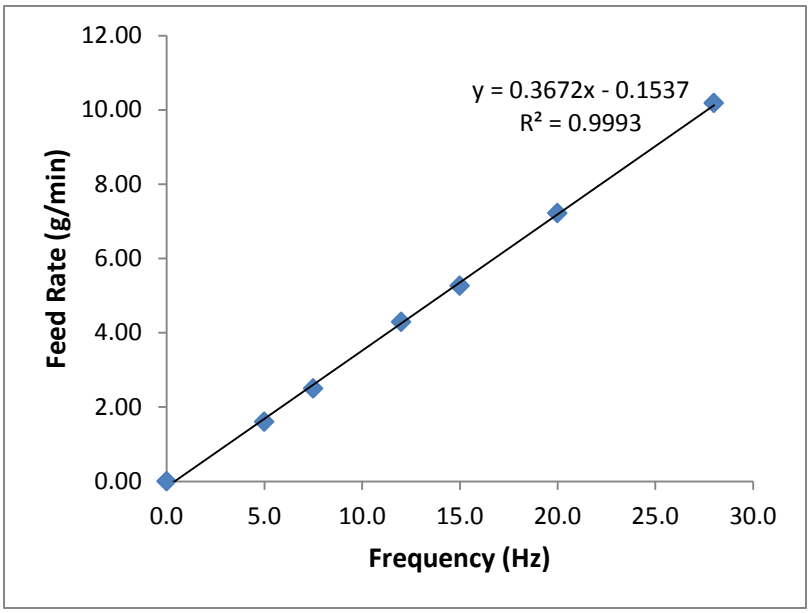

Figure 3.2 **Particle discharge/feed rate (g/min) vs. Frequency of the discharge wheel (Hz)**

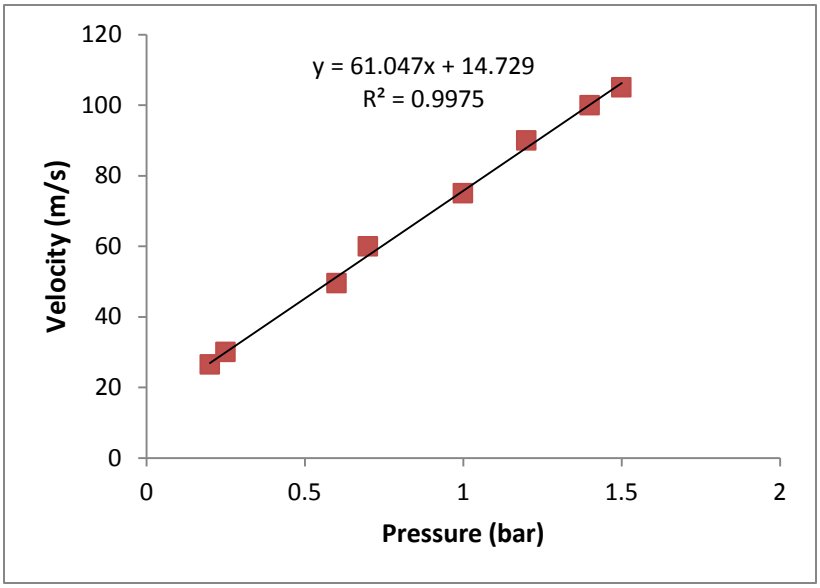

Figure 3.3 **Particle velocity (m/s) vs Pressure (Bar)**

3.2 Test Samples

Solid particle erosion testing was performed on: two different grades of stainless steel, one low-carbon steel and one aluminum alloy. Erosion-corrosion testing was carried out on carbon steel AISI 1020 and stainless steel AISI 316. Detailed composition and grades are listed in Table 3.1. Materials were selected as per their extensive use in applications where they undergo solid particle erosion, such as gas pipelines, valves and gas turbine systems. Vicker's microhardness of the samples were measured using 100-300 gf load, average of four readings were taken per sample and are listed in Table 3.2. All samples were machined into 25 x 25 x 5 mm size and grinded up to 400 grit size paper to give surface roughness Ra of <1 μm. Before each experiment, samples were cleaned ultrasonically in acetone for 10 min, dried and weighed to an accuracy of 0.1 mg using (Starrter weighing balance).

Table 3.1 **Chemical compositions of test materials**

Material	Grade	Fe	Al	Mg	C	Si	Mn	Cr	Ni	Mo	Co	Cu	P	S
Carbon Steel	1020	98.7	…	…	0.21	0.14	0.78	0.03	0.03	…	0.01	0.02	0.02	0.012
Stainless Steel	310S	52.1	…	…	0.08	0.50	1.42	27.21	18.14	0.1	0.18	0.15	0.03	0.008
	316	68.4	…	…	0.08	0.50	1.35	17.05	10.12	1.89	0.21	0.24	0.04	0.003
Aluminum	6060-T4	0.16	98.9	0.44	…	0.40	0.03	…	…	…	…	…	…	…

Table 3.2 **Microhardness of test materials**

Material	Grade	Vickers Hardness				Average
Stainless Steel	310S	274.2	252.8	245.1	278.8	262.7
Low-Carbon Steel	1020	205	203.8	197	196.1	200.5
Stainless Steel	316	193.3	176.6	184.1	179.8	183.5
Aluminum	6060-T4	77.3	86.3	82.3	86.1	83

3.3 Test Procedure

3.3.1 Solid Particle Erosion

Erosion tests were performed as per ASTM G-76-95 test standard [60]. Angular alumina with particle size of 50 µm was used as an erodent in our experiments. Alumina is hygroscopic, hence care was taken to ensure moisture free erodent therefore it was baked in the oven at 110°C for 24 hrs, while stirring at regular intervals before utilizing for the experiments. Compressed air stream used to accelerate alumina particles was first passed through moisture trap and then through air filter to ensure clean and dry air. Tests were carried out at three different velocities: 30m/s, 60m/s and 100m/s corresponding to 0.25 bar, 0.7 bar and 1.4 bar pressure, respectively (Figure 3.3). At each velocity six different impact angles were used: 15°, 30°, 45°, 60°, 75° and 90°. Particle flow rate of 2.5 g/min (corresponding to 7.5 Hz wheel frequency) was kept constant for all the experiments. It was selected to allow adequate particle flux on the sample yet avoiding high inter-particle collisions which are caused by using high mass flow rates [62][63]. Incremental erosion rate calculation method was used.

Initial experiments showed that the steady state erosion rate resulted after 2 min and 5 min for steels and aluminum, respectively. Hence, the test samples were subjected to erosion and removed after every 2 min (for steels) and 5 min (for aluminum). Then, the samples were cleaned and weighed again. This cycle was repeated up to a total time of 10-15 min. Two samples from the same material were tested for each set of parameters (i.e. particle velocity and impingement angle) and their average mass loss versus erodent mass was plotted. Hence the preliminary results from initial solid particle erosion testing

are shown in Figure 3.4. Dimensionless steady state erosion rates will be determined from the slope of the average mass loss vs. erodent mass graph and will be reported as milligrams mass loss of sample per gram of erodent impacting on it (mg/g).

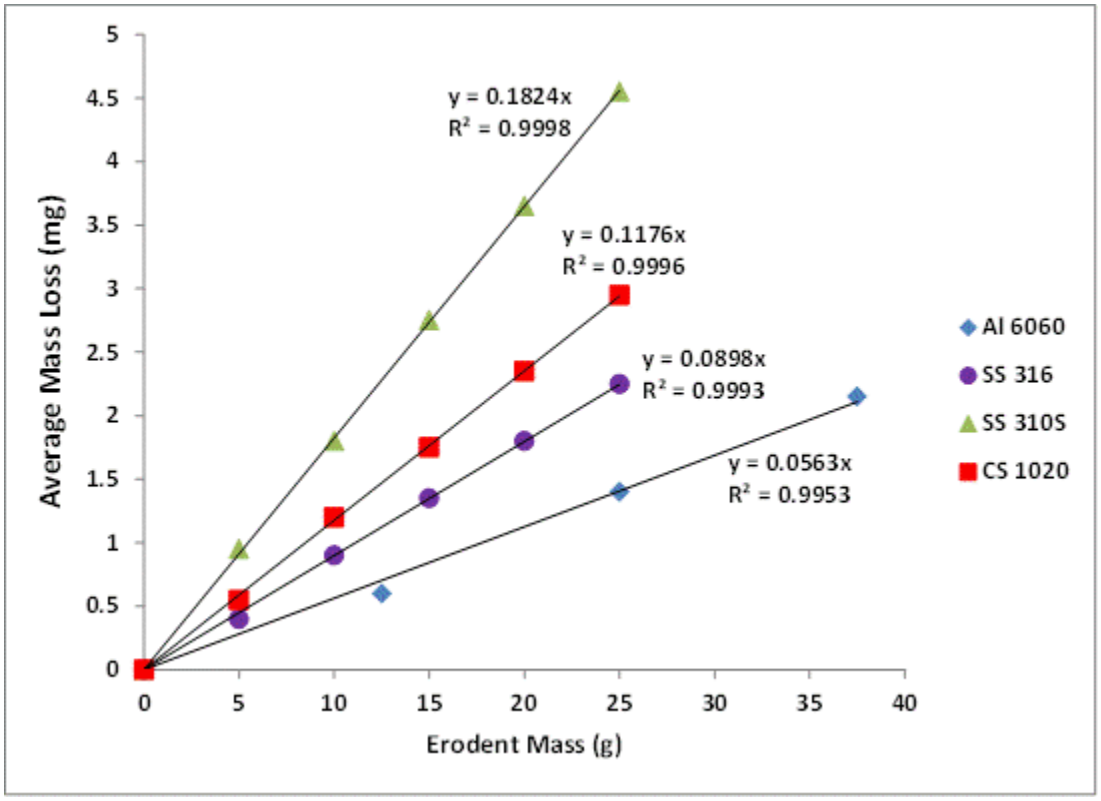

Figure 3.4 **Mass loss (mg) vs. erodent mass (g) for all four materials.**

3.3.2 Erosion-Corrosion

3.3.2.1 Immersion Test

Specimens were subjected to corrosion using the immersion technique. Carbon steel AISI 1020 was immersed in ferric chloride solution (100 g $FeCl_3$ in 900 ml of distilled water) while stainless steel was immersed in HCl saturated with ferric chloride solution. These two solutions were specifically selected to accelerate the corrosion attack relative to other natural corrosive environments. Immersion tests were carried out for 24 h and 48 h, and the weight loss of the two steels was measured.

Before the tests, specimens of size 25 mm x 25 mm x 5 mm were cold mounted in epoxy, this was done to expose only the specimen surface to the corrosive solution and to avoid crevice corrosion at the edges which could influence the weight loss readings. After mounting, specimens were ground up to 400 grit size on SiC abrasive paper, cleaned with distilled water and weighed to an accuracy of 0.0001 g. A reference epoxy sample (without test specimen) of similar size as of other mounts was also immersed in the solution to analyze and eliminate any error in weight loss due to epoxy mounts. Mass loss due to pure corrosion was recorded and surface roughness was measured. Finally, the samples were subjected to SPE and the erosion testing procedure mentioned in section 3.3.1 was followed.

3.3.2.2 Hardness Measurements

Evaluation of hardness measurements for corroded samples was a critical phase of corrosion-enhanced erosion study. CSM Micro Combi Tester (Figure 3.6) was employed to measure the hardness of corroded surface of carbon steels AISI 1020. Corroded samples were cut using a low velocity, diamond blade precision cutter to avoid any tempering of the surface while cutting (Figure 3.5). Samples were then mounted such that the hardness profiles of cross-section could be recorded. This was done to eliminate error of substrate hardness when top surface hardness is measured. Low load of 20 mN was selected to measure the hardness of corrosion products. A total of 6 readings were taken on each specimen and hence, their average value is reported.

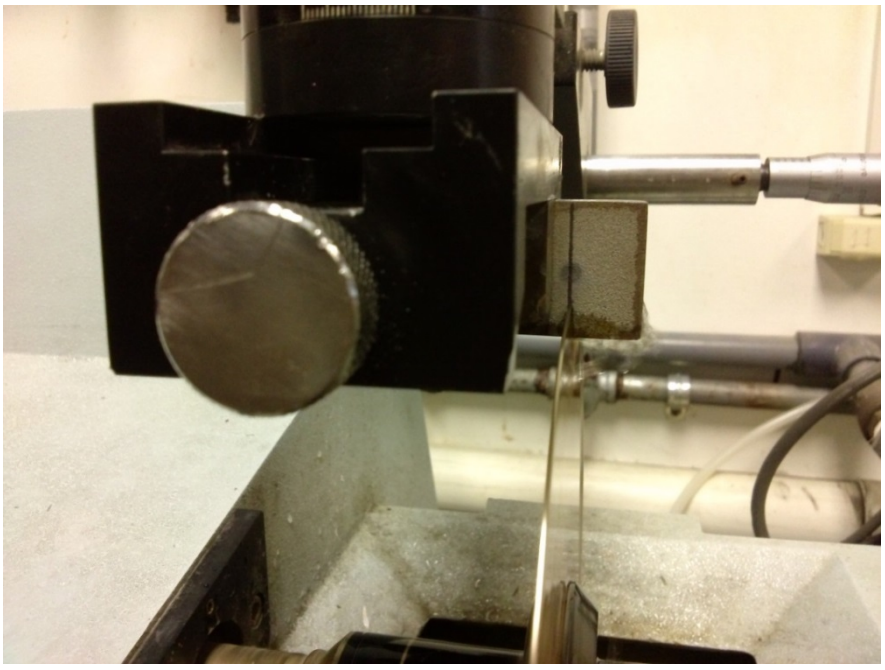

Figure 3.5 Precision diamond cutting

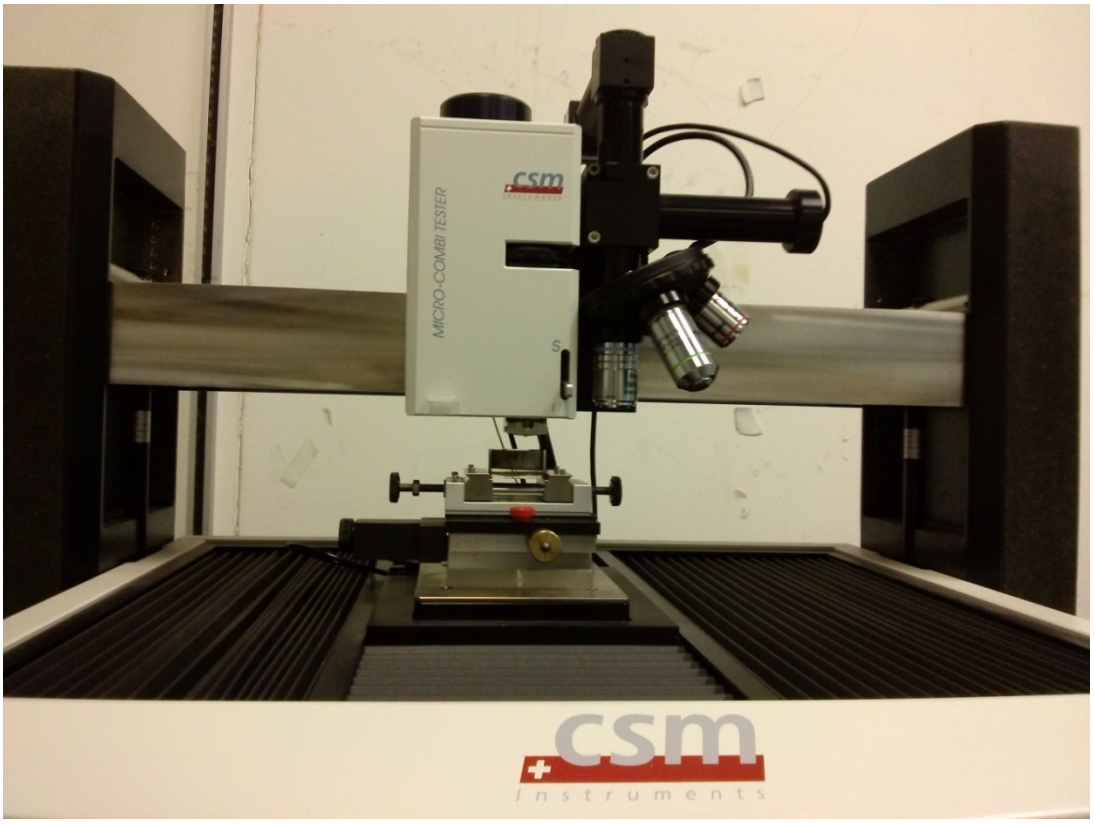

Figure 3.6 **CSM Combi Micro Tester**

3.4 Methodology

3.4.1 Solid Particle Erosion

As discussed in the materials and methods section, AISI 310S, AISI 316, AISI 1020 and Al 6060-T4 alloys were selected to study and compare their erosion behavior. Each material will be subjected to 3 different particle velocities with 6 different impact angle (15°, 30°, 45°, 60°, 75°, 90°) at each velocity. Hence a graph between erosion rate and impact angle will be sketched for each material. Table 3.3 shows the solid particle erosion experimental plan. A total of 144 experiments were be carried out and later on the surface morphology of eroded samples were characterized using scanning electron microscopy to study the erosion mechanism and material degradation.

Experimental data was used to correlate erosion rates (mg/g) of each test material with particle impact angle and particle velocity. These correlations will be useful in comparing the erosion behavior of test materials. Furthermore, the erosion resistance for each material was also evaluated by comparing the bulk hardness of the samples in order to see the effect of hardness on erosion resistance.

Table 3.3 **Solid Particle Erosion experimental plan**

Solid Particle Erosion Experiments Matrix

Velocity (m/s)		30						60						100						Total		Total Samples Per Batch
Sample Size (mm)		20x25x5				25x25x5		20x25x5				25x25x5		20x25x5				25x25x5		20x25x5	25x25x5	
Impact Angle (deg.)		15	30	45	60	75	90	15	30	45	60	75	90	15	30	45	60	75	90			
Carbon Steel	1020	2	2	2	2	2	2	2	2	2	2	2	2	2	2	2	2	2	2	18	18	36
Stainless Steel	316	2	2	2	2	2	2	2	2	2	2	2	2	2	2	2	2	2	2	18	18	36
	310S	2	2	2	2	2	2	2	2	2	2	2	2	2	2	2	2	2	2	18	18	36
Aluminum	6060	2	2	2	2	2	2	2	2	2	2	2	2	2	2	2	2	2	2	18	18	36
Total Samples Per Angle & Velocity		8	8	8	8	8	8	8	8	8	8	8	8	8	8	8	8	8	8	72	72	**144**

3.4.2 Erosion-Corrosion

Austenitic stainless steel AISI 316 and carbon steel AISI 1020 was selected to evaluate the erosion-corrosion behavior. A new approach was used to simulate corrosion-enhanced erosion in these two materials. Samples were subjected to immersion tests (pure corrosion) which were followed by SPE (corrosion-enhanced erosion and pure erosion).

Table 3.4 lists the series of experiments that were carried out. SS AISI 316 was immersed in hydrochloric acid solution saturated with ferric chloride while carbon steel AISI 1020 was immersed in 6% ferric chloride solution. Two immersion times were selected: 24h and 48h. The mass loss of the corroded samples was measured to calculate corrosion rate of the materials in their respective environments. Finally the corroded samples were subjected to SPE to analyze corrosion-enhanced erosion behavior and compare that with pure erosion (SPE on un-corroded samples).

Table 3.4 **Corrosion-Enhanced Erosion experimental plan**

Immersion Test + SPE Experiments Matrix

Immersion Time		24 h																48 h												Total Samples Per Batch
Velocity (m/s)		30								60								30								60				
Sample Size (mm)		20x25x5				25x25x5				20x25x5				25x25x5				20x25x5				25x25x5				20x25x5				25x25x5			
Impact Angle (deg.)		15	30	45	60	75	90	15	30	45	60	75	90	15	30	45	60	75	90	15	30	45	60	75	90	15	30	45	60	75	90	
Carbon Steel	1020	1	1	1	1	1	1	1	1	1	1	1	1	1	1	1	1	1	1	1	1	1	1	1	1	1	1	1	1	1	1	24
Stainless Steel	316	1	1	1	1	1	1	1	1	1	1	1	1	1	1	1	1	1	1	1	1	1	1	1	1	1	1	1	1	1	1	24
Total Samples Per Angle & Velocity		2	2	2	2	2	2	2	2	2	2	2	2	2	2	2	2	2	2	2	2	2	2	2	2	2	2	2	2	2	2	**48**

CHAPTER 4

RESULTS AND DISCUSSIONS

4.1 Solid Particle Erosion behavior of Metals

4.1.1 Effect of Impact Angle on Erosion Rate

Ductile and brittle materials showed different erosion rates with respect to the solid particle impact angle. A comparison of erosion rates of aluminum (ductile) and alumina (brittle) with respect to impact angle, obtained from the curves of Finnie and Sheldon [64], is shown in Figure 4.1. It was observed that ductile materials generally show maximum erosion rates in the range of 15°-30° impact angle while brittle materials show maximum erosion rate at normal angle.

Similarly, the tests performed by Oka et al. [32] showed that the shape of the erosion curves is dependent on the material hardness. They attribute the maximum erosion rate at any given angle to the high shear forces incurred on the surface and the ability of the material to resist these forces. Consequently, materials with high hardness such as ceramics resist erosion at oblique angles, while the ductile materials are prone to shear forces and erodes more at oblique angles.

Furthermore, Shewmon et al. [17] explained that the high mass loss for ductile metals at oblique angles is due to lip formation by effective penetration of the incident particles. These extruded lips are then sheared off by subsequent impacts. Whereas, at normal

incident angle, the ductile metals absorb most of the kinetic energy of incoming particles resulting in lower mass loss.

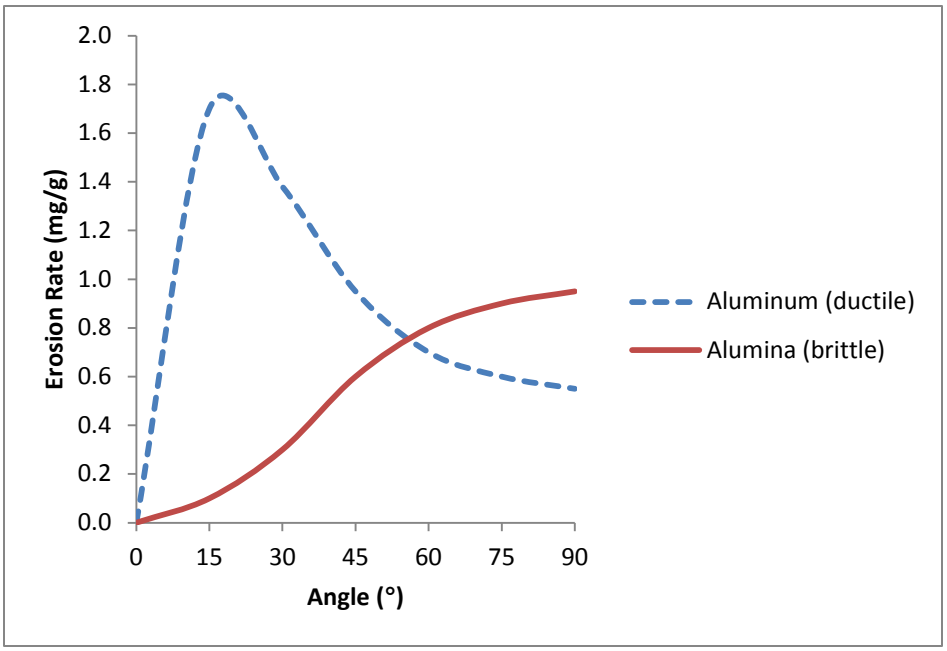

Figure 4.1 **Comparison between erosion characteristics of ductile and brittle materials [64]**

Figure 4.2 shows the effect of impact angle on the erosion rate for the four tested materials keeping the erodent impact velocity unchanged (60 m/s). It is clear from the figure that the maximum erosion rates occur between 15°-30° impact angle. Accordingly, all four metallic alloys are showing ductile erosion behavior. Also, Sundararajan [13] discussed the dependence of the maximum erosion rate and the corresponding impact angle on the coefficient of friction, μ. His model indicated that with increasing μ, the peak erosion rate shifts towards lower impact angles. Since there are many variables involved (material properties, particle characteristics), the shift in impact angles for peak erosion rates within ductile metals is quite complex. One such variable is coefficient of friction which could have resulted in the peak shift of carbon steel AISI 1020 to 30° angle, compared to the peaks of other materials which occurred at the impact angle of 15°.

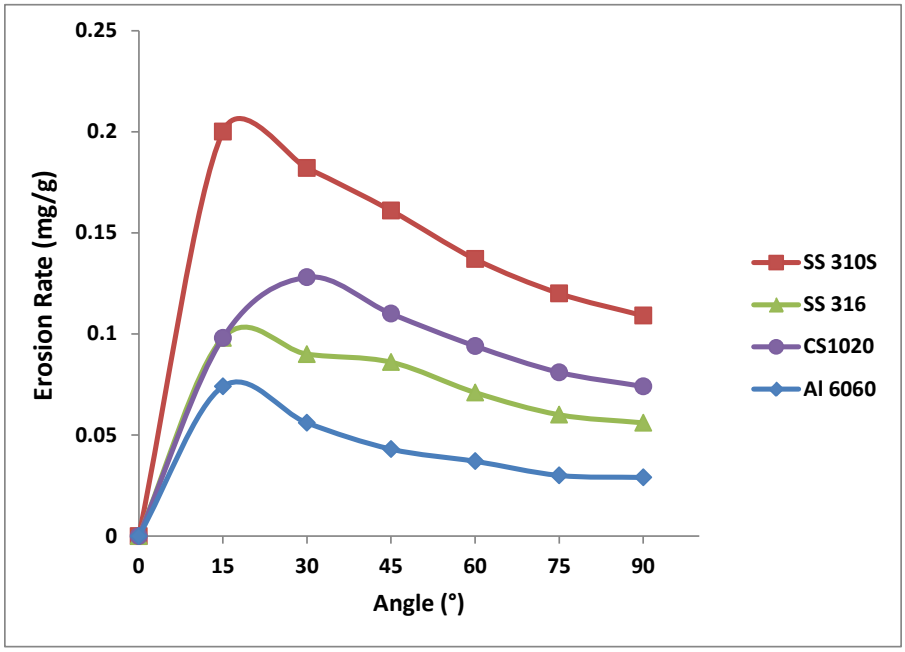

Figure 4.2 Effect of impact angle on erosion rate of four materials at impact velocity of 60 m/s

4.1.2 Effect of Impact Velocity on Erosion Rate

The increase in erosion rate is very strongly related to particle impact velocity. The correlation between erosion rate and velocity is generally reported as a power law equation in the form $E = K (V)^n$, where E is erosion rate, K is the material constant which depends on particle size and impact angle, V is the particle velocity and n is velocity exponent with value between 1.0 and 2.5 [14]. The effect of impact velocity on erosion rate for the four test materials is shown in Figure 4.3-4.6 and their respective erosion rate values are given in Table 4.1-4.4. As expected, there is a strong increase in erosion rates with increasing impact velocity, observed by positive y-axis translation of curves. This is attributed to the increase in particle kinetic energy with an increase in particle flow velocity resulting in higher shear stresses which causes more mass loss as discussed earlier by Levy and Liebhard [65]. Furthermore, it can be seen that the erosion behavior with respect to impact angle is independent of the velocity. Similar observation has been reported by other authors previously such as Oka et al. [32] and Morrison et al. [66].

The maximum erosion rate for carbon steel 1020 increased from 0.043 mg/g at 30 m/s to 0.128 mg/g at 60 m/s showing a 3 fold increase and the erosion rate of 0.230 mg/g at 100 m/s velocity shows approximately 5 fold increase in erosion rate from that at 30 m/s velocity. The erosion rate increased with velocity in the same proportion was noted for all materials tested. This indicates that the increase in erosion rate with particle velocity is strongly dependent on eroding particle kinetics rather than on the material properties.

Table 4.1 **Erosion Rate values for stainless steel AISI 310S at velocities of 30, 60 and 100 m/s.**

Stainless Steel AISI 310S					
Velocity = 30 m/s		Velocity = 60 m/s		Velocity = 100 m/s	
Angle (°)	Erosion Rate (mg/g)	Angle (°)	Erosion Rate (mg/g)	Angle (°)	Erosion Rate (mg/g)
0	**0**	**0**	**0**	**0**	**0**
15	0.06	15	0.20	15	0.34
30	0.06	30	0.18	30	0.30
45	0.05	45	0.16	45	0.26
60	0.04	60	0.14	60	0.21
75	0.04	75	0.12	75	0.18
90	0.04	90	0.11	90	0.17

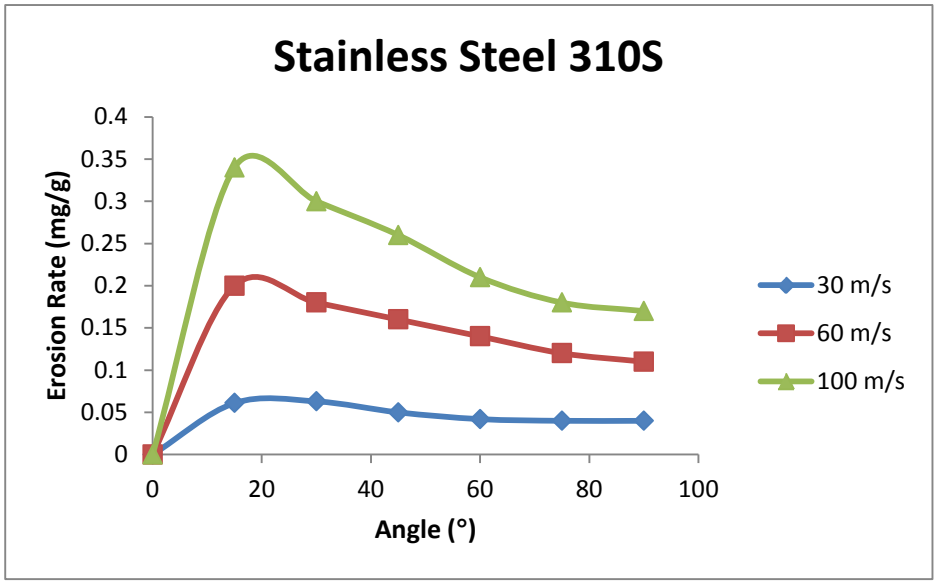

Figure 4.3 **Effect of impact velocity on erosion rate for stainless steel AISI 310S**

Table 4.2 **Erosion Rate values for stainless steel AISI 316 at velocities of 30, 60 and 100 m/s.**

Stainless Steel AISI 316					
Velocity = 30 m/s		Velocity = 60 m/s		Velocity = 100 m/s	
Angle (°)	Erosion Rate (mg/g)	Angle (°)	Erosion Rate (mg/g)	Angle (°)	Erosion Rate (mg/g)
0	0.000	0	0.000	0	0.000
15	0.036	15	0.098	15	0.173
30	0.036	30	0.090	30	0.158
45	0.032	45	0.086	45	0.141
60	0.025	60	0.071	60	0.126
75	0.020	75	0.060	75	0.109
90	0.019	90	0.056	90	0.096

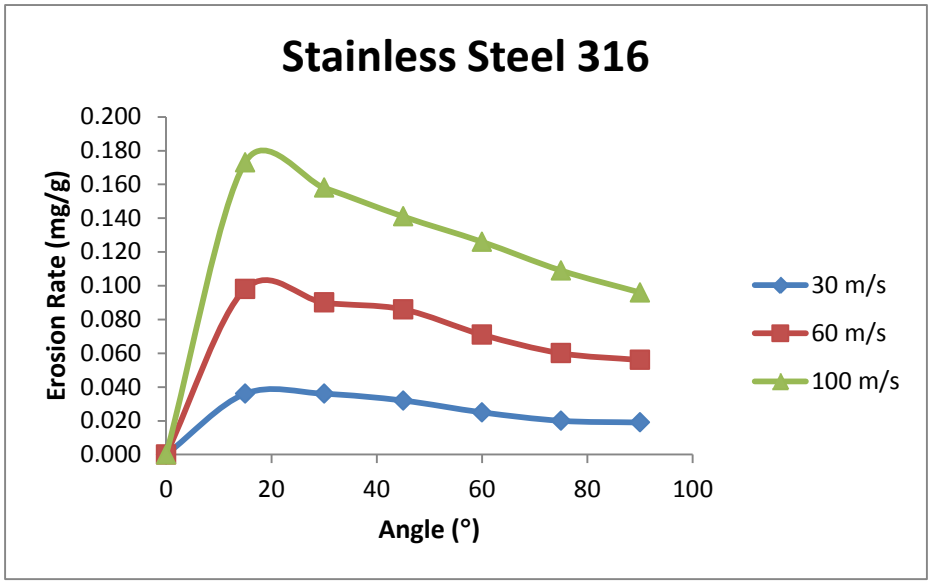

Figure 4.4 **Effect of impact velocity on erosion rate for stainless steel AISI 316**

Table 4.3 **Erosion Rate values for carbon steel AISI 1020 at velocities of 30, 60 and 100 m/s.**

Carbon Steel AISI 1020					
Velocity = 30 m/s		Velocity = 60 m/s		Velocity = 100 m/s	
Angle (°)	Erosion Rate (mg/g)	Angle (°)	Erosion Rate (mg/g)	Angle (°)	Erosion Rate (mg/g)
0	0.000	0	0.000	0	0.000
15	0.034	15	0.098	15	0.193
30	0.043	30	0.128	30	0.230
45	0.040	45	0.110	45	0.200
60	0.030	60	0.094	60	0.165
75	0.027	75	0.081	75	0.138
90	0.025	90	0.074	90	0.121

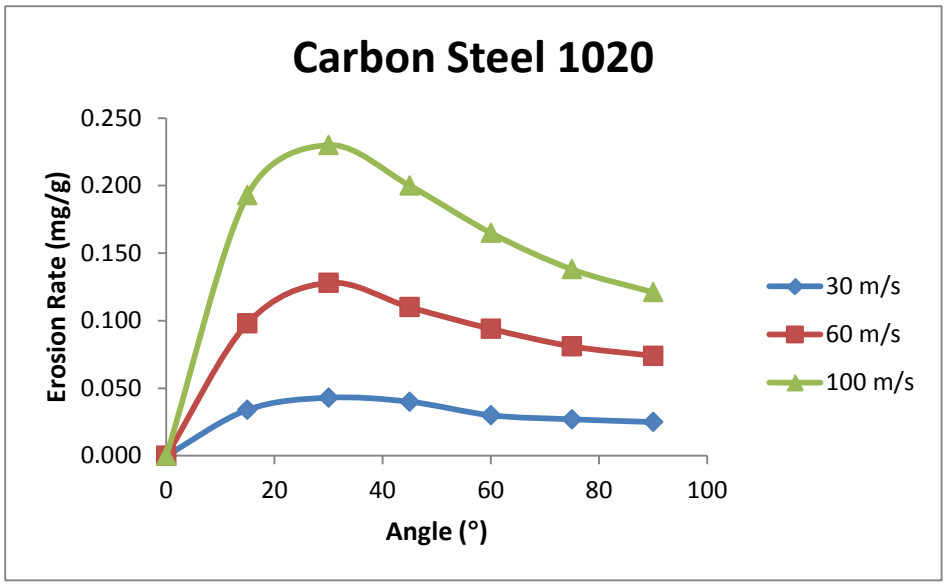

Figure 4.5 **Effect of impact velocity on erosion rate for carbon steel AISI 1020**

Table 4.4 **Erosion Rate values for Aluminum 6060-T4 at velocities of 30, 60 and 100 m/s.**

Aluminum 6060-T4					
Velocity = 30 m/s		Velocity = 60 m/s		Velocity = 100 m/s	
Angle (°)	Erosion Rate (mg/g)	Angle (°)	Erosion Rate (mg/g)	Angle (°)	Erosion Rate (mg/g)
0	0.000	0	0.000	0	0
15	0.029	15	0.074	15	0.121
30	0.019	30	0.056	30	0.094
45	0.017	45	0.043	45	0.073
60	0.012	60	0.037	60	0.054
75	0.010	75	0.030	75	0.047
90	0.010	90	0.029	90	0.042

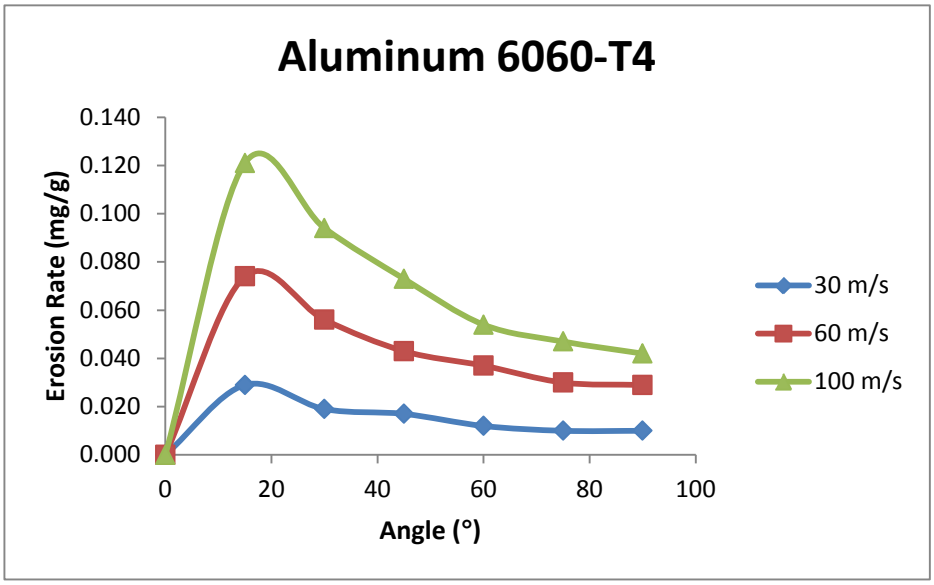

Figure 4.6 **Effect of impact velocity on erosion rate for Aluminum 6060-T4**

4.1.3 Correlation with Erosion Model

Quantification of erosion rate experimental data in form of correlations is useful to simulate erosion problems at desired conditions. Erosion models are generally defined as a function of impact velocity, impact angle, erodent size and material properties (hardness, fracture strain). Most widely used erosion models are of Hutchings [29], [67] and Sundararajan [27]. In addition, a famous erosion model which can be applied to all metals is given by Oka et. al [30]:

$$E_{(\alpha)} = g(\alpha)E_{90} \quad (1)$$

$$g(\alpha) = (\sin \alpha)^{n1} (1+Hv(1-\sin \alpha))^{n2} \quad (2)$$

$$E_{90} = Cv^{n} \quad (3)$$

$$\text{Gives, } E = (\sin \alpha)^{n1} (1+Hv(1-\sin \alpha))^{n2}[Cv^{n}] \quad (4)$$

Where g(α) is defined as normalized erosion rate i.e., ratio of erosion rate at a given angle α to erosion rate at normal angle. Combining eq. 1-3 gives E (mm^3Kg^{-1}) as a function of Vickers hardness Hv, impact angle α, impact velocity v and velocity exponent n with C, n_1, n_2 as constants.

In the present work, the experimental data was correlated with Oka et al. [30] erosion model and values of C, n_1, n_2 and n were determined by performing regression analysis using MATLAB software. Lower and upper bounds for n_1, n_2 were selected to be 0 and 2, respectively, while for velocity exponent n, between 1 and 3. Constant values of Vickers hardness HV given in Table 3.2 were used. Hence, the constants determined by

regression analysis are shown in Table 4.5. Values of the correlation coefficient R^2> 90% of all materials are indicating a good fit using the given parameters.

Furthermore, using Eq. (4) and the parameters given in Table 4.5, erosion rates were calculated at v = 60 m/s and α ranging from 15° to 90°. A comparison between the experimental erosion rate curves with those calculated using Oka et al. [30] model is shown in Figure 4.7-4.10 and their respective erosion rate values are given in Table 4.6-4.9. The calculated erosion rate shows a good agreement with experimental data of stainless steels, carbon steel and aluminum. This indicated that Oka et al. [30] model can be used to simulate erosion problems. However, the parameters for this model given in Table 3 are specific to current test materials and present conditions.

Table 4.5 **Curve fitting constants for the test materials**

Materials	c	n1	n2	n	R^2
SS 316	0.04387	3.69E-10	0.1302	1.199	99%
SS 310S	0.08848	1.25E-08	0.1524	1.158	97%
CS 1020	0.04034	0.1308	0.1542	1.273	98%
Al 6060-T4	0.06548	9.88E-09	0.3136	1.117	96%

Table 4.6 **Comparison of experimental and Oka et al. model curve fitting erosion rate values for stainless steel AISI 310S.**

Stainless Steel AISI 310S

Velocity (m/s)	Angle (°)	Erosion Rate (mg/g)	Oka et. al. model Erosion Rate -E (mg/g)
60	0	0	0.00000
60	15	0.200	0.17558
60	30	0.182	0.16542
60	45	0.161	0.15260
60	60	0.137	0.13578
60	75	0.120	0.11151
60	90	0.109	0.07857

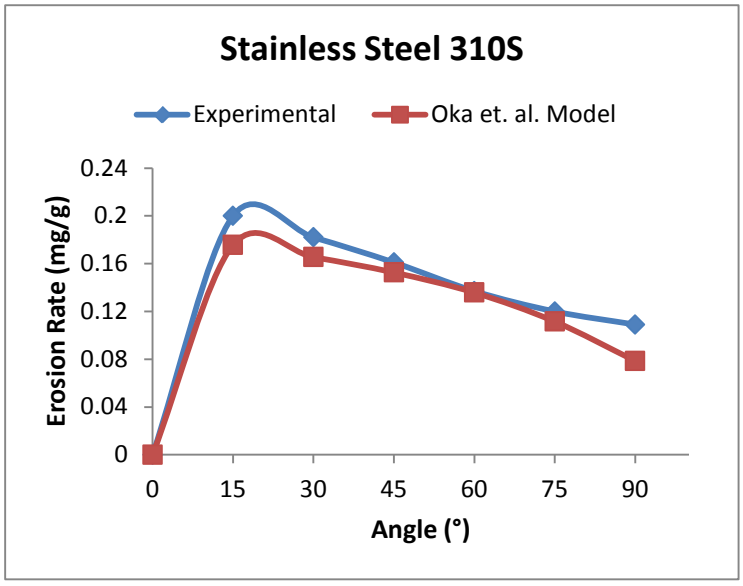

Figure 4.7 **Comparison of experimental and Oka et al. model curve fitting erosion rate curves for stainless steel AISI 310S.**

Table 4.7 **Comparison of experimental and Oka et al. model curve fitting erosion rate values for stainless steel AISI 316.**

Stainless Steel AISI 316

Velocity (m/s)	Angle (°)	Erosion Rate (mg/g)	Oka et. al. model Erosion Rate - E (mg/g)
60	0	0.000	0.00000
60	15	0.098	0.09025
60	30	0.090	0.08578
60	45	0.086	0.08009
60	60	0.071	0.07254
60	75	0.060	0.06156
60	90	0.056	0.04756

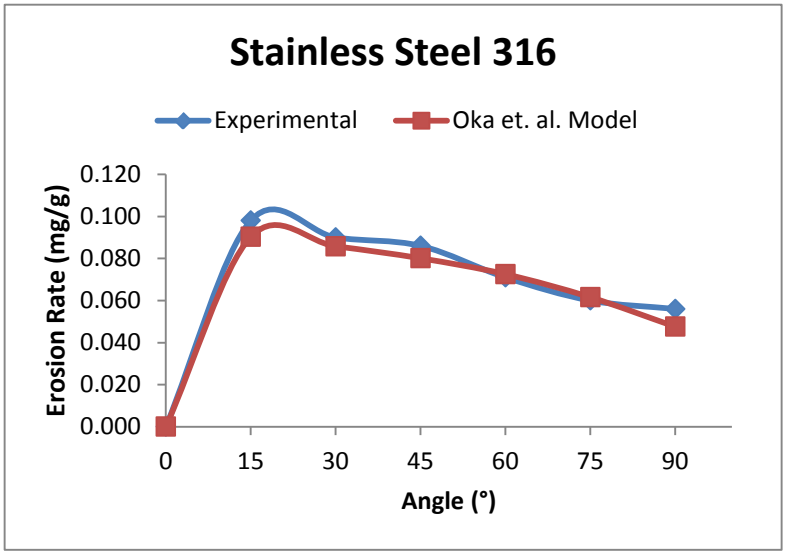

Figure 4.8 **Comparison of experimental and Oka et al. model curve fitting erosion rate curves for stainless steel AISI 316.**

Table 4.8 **Comparison of experimental and Oka et al. model curve fitting erosion rate values for carbon steel AISI 1020.**

Carbon Steel AISI 1020

Velocity (m/s)	Angle (°)	Erosion Rate (mg/g)	Oka et. al. model Erosion Rate -E (mg/g)
60	0	0.000	0.00000
60	15	0.098	0.10566
60	30	0.128	0.10843
60	45	0.110	0.10459
60	60	0.094	0.09549
60	75	0.081	0.07965
60	90	0.074	0.05825

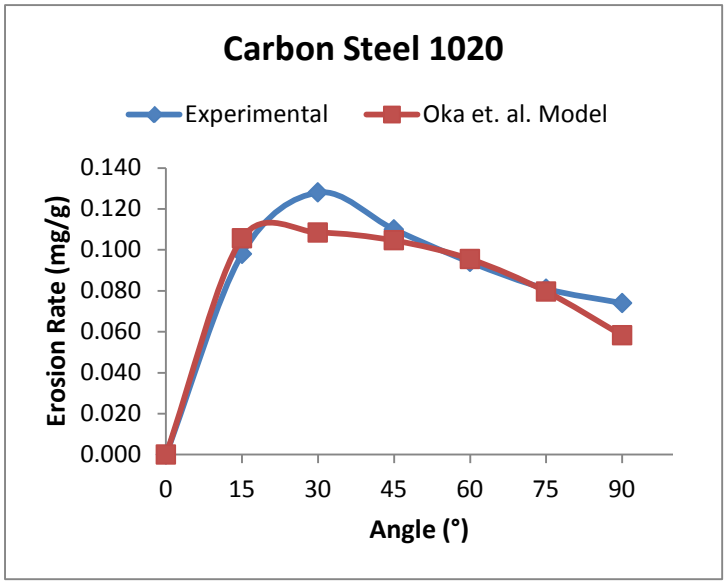

Figure 4.9 **Comparison of experimental and Oka et al. model curve fitting erosion rate curves for carbon steel AISI 1020.**

Table 4.9 **Comparison of experimental and Oka et al. model curve fitting erosion rate values for aluminum 6060-T4.**

Aluminum 6060-T4

Velocity (m/s)	Angle (°)	Erosion Rate (mg/g)	Oka et. al. model Erosion Rate -E (mg/g)
60	0	0.000	0.00000
60	15	0.074	0.06265
60	30	0.056	0.05550
60	45	0.043	0.04718
60	60	0.037	0.03745
60	75	0.030	0.02609
60	90	0.029	0.01713

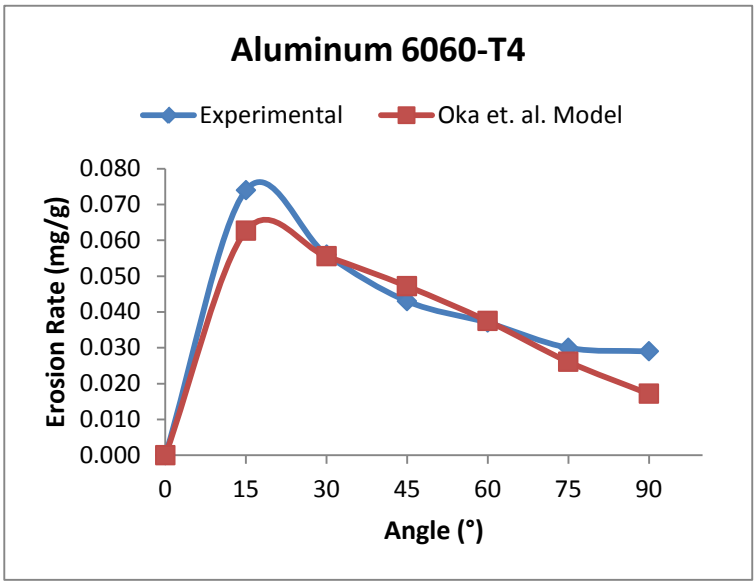

Figure 4.10 **Comparison of experimental and Oka et al. model curve fitting erosion rate curves for aluminum 6060-T4.**

4.1.4 Erosion Rate and Mechanism

Figure 4.11 (a-c) shows the comparison of erosion behavior between AISI 310S, AISI 316, AISI 1020 and Aluminum 6060-T4, at three different velocities. For steels, the erosion rate found to increase as hardness increases (Table 3.2 & Figure 4.11). Moreover, at velocity of 60 m/s, AISI 310S and an average bulk hardness of 262.7 HV, the peak erosion rate found to be 0.2 mg/g. However, for AISI 316 with a hardness of 183.5 HV, the peak erosion rate found to be 0.098 mg/g. Also, for AISI 1020 with an intermediate hardness, the erosion rate found to be a value between 0.089 and 0.2 mg/g. Moreover, it can be seen that aluminum being the most ductile is showing highest erosion resistance compared to steels. This is because ductility helps erosion resistance by absorbing the kinetic energy of impacting particles and plastically deform the surface while maintaining within the fracture strain limits [16].

Various studies have concluded that the increase in hardness either by heat-treatment, work-hardening or solution annealing, causes decrease in erosion resistance [12], [13], [65], [66], [68]. For example, Sundararajan [13] study the effect of hardness in pure metals and alloys on their erosion resistance and concludes that the erosion resistance decrease in steels as the hardness increases and this attributed to fully adiabatic heating. However, the abrasion resistance increases with increasing hardness pertaining to a non-adiabatic wear process. Similarly in the present study, steels have shown an increase in erosion rate with increasing hardness. However, direct relationship between erosion rate and bulk material hardness cannot be established. This is mainly because other factors may play important role during the erosion process such as localized hardening and adiabatic heating.

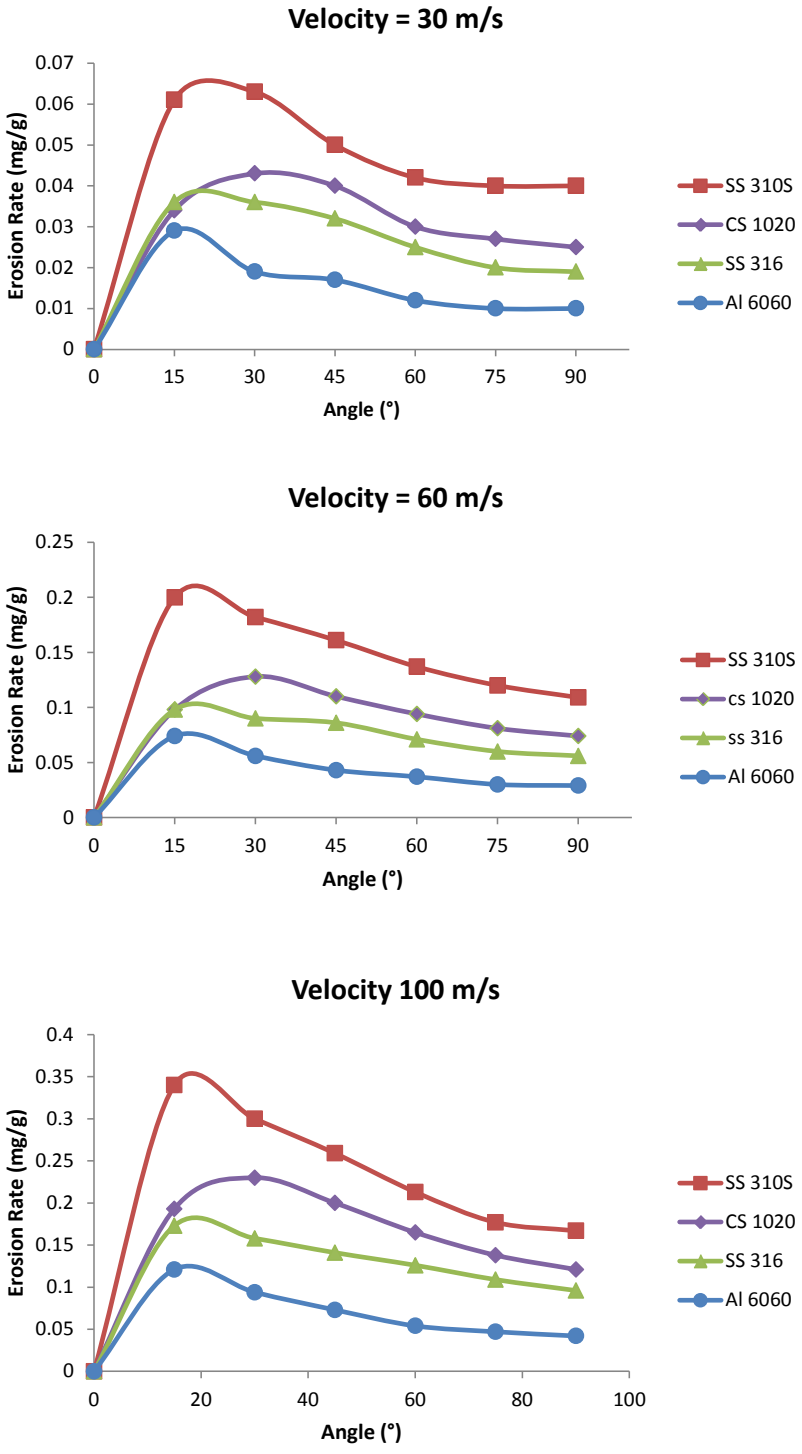

Figure 4.11 **Comparison between the erosion characteristics of AISI 310S, AISI 316, AISI 1020 and Aluminum 6060-T4 at three different velocities; a) 30 m/s, b) 60 m/s and c) 100 m/s**

It is clear from the erosion rate dependence on the impact angle that all four materials are following ductile erosion behavior. To understand this ductile erosion mechanism, scanning electron microscopy was carried out. Figure 4.12 (a-b) shows SEM micrographs of alumina eroding particles before erosion. 50 µm uniformly sized alumina with angular shape and sharp cutting edges can be seen from the micrographs. The high mass loss is caused by hard and angular particles compared to soft and round particles as discussed by Levy and Liebhard [65] and Vite-Torres [24]. They relate the high wear losses and material degradation to the angular alumina erodent.

Figure 4.13 (a-b) shows SEM images of stainless steel 310S eroded at impact angle of 15° and 90°. As shown in Figure 4.13 (a), the severe material degradation is caused by extrusion/ploughing action. Moreover, the indications of material removal such as deformation scratches are also shown. Also, the damage at normal angle as shown in Figure 4.13 (b) is much less severe with no deformation scratches. In this case, crates and pits are visible indicating that most of the kinetic energy of incident particles is dissipated in deforming/displacing the material rather than actual material removal.

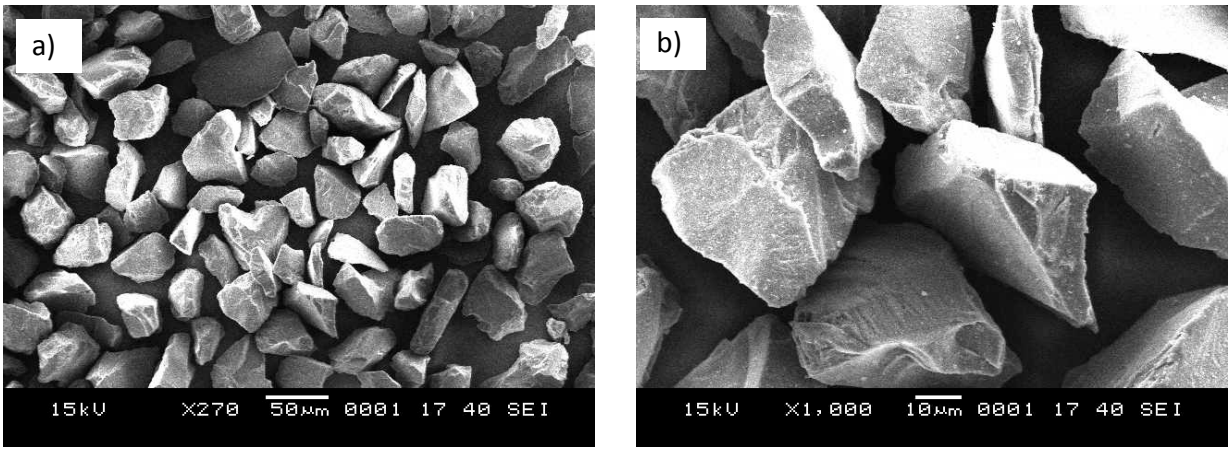

Figure 4.12 **Alumina abrasive particles 50 µm at magnification a) 270X and b) 1,000X**

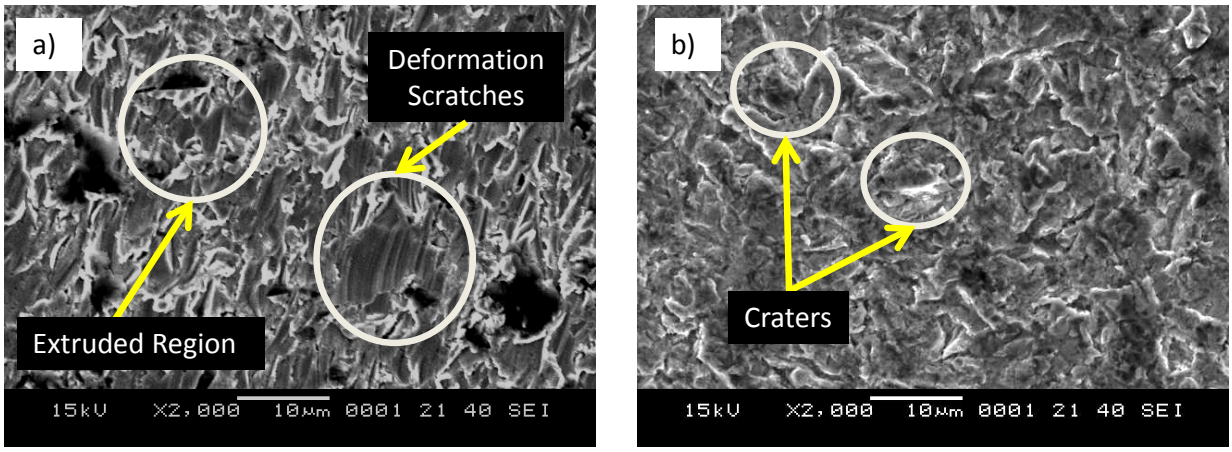

Figure 4.13 **Stainless Steel 310S Eroded Surface at impact angle a) 15° and b) 90°**

The eroded surfaces of carbon steel 1020 are shown In Figure 4.14 (a-b). Once again, the impact angle of 15° more wear damage is observed compared to 90°. Also, deformation scratches and lip formation due to plastic deformation by extrustion/ploughing action are shown. This is consistent with the findings of Levy [5], Hein [17], Finnie [69]. On the other hand, at 90° impact angle, the ductile erosion behavior in carbon steel AISI 1020 is characterized by dimples, pits and crater morphologies (Figure 4.14 (b)) which is generally observed in ductile metals at normal impacts as indicated by Laguna-Camacho [7]. Similar erosion morphologies were observed in stainless steel 316, as in stainless 310S and carbon steel 1020.

For ductile erosion mechanism, quite different erosion morphologies are observed in the case of aluminum 6060-T4 compared to other three materials. As shown in Figure 4.15 (a-b), the higher erosion resistance of aluminum alloy is characterized by the formation of flakes and distressed regions where the ductility of aluminum prevents the material detachment. Furthermore, the lower magnification images of eroded aluminum alloy surface (Figure 4.15 (c-d)) showing a wavy structure and formation of grooves, which are attributed to the lower hardness of aluminum that results in extensive material displacement. In addition, at higher velocity of 100 m/s (Figure 4.15 (d)), waves are slightly more compact and dense showing higher plastic deformation but again less material removal. As a result of which, aluminum 6060-T4 having lowest hardness of HV 83 is also showing the lowest erosion rates at all velocities.

.

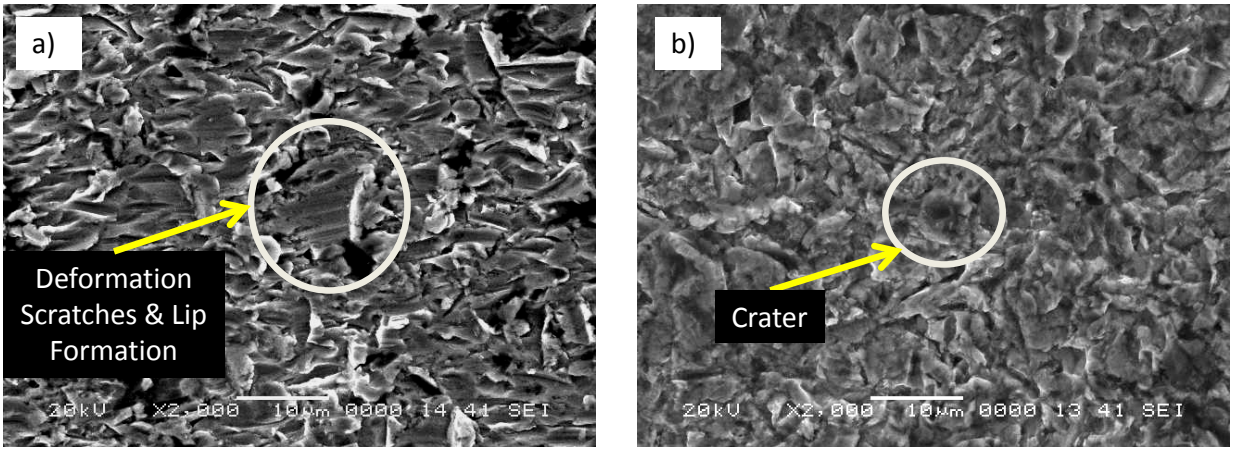

Figure 4.14 **Carbon Steel AISI 1020 eroded surface at impact angle a) 15° and b) 90°**

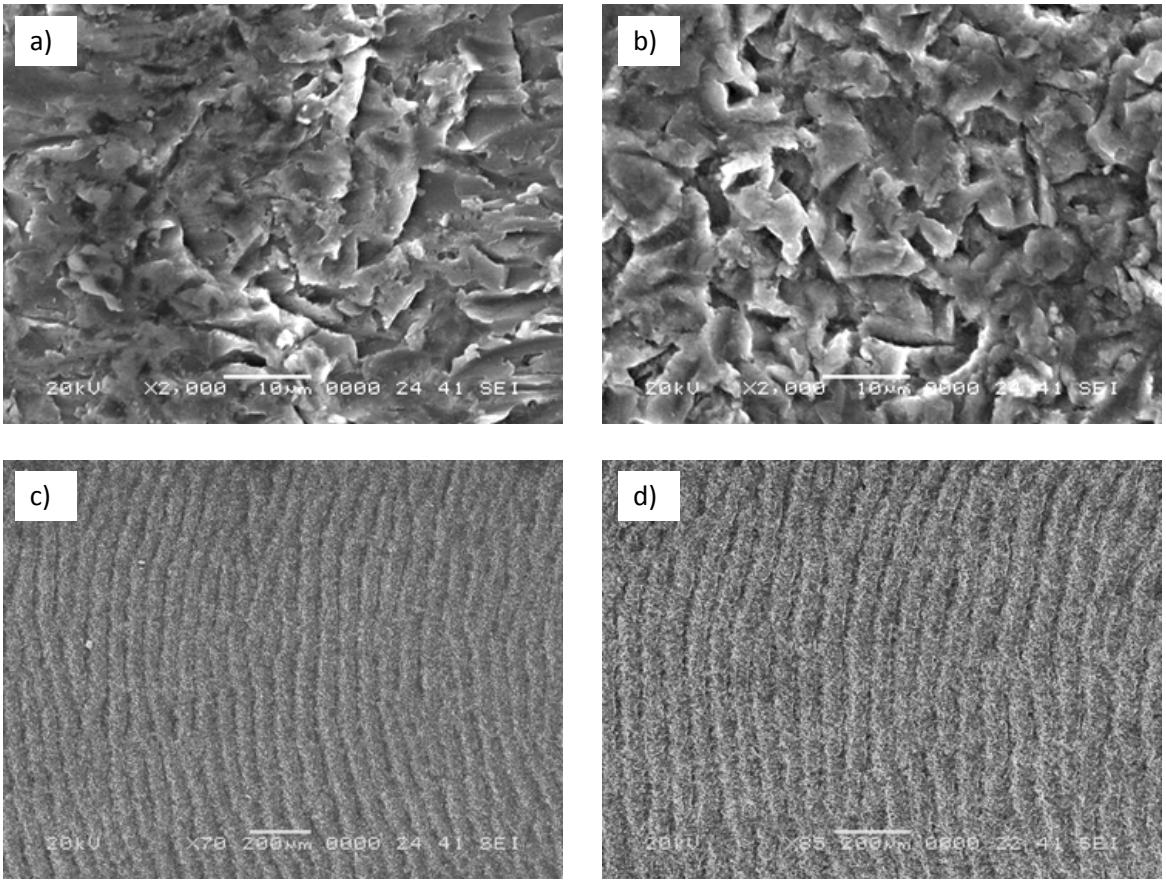

Figure 4.15 **Aluminum eroded surface at impact angle a) 15°, b) 90°, c) 15° (velocity = 60 m/s) and d) 15° (velocity = 100 m/s)**

4.2 Corrosion-Enhanced Erosion behavior of Metals.

4.2.1 Corrosion investigation using immersion test

Figure 4.16 (a-b) shows the microstructure of carbon steel AISI 1020 and stainless steel AISI 316. Fine grained microstructure comprising of pearlite and ferrite in the optical micrograph of carbon steel, whereas, grains of austenite are clearly seen in the microstructure of austenitic stainless steel. Scanning electron microscopy of the 24 h immersed carbon steel specimen reveals severe surface degradation due to active corrosion attack by chloride ions (Figure 4.17 (a)). Moreover, crack formation leaving loosely adhered corrosion products can also be seen in Figure 4.17 (b). Conversely, Figure 4.18 (a) and Figure 4.18 (b) reveals the 24 h immersed specimens of stainless steel 316 which is characterized by formation of dimples and grooves throughout the surface suggesting general corrosion attack by Cl^- and H^+ ions. Unlike carbon steel, the passive nature of austenitic stainless steel 316 helps to resist the corrosion attack in chloride bearing environments [50].

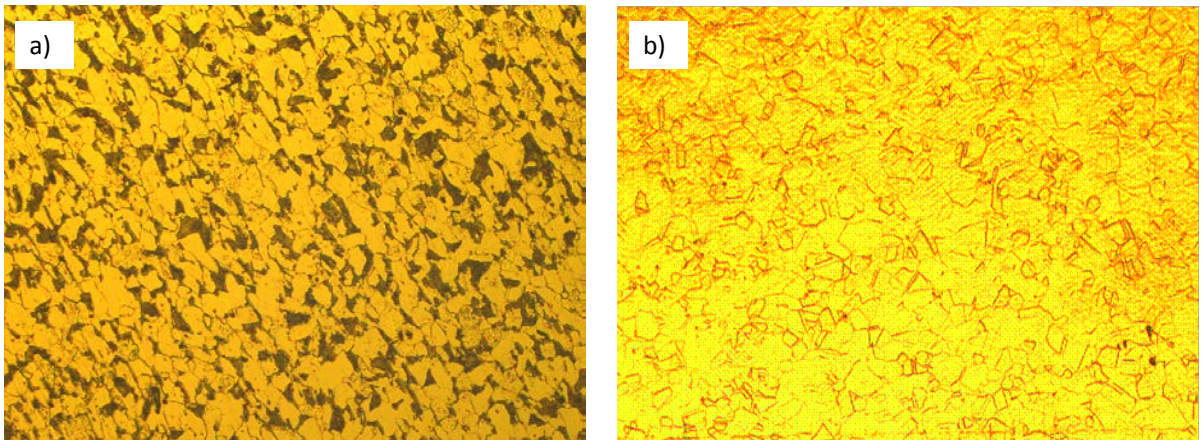

Figure 4.16 (a) Optical micrograph of carbon steel AISI 1020 at 100X magnification, (b) Optical micrograph of stainless steel AISI 316 at 100X magnification.

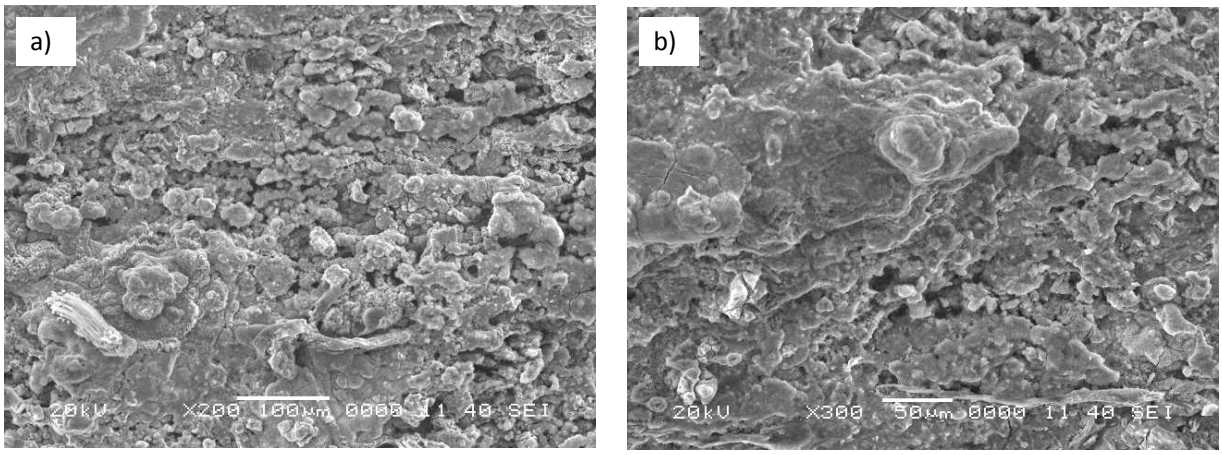

Figure 4.17 **(a) SEM micrograph of 24 h immersed carbon steel AISI 1020 showing loosely adherent corrosion products, (b) SEM micrograph of 24 h immersed carbon steel AISI 102 revealing cracks on the oxide corrosion product.**

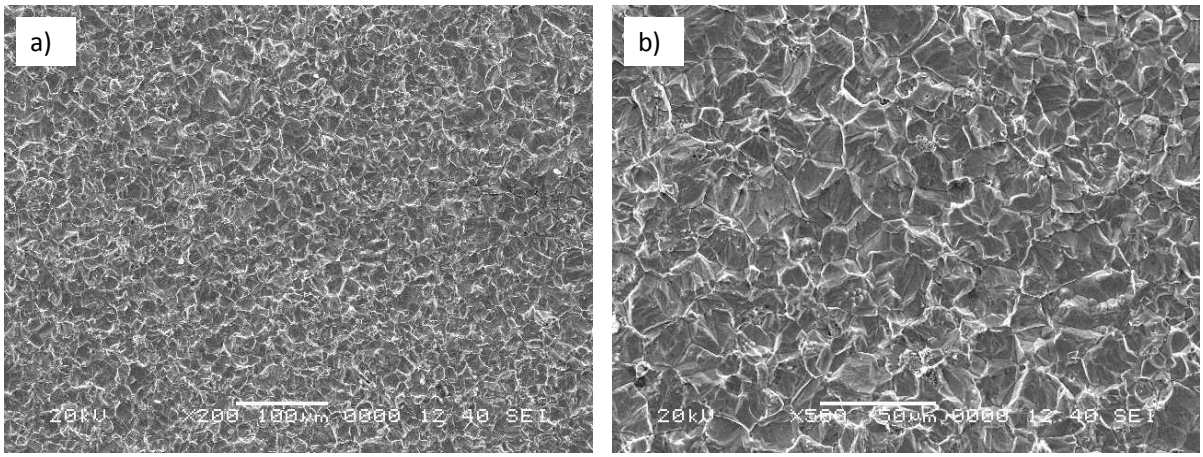

Figure 4.18 **(a) SEM micrograph of 24 h immersed stainless steel AISI 316 showing uneven morphology, (b) SEM micrograph of 24 h immersed stainless steel AISI 316 showing dimples and grooves.**

Table 4.10 and Table 4.11 show the weight loss recorded after immersion tests for carbon steel AISI 1020 and stainless steel AISI 316, respectively. From Table 4.10, it can be seen that an average weight loss of 1.3807g was recorded for AISI 1020 after 24 h which is considerably higher than the weight loss of AISI 316 (0.3593 g) for similar exposure time. Furthermore, after 48 h immersion of AISI 1020 in ferric chloride, significant increase in weight loss compared to 24 h exposure is observed. K. E. Garcia et. al [70] studied the adherent and non-adherent rust formation on carbon steel AISI 1020 after immersion in chloride solution and found that the weight of non-adherent rust that is lost during the corrosion process, initially increases with time, on the other hand, a more adherent layer of rust is formed. Hence, the increase in weight loss for AISI 1020 with time can be attributed to the loss of non-adherent layer of rust during immersion. Nevertheless, AISI 316 showed approximately 50% increase in weight loss after 48 h immersion compared to 24 h immersion in HCl saturated with ferric chloride solution.

The corrosion rates (CR) for both materials were calculated based on the weight loss method using the following equation [71]:

$$\text{CR} = \left\lfloor \frac{weight\ loss\ (g)}{surface\ area\ (mm^2) \times density(g/mm^3) \times time\ (h)} \right\rfloor \times 8760\ yr^{-1} \qquad (1)$$

The calculated corrosion rates are given in Table 4.12 and graphically illustrated in the Figure 4.19. As expected, the corrosion rates of AISI 1020 are much higher than AISI 316. Maximum corrosion rate for AISI 1020 is 102.4 mm/yr calculated after 24 h exposure to ferric chloride. In addition, AISI 316 was calculated to be 26.2 mm/yr and 19.3 mm/yr after 24 h and 48 h immersion in HCl saturated with ferric chloride, respectively. For stainless steel, the relative decrease in corrosion rate with time is due to

the formation of cation barrier at the metal surface which hinders the ion transport and hence slows down the corrosion reaction [72].

Table 4.10 **Weight loss measurements after immersion of AISI 1020 in ferric chloride, for (a) 24 h and (b) 48 h.**

a)	Carbon Steel Immersion for 24 h			
Sample no.	**Initial Mass (g)**	**Final Mass (g)**	**Mass Loss (g)**	**Mass Loss After Error Adjustment (g)**
Refernce	31.0708	31.0900	-0.0192	0.0000
1	57.1403	55.8003	1.3400	1.3592
2	50.3718	49.1448	1.2270	1.2462
3	44.5715	43.1221	1.4494	1.4686
4	42.4932	41.2003	1.2929	1.3121
5	51.1243	49.7186	1.4057	1.4249
6	55.9485	54.5148	1.4337	1.4529
7	46.3080	44.9031	1.4049	1.4241
8	52.1274	50.7893	1.3381	1.3573
Average Loss (g)			**1.3615**	**1.3807**

b)	Carbon Steel Immersion for 48 h			
Sample no.	**Initial Mass (g)**	**Final Mass (g)**	**Mass Loss (g)**	**Mass Loss After Error Adjustment (g)**
Refernce	23.7930	23.8246	-0.0316	0.0000
1	50.6627	48.2817	2.3810	2.4126
2	51.3688	48.9865	2.3823	2.4139
3	50.7290	47.9384	2.7906	2.8222
4	53.2838	50.5633	2.7205	2.7521
5	50.2301	47.8346	2.3955	2.4271
6	51.1595	48.7473	2.4122	2.4438
7	50.5525	48.0072	2.5453	2.5769
8	52.6833	50.2012	2.4821	2.5137
Average Loss (g)			**2.5137**	**2.5453**

Table 4.11 **Weight loss measurements after immersion of AISI 316 in HCl saturated with ferric chloride, for (a) 24 h and (b) 48 h.**

a)	Stainless Steel Immersion for 24 h			
Sample no.	**Initial Mass (g)**	**Final Mass (g)**	**Mass Loss (g)**	**Mass Loss After Error Adjustment (g)**
Refernce	24.9195	24.9403	-0.0208	0.0000
1	38.8716	38.4989	0.3727	0.3935
2	40.7372	40.4273	0.3099	0.3307
3	36.6236	36.2443	0.3793	0.4001
4	31.5759	31.2284	0.3475	0.3683
5	34.0805	33.7778	0.3027	0.3235
6	33.9534	33.6344	0.3190	0.3398
7	35.9015	35.5727	0.3288	0.3496
8	35.7022	35.3734	0.3288	0.3496
Average Loss (g)			**0.3385**	**0.3593**

b)	Stainless Steel Immersion for 48 h			
Sample no.	**Initial Mass (g)**	**Final Mass (g)**	**Mass Loss (g)**	**Mass Loss After Error Adjustment (g)**
Refernce	24.9446	24.9780	-0.0334	0.0000
1	47.5692	47.0931	0.4761	0.5095
2	48.5816	48.1260	0.4556	0.4890
3	40.4552	39.8671	0.5881	0.6215
4	38.3169	37.7669	0.5500	0.5834
5	42.5615	42.1114	0.4501	0.4835
6	38.7510	38.3046	0.4464	0.4798
7	37.5368	37.0494	0.4874	0.5208
8	33.4255	32.8875	0.5380	0.5714
Average Loss (g)			**0.4944**	**0.5278**

Table 4.12 **Weight loss and corrosion rate values for carbon steel AISI 1020 and stainless steel AISI 316 after 24 h and 48 h immersion**

Material	Exposed Area (mm3)	Density (g/mm3)	Time (h)	Weight Loss (g)	Corrosion Rate (mm/yr)
AISI 1020	625	0.00787	24	1.3807	102.4
AISI 316	625	0.00800	24	0.3593	26.2
AISI 1020	625	0.00787	48	2.5435	94.4
AISI 316	625	0.008	48	0.5278	19.3

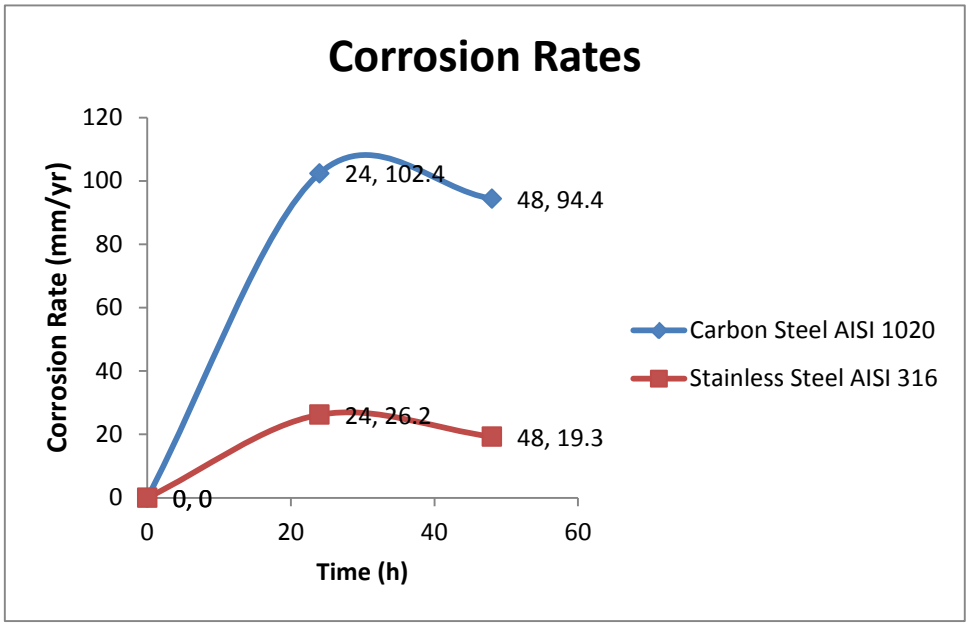

Figure 4.19 **Graph of instantaneous corrosion rate values for AISI 1020 and AISI 316**

4.2.2 Corrosion Enhanced Erosion

Corroded specimens were subjected to solid particle erosion, thus the enhancement in erosion rates due corrosion were analyzed by comparing the corrosion enhanced erosion rates against pure erosion rates (erosion on polished specimens). Erosion tests were carried out at particle velocity of 30 m/s and 60 m/s. At each impact velocity, six impact angles from 15° to 90° were used.

Figure 4.20 (a) and (b) shows the erosion rates comparison for corroded and polished stainless steel AISI 316 specimen. Figure 4.21 (a) and (b) shows the comparison between pure erosion and corrosion enhanced erosion of carbon steel AISI 1020 at velocity of 30 m/s and 60 m/s, respectively. In both cases, polished and corroded specimens follow ductile erosion behavior with peak erosion rates within 15°-30° impact angles. No significant increase in erosion rate is observed in stainless steel, however, the erosion rates for corroded specimens is slightly on the higher side as compared to the erosion rates of un-corroded specimens. On the other hand, substantial increase in erosion rates for the corroded carbon steel AISI 1020 is observed.

Stainless Steel AISI 316

Velocity (m/s)	Angle (°)	Erosion Rate Corr for 48h (mg/g)	Erosion Rate Corr for 24h (mg/g)	Erosion Rate Uncorr (mg/g)
30	0	0.000	0.000	0.000
30	15	0.045	0.044	0.039
30	30	0.045	0.041	0.039
30	45	0.037	0.040	0.038
30	60	0.034	0.036	0.033
30	75	0.030	0.030	0.026
30	90	0.028	0.030	0.025

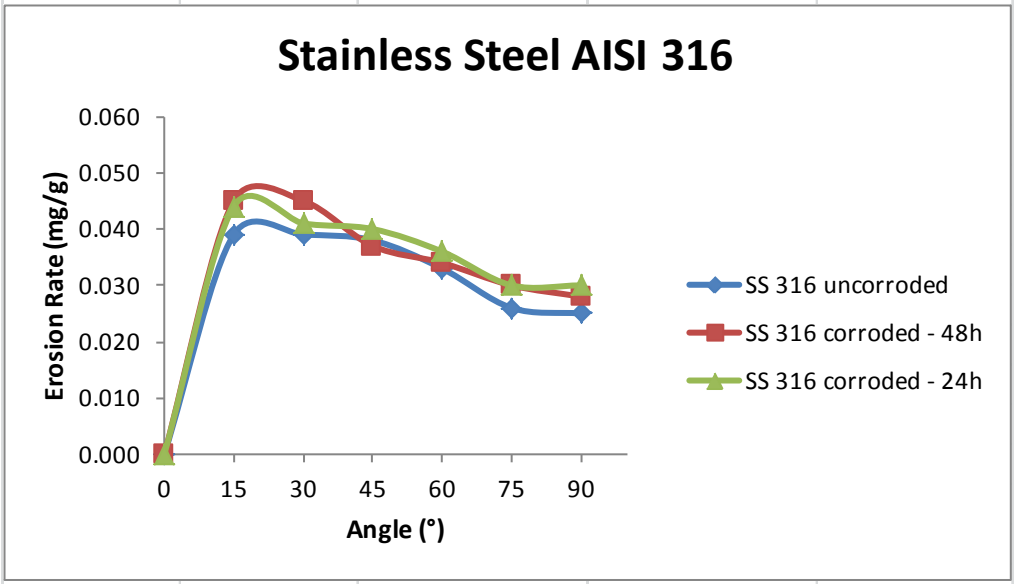

Figure 4.20 (a) Corrosion enhanced erosion and pure erosion comparison of stainless steel AISI 316 at velocity of 30 m/s

Stainless Steel AISI 316

Velocity (m/s)	Angle (°)	Erosion Rate Corr for 48h (mg/g)	Erosion Rate Corr for 24h (mg/g)	Erosion Rate Uncorr (mg/g)
60	0	0.000	0.000	0.000
60	15	0.097	0.095	0.097
60	30	0.092	0.090	0.085
60	45	0.081	0.075	0.079
60	60	0.069	0.072	0.070
60	75	0.062	0.058	0.053
60	90	0.060	0.055	0.057

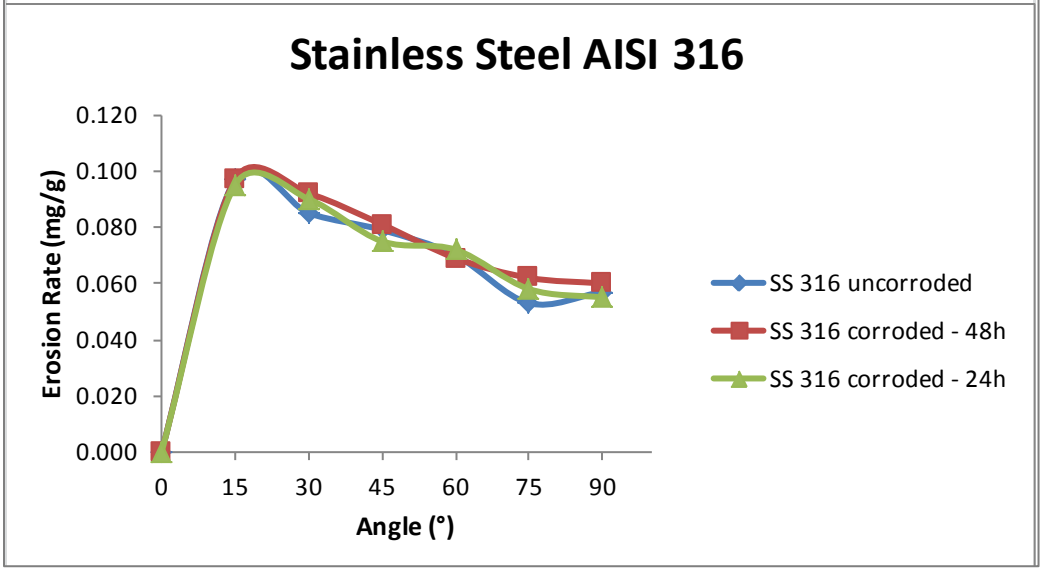

Figure 4.20 (b) Corrosion enhanced erosion and pure erosion comparison of stainless steel AISI 316 at velocity of 60 m/s

Carbon Steel AISI 1020

Velocity (m/s)	Angle (°)	Erosion Rate Corr for 48h (mg/g)	Erosion Rate Corr for 24h (mg/g)	Erosion Rate Uncorr (mg/g)
30	0	0.000	0.000	0.000
30	15	0.056	0.072	0.042
30	30	0.054	0.062	0.046
30	45	0.046	0.056	0.041
30	60	0.040	0.054	0.035
30	75	0.034	0.052	0.030
30	90	0.030	0.044	0.027

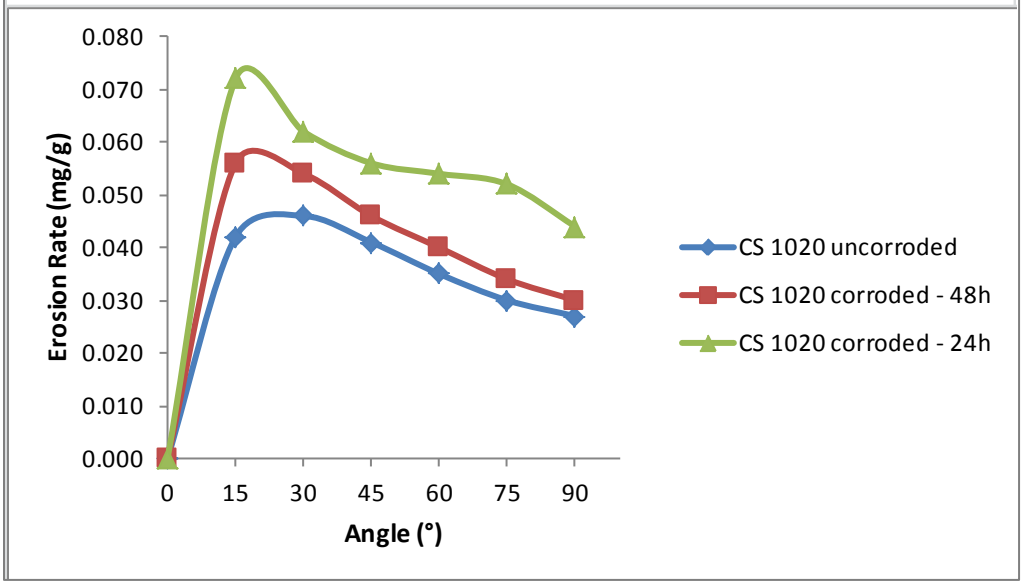

Figure 4.21 **(a) Corrosion enhanced erosion and pure erosion comparison of carbon steel AISI 1020 at velocity of 30 m/s**

Carbon Steel AISI 1020

Velocity (m/s)	Angle (°)	Erosion Rate Corr for 48h (mg/g)	Erosion Rate Corr for 24h (mg/g)	Erosion Rate Uncorr (mg/g)
60	0	0.000	0.000	0.000
60	15	0.088	0.128	0.081
60	30	0.092	0.114	0.086
60	45	0.084	0.108	0.074
60	60	0.078	0.096	0.065
60	75	0.072	0.082	0.058
60	90	0.060	0.078	0.049

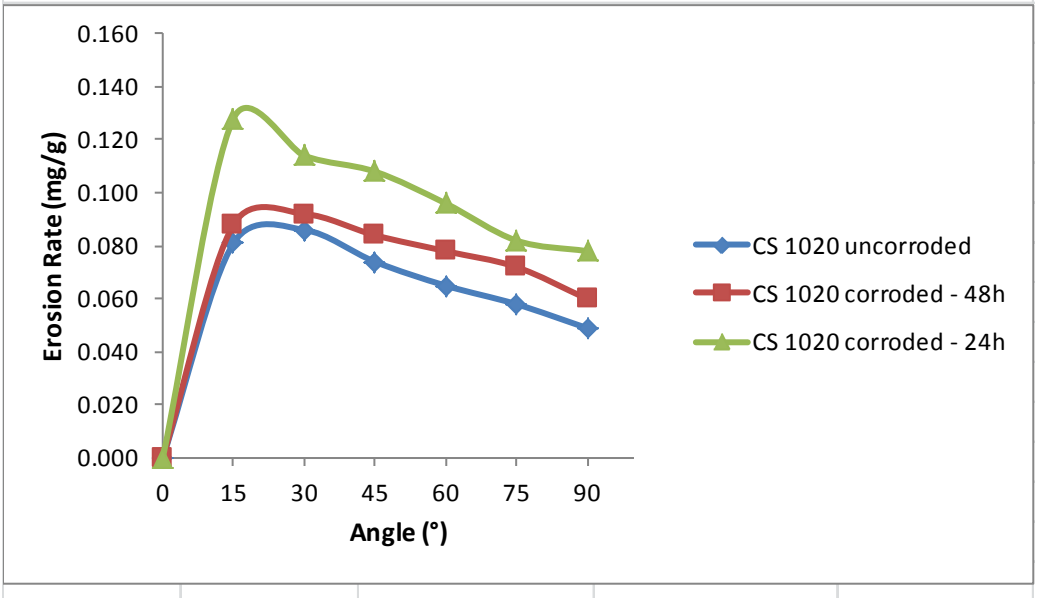

Figure 4.21 (b) Corrosion enhanced erosion and pure erosion comparison of carbon steel AISI 1020 at velocity of 60 m/s.

Table 4.13 reveals the average of surface roughness measured on various corroded and polished specimens. There is a drastic increase in surface roughness of AISI 1020 from 0.32 µm (polished surface) to 9.53 µm (24h immersed specimens). Surface degradation in carbon steel is mainly due to its inability to form a protective adherent passive layer [73]. Consequently, a combination of adherent and non-adherent rust is formed which contributes to the surface roughness. The formation of asperities and loosely bound corrosion products are the main factors which are increasing the erosion rate of AISI 1020 after the corrosion.

In case of stainless steel AISI 316, there is only a marginal increase in surface roughness from 0.31 µm (polished surface) to 1.56 µm (24h immersed specimens). This is attributed to the protective chromium oxide layer on stainless steel 316 which protects the material against corrosion. However, the mirror finish of the stainless steel surface is diminished due to local breakdown of passive layer, after exposure to corrosive solution. Hence, the difference in the corrosion enhanced erosion characteristics of carbon steel and stainless steel can be attributed to the surface roughness and loosely adherent rust on carbon steel surface.

Table 4.13 **Surface Roughness (Ra, µm) for polished and corroded carbon steel AISI 1020 and stainless steel AISI 316 immersed for 24 h.**

Surface Roughness for 24h immersed specimens				
#	Carbon Steel 1020 Corroded	Carbon Steel 1020 Uncorroded	Stainless Steel 316 Corroded	Stainless Steel 316 Uncorroded
1	9.42	0.24	1.74	0.42
2	6.60	0.26	1.70	0.96
3	7.72	0.36	1.52	0.12
4	9.62	0.24	1.86	0.24
5	9.82	0.22	1.80	0.10
6	8.66	0.26	1.42	0.38
7	13.92	0.66	1.16	0.20
8	11.02	0.18	1.68	0.26
9	8.95	0.38	1.16	0.28
10	9.55	0.40	1.60	0.18
Average	**9.53**	**0.32**	**1.56**	**0.31**

Another important observation for carbon steel AISI 1020 is the maximum erosion rate for specimens immersed for 24 h whereas the erosion rate for 48 h immersed specimens is found to be in between polished and 24 h immersed specimens. This phenomenon was contradicting the expectation of increased erosion rate with an increase in immersion time. However, a direct relationship between the effect of immersion time and subsequent enhancement in erosion rate cannot be established for the given data at this stage, because erosion rate is more dependent on the material properties such as hardness [68], ductility [5], strength and surface roughness. Whereas, the time of immersion mainly results in mass loss which correlates to corrosion rate but in most cases the surface conditions (hardness and surface roughness after corrosion) also varies considerably with time. Hence, to understand the change in surface conditions of the specimens with immersion time and its subsequent effect on erosion rates; a series of immersion tests at different times were carried out for carbon steel AISI 1020 in ferric chloride solution. Table 4.14 and Figure 14.22 shows the variation in corrosion rates for carbon steel with time. A bar graph illustrating the increase in mass loss with time is given in Figure 14.23.

Table 4.14 Mass loss and corresponding corrosion rates for carbon steel AISI 1020 immersed for 12h, 24h, 36h, 48h and 60h. With 0h representing the polished specimen

Immersion Time (h)	0	12	24	36	48	60
Mass Loss (g)	0	0.72	1.34	1.95	2.57	2.74
Density (g/mm3)	7.87x10E-3	7.87x10E-3	7.87x10E-3	7.87x10E-3	7.87x10E-3	7.87x10E-3
Exposed Area (mm2)	625	625	625	625	625	625
Corrosion Rate (mm/yr)	0	106.8	99.4	96.5	95.4	81.3

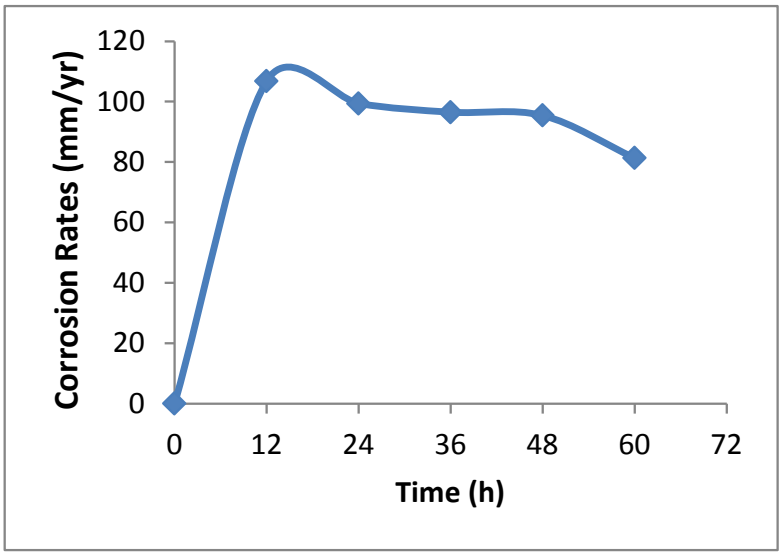

Figure 4.22 **Corrosion rates variation for carbon steel AISI 1020 with time.**

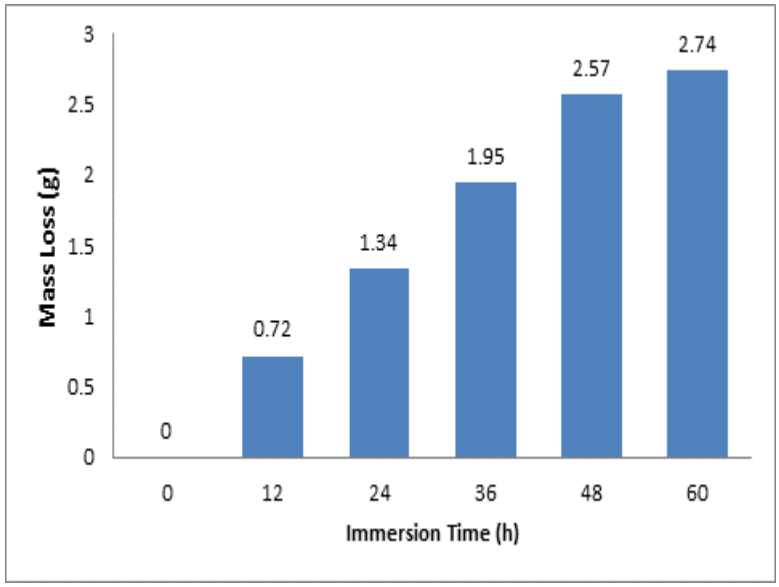

Figure 4.23 **Mass loss (g) of carbon steel AISI 1020 after immersion in ferric chloride solution for 12h, 24h, 36h, 48h and 60h.**

It is clear from the data that as the time increase the mass loss increases but the corrosion rate decreases. For 12 h immersion the corrosion rate is highest due aggressive oxidation attack on bare metal surface. However, as the immersion time is increased the rate stabilizes and then decreases again pertaining to the formation of more adherent rust which retards further corrosion attack.

Figure 4.24 shows the result of erosion tests carried on these immersed specimens. Erosion tests were carried out at a single impact angle of 90° and an impact velocity of 60 m/s. It can be seen from the figure that the erosion rate varies with immersion time. Nevertheless, the specimen immersed for 24h persistently showed highest erosion rate as compared to other corroded specimens. The variation in erosion rate is directly related to the surface condition. Hence, to correlate the erosion rate with the surface conditions, two important parameters Vickers hardness and surface roughness of the corroded specimens was measured (procedure explained in experimental methods section). An overlay of hardness and erosion rates for corroded specimens is given in the double axis graph shown in Figure 4.25 (values listed in Table 4.15 and Table 4.16). Surprisingly, the variation in erosion rate directly corresponds to the surface hardness of the corroded specimens. The increase in erosion rate with hardness relates to the inability of harder surface to absorb the kinetic energy of the impacting solid particles [16]. A similar conclusion was reached in our previous work where aluminum 6060-T4 alloy having lower hardness compared to steels, exhibited higher erosion resistance [74].

Table 4.15 **Vickers hardness measured at the cross section surface of the corroded specimens.**

Time (h)	Vickers Hardness					Average
0	240.95	233.83	236.69	235.45	237.39	236.86
12	274.62	364.74	292.17	282.81	336.89	310.25
24	279.06	362.44	346.02	355.59	328.18	334.26
36	286.22	258.08	260.33	211.4	276.05	258.42
48	268.89	246.31	261.85	239.74	256.11	254.58
60	226.93	311.96	269.4	250.4	308.29	273.40

Table 4.16 **Variation of erosion rate (mg/g) with immersion time (h)**

Velocity (m/s)	Angle (°)	Immersion Time (h)	Erosion Rate (mg/g)
60	90	0	0.049
60	90	12	0.074
60	90	24	0.082
60	90	36	0.070
60	90	48	0.066
60	90	60	0.068

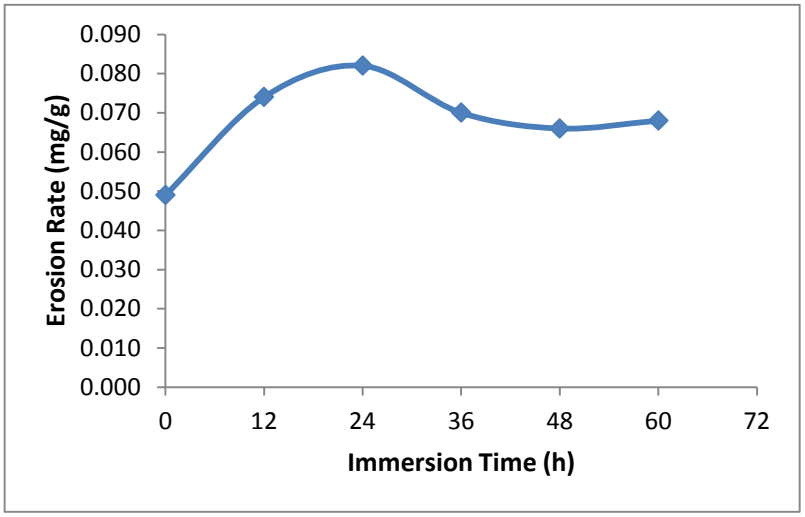

Figure 4.24 **Variation in erosion rate (mg/g) with immersion time (h) for carbon steel AISI 1020**

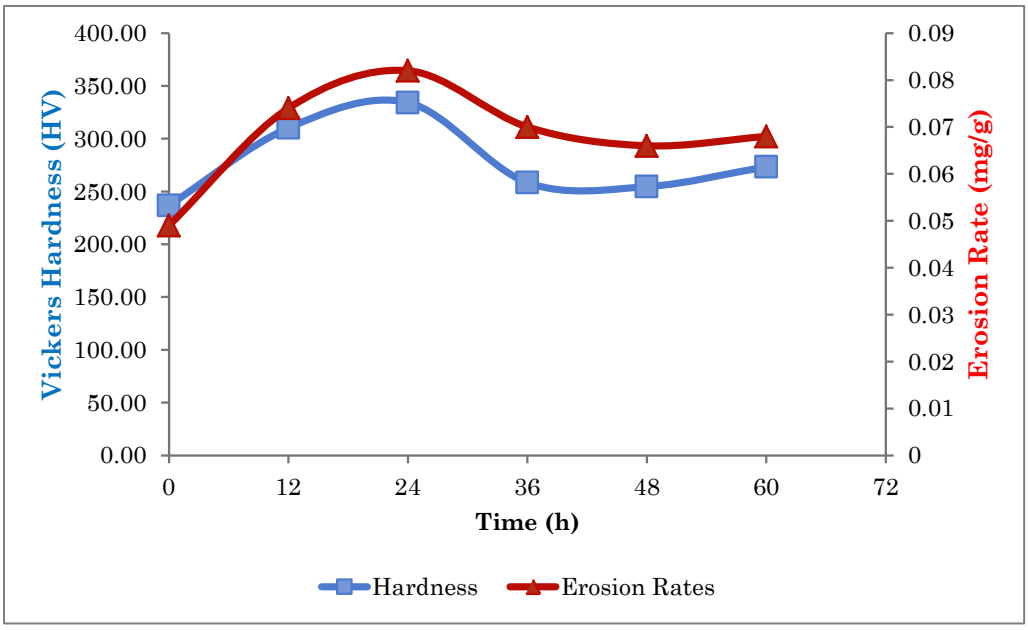

Figure 4.25 **An overlay of erosion rate and Vickers hardness values for different immersion times.**

Similarly, the measured surface roughness (Ra, µm) values and erosion rates were superimposed. Figure 4.26 (values in Table 4.17) clearly shows the variation of erosion rates with surface roughness in a similar fashion as the Vickers hardness. Surface roughness of the target materials plays a vital role and can affect the erosion process of the target material [75]. Both, surface roughness and hardness contributed to the variation in the erosion rates. However, it cannot be quantitatively established that which of the two parameters has strongly influenced the erosion rates as both parameters were affected simultaneously during the corrosion process.

Table 4.17 Surface roughness values in Ra (µm) for carbon steel AISI 1020 after immersion at different times.

Surface Roughness - Carbon Steel AISI 1020						
Reading / Immersion Time	**0**	**12**	**24**	**36**	**48**	**60**
1	0.24	7.80	9.42	4.30	5.16	7.40
2	0.26	6.82	6.60	6.62	5.16	5.82
3	0.36	7.48	7.72	10.86	8.40	10.06
4	0.24	9.64	9.62	7.82	6.58	9.66
5	0.22	11.54	9.82	7.94	10.58	8.30
6	0.26	10.58	8.66	9.18	7.08	6.29
7	0.66	8.44	13.92	7.38	8.36	8.54
8	0.18	7.84	11.02	10.50	10.96	9.74
Average	**0.30**	**8.77**	**9.60**	**8.08**	**7.79**	**8.23**

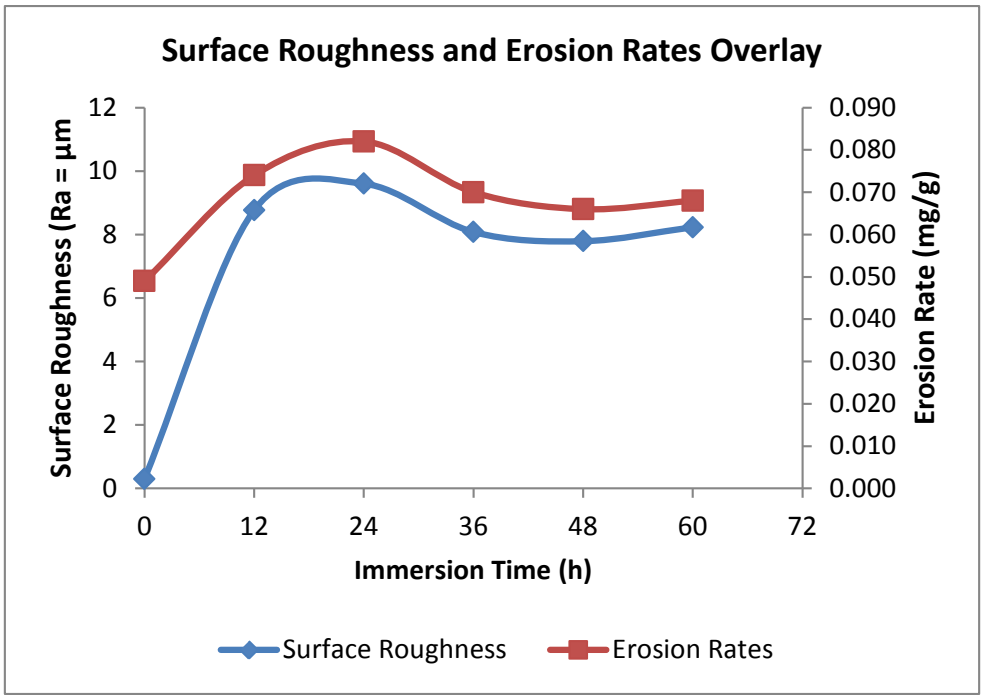

Figure 4.26 **An overlay of erosion rate and surface roughness values for different immersion times.**

X-Ray diffraction scans were carried out on carbon steel AISI 1020 (24 h and 48 h immersed specimens) in order to characterize the corrosion products and explain the possible reason for the increase in hardness and surface roughness. Figure 4.27 shows the XRD patterns for the polished, 24 h corroded and 48 h corroded carbon steel AISI 1020 specimens. The XRD patterns of the corroded samples were obtained from the rust which was scraped and collected from the corroded specimens. The fittings of the patterns were adequately done using the following components: pure Fe (F), magnetite (M), hematite (H) and another possible compound barringerite (B).

The relative decrease in intensity of the F peaks is visible from the patterns. This indicates the conversion of into oxides and other compounds after the immersion tests. Presence of M and H compounds is clearly marked on the XRD patterns of both the corroded specimens. The new peaks of rather lower intensity (abundances) in the patterns of corroded specimens are mostly characteristic of magnetite and hematite phases. Hence, the increase in the surface hardness after corrosion may be attributed to the presence of these brittle phases. In addition, another compound barringerite (Fe_2P) was seen to be in good fit with various peaks of the 24 h corroded specimen. Barringerite is brittle in nature with fine grain size and could be another reason behind the increase in hardness and subsequent erosion rate of the 24 h immersed specimens.

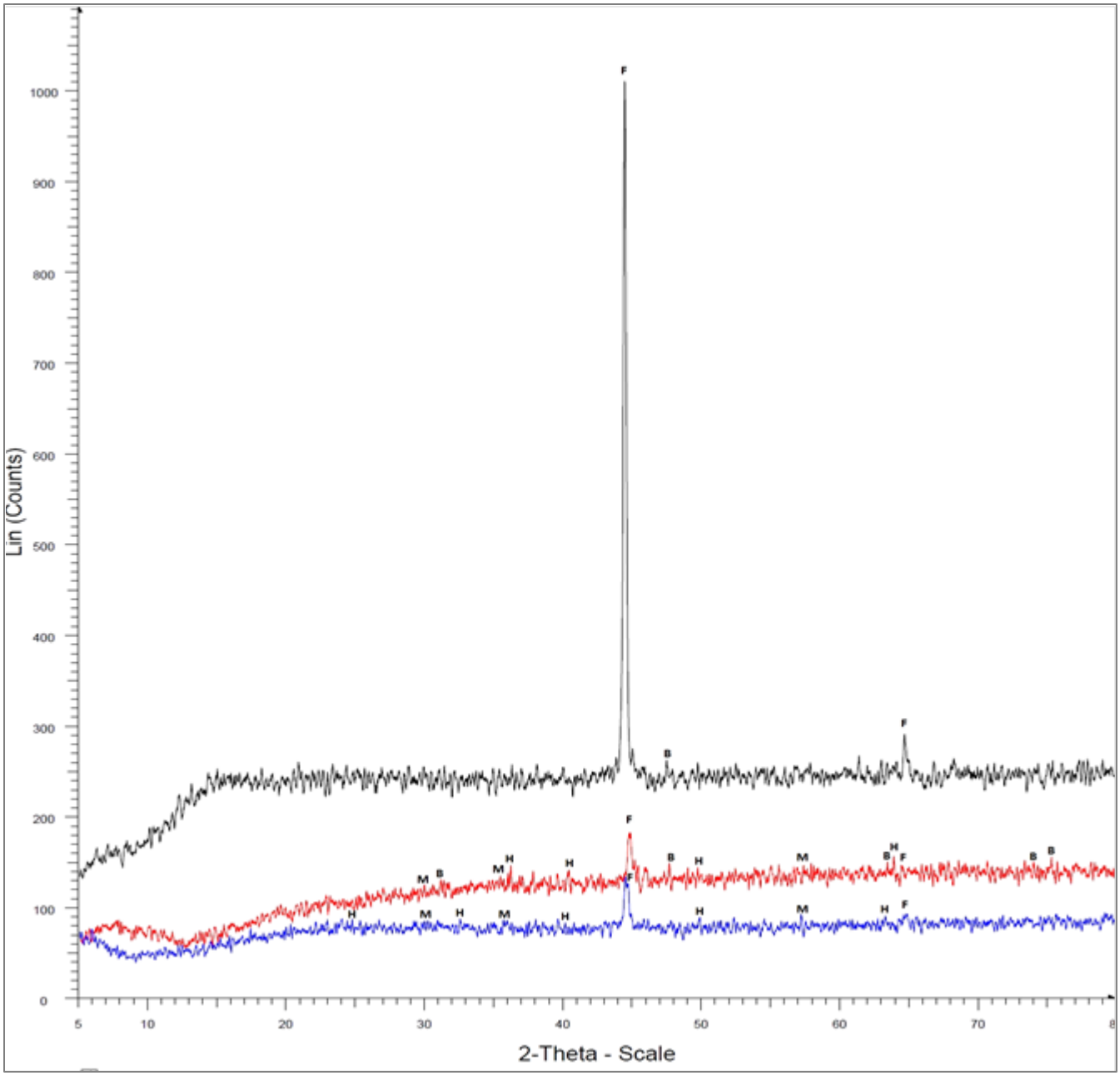

Figure 4.27 **XRD patterns of polished (top curve), 24h corroded (middle curve) and 48h corroded (bottom curve). Peaks labeling: magnetite (M), hematite (H), barringerite (B) and iron (F).**

4.2.3 Effect of Impact Velocity on Erosion Rate

The increase in erosion rate with an increase in velocity is as expected. From 30m/s to 60 m/s, the erosion rate of AISI 1020 immersed for 24 h, increased from 0.072 mg/g to 0.128 mg/g at an impact angle of 15°. This is due to the increase in particle kinetic energy with increase in flow velocity resulting in higher shear stresses which in turn causes more mass loss [65]. Furthermore, it can be seen that the erosion behavior with respect to impact angle is independent of the velocity, similar observation has been reported by other authors previously [32][66]. This indicates that the increase in erosion rate with particle velocity is strongly dependent on eroding particles kinetics rather than on material properties.

4.2.4 Effect of Impact Angle on Erosion Rate

Ductile and brittle materials exhibit different erosion rates with respect to impact angle. Finnie and Sheldon [64] observed that ductile materials generally show maximum erosion rates in the range of 15°-30° impact angle while brittle materials show maximum erosion rate at normal angle. Similarly, Oka et al. [32] in their erosion rate study of various metals, a plastic and a ceramic showed that the shape of the erosion curves with respect to impact angle depends on material hardness. In addition, the maximum erosion rate at any given angle was associated with high shear forces incurred on the surface and the ability of the material to resist them. Consequently, materials with high hardness such as ceramics resist material removal at oblique angles while metals being more ductile are prone to shear forces therefore erodes more at oblique angles compared to 90° angle.

Furthermore, Shewmon et al. [17] explained that the high mass loss for ductile metals at oblique angles is due to lip formation by effective penetration of the incident particles.

These extruded lips are then sheared off by subsequent impacts whereas at normal incident angle the ductile metals absorb most of the kinetic energy of incoming particles resulting in lower mass loss.

Figure 4.14 (a-b) and Figure 4.15 (a-b) also shows the effect of impact angle on the erosion rate for carbon steel AISI 1020 and stainless steel AISI 316, respectively. It is clear from the figures that the maximum erosion rates occur between 15°-30° impact angle. Accordingly, both the steels are showing ductile erosion behavior.

4.2.5 Pure Erosion Mechanism

It is clear from the erosion rate dependence on impact angle that all four materials are following ductile erosion behavior. To understand this ductile erosion mechanism, scanning electron microscopy was carried out. Figure 4.28 (a) and (b) shows SEM images of stainless steel 316 eroded at impact angle of 15° and 90°, respectively. From Figure 4.28 (a), severe material degradation caused by extrusion/ploughing action can be seen. Indications of material removal such as deformation scratches are also clearly visible. Conversely, the damage at normal angle as shown in Figure 4.28 (b) is much less severe with no deformation scratches, however, crates and pits are visible indicating that most of the kinetic energy of incident particles is dissipated in deforming/displacing the material rather than actual material removal.

Similarly, Fig. 4.29 (a) and (b) shows the eroded surfaces of carbon steel 1020 at particle velocity of 60 m/s, again, at the impact angle of 15° more wear damage is observed compared to 90°. Deformation scratches and lip formation due to plastic deformation by extrustion/ploughing action can be seen, which is consistent with the findings of other

authors [5][17][69]. At 90° impact angle, the ductile erosion behavior in carbon steel AISI 1020 is characterized by dimples, pits and crater morphologies (Fig. 4.29 (b)) which is generally observed in ductile metals at normal impacts [7].

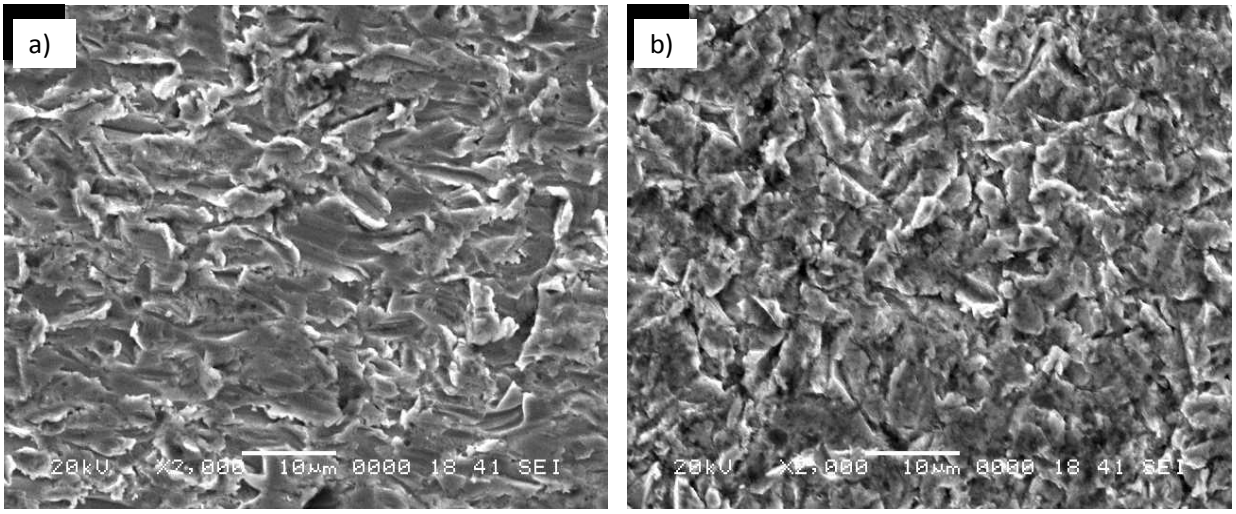

Figure 4.28 **Stainless Steel 316 eroded Surface at impact angle a) 15° and b) 90°**

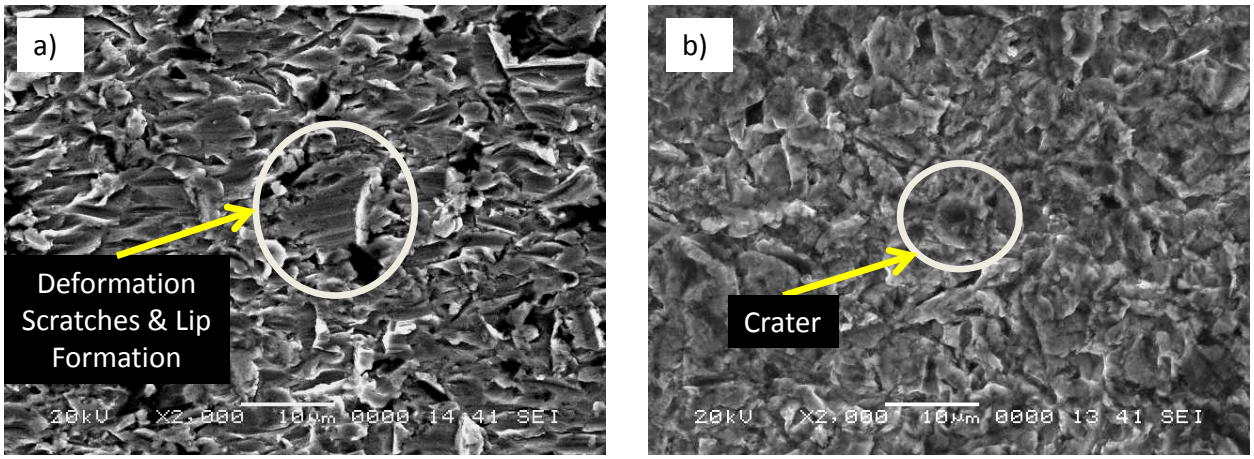

Figure 4.29 **Carbon Steel AISI 1020 eroded surface at impact angle a) 15° and b) 90°**

4.2.6 Corrosion Enhanced Erosion Mechanism

Scanning electron microscopy of polished, corroded (24h and 48h), eroded and eroded + corroded (24h and 48h) carbon steel AISI 1020 specimens was carried out to study the corrosion-enhanced erosion mechanism. Figure 4.30 (a-d) shows the comparison of the above mentioned four specimens' stages at 24h, while Figure 4.31 (a-d) compares the specimens immersed for 48h. Images reveal severe surface degradation on corroded carbon steel surface exposed to erosion test at an impact angle of 15° and velocity of 60 m/s. Evidence of heavy plastic deformation by extrusion and forging is clearly visible. Moreover, material cutting, shredding and localized fractures are also dominant during corrosion enhanced erosion of AISI 1020. Extruded lip morphologies, which were observed in pure erosion of AISI 1020, are replaced with fracture induced flattened platelets on corrosion enhanced eroded surface; similar observation was made by Md. Aminul Islam et al. [53] in their study of corrosion enhanced erosion of API X- 70 pipeline steel. The contrasting erosion mechanism on corroded carbon steel compared to pure erosion mechanism is instigated by the presence of porous and brittle oxide products formed on the carbon steel surface after immersion in ferric chloride solution. The brittle nature of the oxide film makes the specimen vulnerable to erosion attack under subsequent aluminum oxide particle impacts. As a result, increase in erosion rates is observed in the corroded surface with some evidence of metal cuts and platelet fractures.

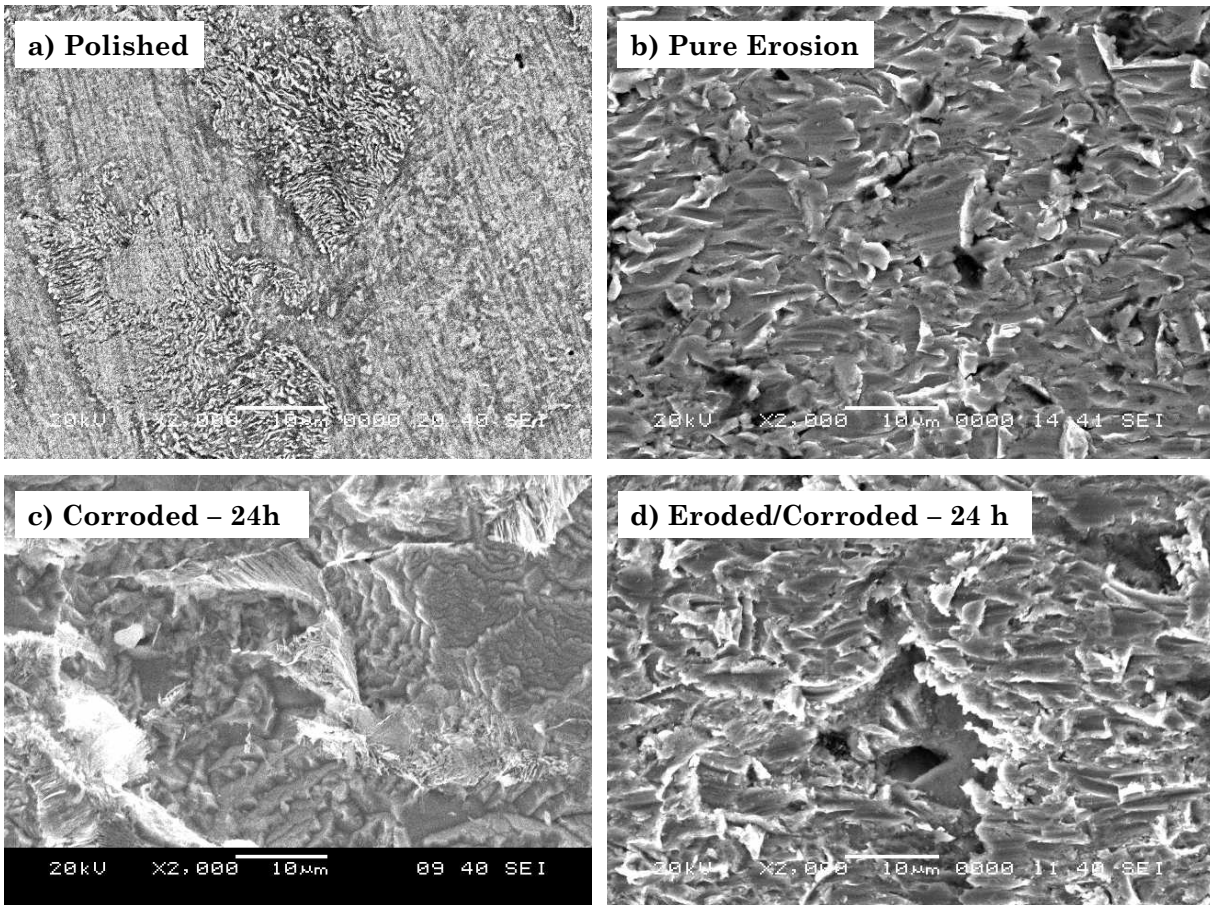

Figure 4.30 **Carbon Steel AISI 1020 a) Polished, b) Eroded (impact angle 15°, impact velocity 60 m/s), c) After immersion for 24h, and d) Eroded-corroded (after 24 immersion and eroded at impact angle of 15° and velocity of 60 m/s).**

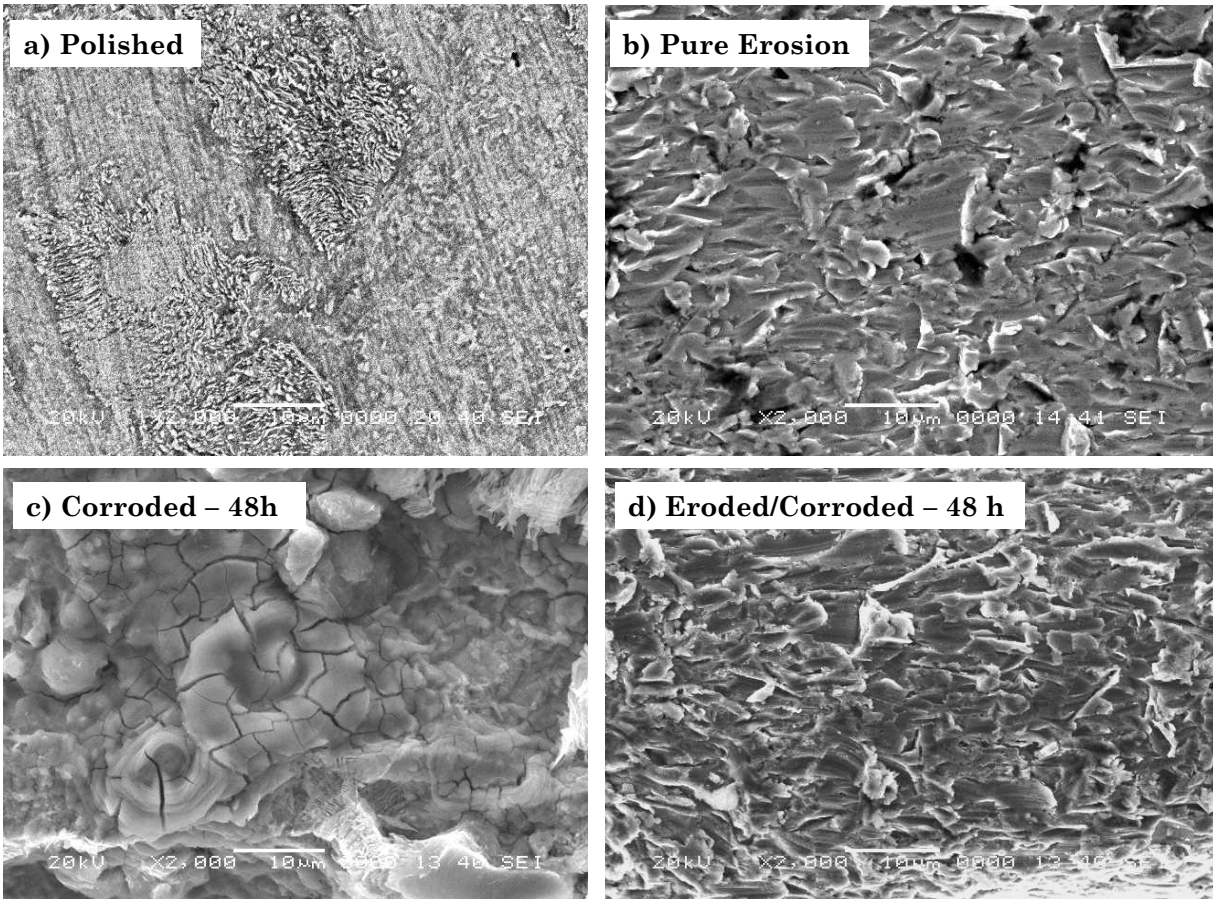

Figure 4.31 **Carbon Steel AISI 1020 a) Polished, b) Eroded (impact angle 15°, impact velocity 60 m/s), c) After immersion for 48h, and d) Eroded-corroded (after 48 immersion and eroded at impact angle of 15° and velocity of 60 m/s).**

In contrast to carbon steel AISI 1020, stainless steel AISI 316 is much less susceptible to corrosion-enhanced erosion. Figure 4.32 (a) and (b) compares the corroded and eroded-corroded (24h immersion) surface of AISI 316. Extensive plastic deformation by extrusion and forging is seen, unlike AISI 1020, no platelet fractures are visible. However, extruded lip morphologies as seen in un-corroded AISI 316 still persists. This proves that stainless steel maintains enough ductility even after corrosion, thus resisting fracture marks and metal cuts by absorbing the kinetic energy of the incident alumina particles [16]. Similar erosion mechanism observations were made on polished and 48h immersed specimens.

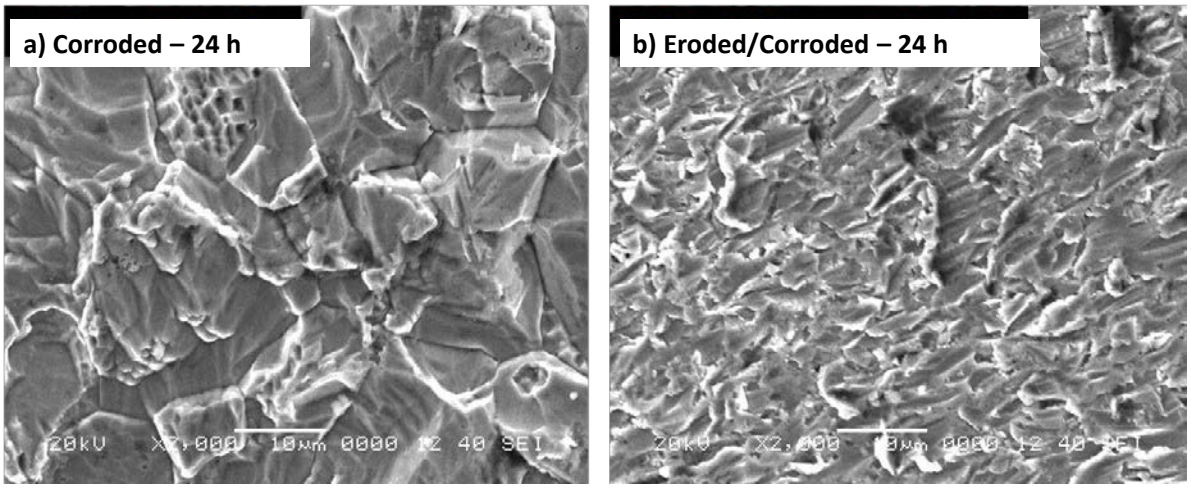

Figure 4.32 Stainless Steel AISI 316 a) After immersion for 24h, and b) Eroded-corroded (after 24 immersion and eroded at impact angle of 15° and velocity of 60 m/s).

CHAPTER 5

CONCLUSIONS AND FUTURE RECOMMENDATIONS

5.1 Conclusions: Pure Erosion Experiments

Experiments were carried out to investigate the solid particle erosion characteristics of AISI 310S, AISI 316, AISI 1020 and aluminum 6060-T4. Angular alumina erodent with 50 μm average particle size was used as an erodent and the erosion measurements were conducted for six different impingement angles ranging from 15° to 90° in steps of 15°, using three different impact velocities (30 m/s, 60 m/s and 100 m/s) at each angle. Based on the obtained results, the following conclusions can be drawn:

1) Comparisons of erosion behavior between steels and aluminum 6060-T4 alloy have shown that the increase in erosion rate is directly proportional to bulk hardness. Aluminum 6060-T4 showed maximum erosion resistance compared to steels at all velocities. This attributes to the lower hardness and sufficient ductility, which prevents mass loss by dissipating solid particle kinetic energy in the form of heat and plastic deformation.

2) SEM analyses of the eroded surfaces have shown ductile erosion mechanisms in all four metals. Various morphologies such as extrusion/ploughing, deformation scratches, lip formation, dimples and pits were observed in steels. However, for aluminum 6060-T4, eroded surface was characterized by formation of flakes and

distressed platelets. Also, at lower magnification, wavy texture was observed which further substantiates the ability of aluminum 6060-T4 to resist erosion.

3) The increase in erosion rate with the increase of particle impact velocity for all four alloys has shown that the effect of velocity on erosion rate is independent of material properties.

4) All four alloys showed ductile erosion behavior with the peak erosion rate in the range between 15° to 30° impact angle. Furthermore, the effect of impact angle on erosion rate was found to be independent of velocity.

5.2 Conclusions: Corrosion-Enhanced Erosion Experiments

Experiments were carried out to investigate the corrosion enhanced erosion behavior of stainless steel AISI 316 and carbon steel AISI 1020. Specimens were immersed in corrosive solution for 24 h and 48 h. Both, corroded and polished specimens were then subjected to erosion at six different impingement angles 15°, 30°, 45°, 60°, 75° and 90°, using two different impact velocities (30 m/s and 60 m/s) at each angle. Additionally, corrosion and corrosion-enhanced erosion of Carbon Steel AISI 1020 was analyzed after various immersion times. Based on the obtained results, the following conclusions can be drawn:

1. Immersion of carbon steel 1020 in 6% ferric chloride solution for 24 h, led to the formation of brittle oxide compound, whereas stainless steel 316 relatively resisted corrosion attack in HCl saturated with ferric chloride solution due to protective passive layer.

2. Significant increase in erosion was observed for corroded carbon steel 1020 which is attributed to the hard, brittle and porous corrosion products (characterized using SEM and XRD) after immersion in ferric chloride solution. However, stainless steel 316 was found to be less susceptible to corrosion-enhanced erosion due to its passive nature.

3. Analysis of surface conditions for carbon steel AISI 1020 after different immersion time revealed that the variation in erosion rate of the corroded samples is directly related to surface roughness and hardness.

4. An increase in erosion rate with increase in velocity was observed for carbon steel AISI 1020 and stainless steel AISI 316. This is attributed to the increase in particle kinetic energy with an increase in particle flow velocity resulting in higher shear stresses which causes more mass loss.

5. SEM revealed evidence of material cutting, shredding and localized fracture in eroded-corroded AISI 1020. Extensive plastic deformation by extrusion and forging is observed in AISI 316 but without any evidence of fracture marks.

5.3 Future Recommendations

In this thesis, detailed experimentation and discussions have been provided to substantiate the higher erosion resistance of aluminum 6060-T4 and corrosion-enhanced erosion phenomenon of carbon steel AISI 1020. However, in order to take this work a step further and fully understand the erosion behavior of aluminum alloys and corrosion mechanism of carbon steel, following recommendation are made:

1. Solid particle erosion comparison between various aluminum alloys to understand the effect of heat treatments and alloys additions on the erosion behavior of Al.

2. In-situ characterization of scales and corrosion products formed on carbon steel during immersion can give us real-time information about the mechanism of corrosion.

3. In the present study, SEM and Starret surface roughness tester were used to study the surface degradation. However, for in-depth surface analysis, AFM can be employed to study the damage incurred after corrosion and erosion.

4. Predictive models for corrosion-induced erosion phenomenon are rarely found in the literature. Hence, it is suggested to develop a corrosion-enhanced erosion model which would incorporate surface roughness, hardness, pH, and immersion time. The model can be partly validated by using the corrosion-enhanced erosion experimental results provided in this thesis.

REFERENCES

[1] A. V Levy, “Solid particle erosion and erosion-corrosion of materials,” *ASTM Int.*, 1995.

[2] P. R. Roberge, *Corrosion Testing Made Easy: Erosion-Corrosion*. NACE International, 2004.

[3] H. Badr, M. Habib, R. Ben-Mansour, and S. A. . Said, “Effect of flow velocity and particle size on erosion in a pipe with sudden contraction,” *6th Saudi Eng. Conf.*, vol. 5, no. December, 2002.

[4] I. Finnie, “Erosion of surfaces by solid particles,” *Wear*, vol. 3, pp. 87–103, 1960.

[5] A. V Levy, “The platelet mechanism of erosion of ductile metals,” *Wear*, vol. 108, no. 1, pp. 1–21, Mar. 1986.

[6] G. Sheldon and A. Kanhere, “An investigation of impingement erosion using single particles,” *Wear*, vol. 21, 1972.

[7] J. R. Laguna-Camacho, A. Marquina-Chávez, J. V. Méndez-Méndez, M. Vite-Torres, and E. a. Gallardo-Hernández, “Solid particle erosion of AISI 304, 316 and 420 stainless steels,” *Wear*, Jan. 2013.

[8] G. Zambelli and A. V. Levy, “Particulate erosion of NiO scales,” *Wear*, vol. 68, no. 3, pp. 305–331, May 1981.

[9] R. E. Winter and I. M. Hutchings, “The role of adiabatic shear in solid particle erosion,” *Wear*, vol. 34, no. 2, pp. 141–148, Sep. 1975.

[10] R. Brown and J. W. Edington, “The melting of metal targets during erosion by hard particles,” *Wear*, vol. 71, no. 1, pp. 113–118, Sep. 1981.

[11] T. Christman and P. G. Shewmon, “Adiabatic shear localization and erosion of strong aluminum alloys,” *Wear*, vol. 54, no. 1, pp. 145–155, May 1979.

[12] J. Salik, D. Buckley, and W. A. Brainard, “The effect of mechanical surface and heat treatments on the erosion resistance of 6061 Aluminum Alloy,” *Wear*, vol. 65, pp. 351–358, 1981.

[13] G. Sundararajan, “The differential effect of the hardness of metallic materials on their erosion and abrasion resistance,” *Wear*, vol. 162464, pp. 773–781, 1993.

[14] H. C. Laura P, McCabe, Gordon A. Sargebt, “Effect of microstructure on the erosion of steels by solid particles,” *Wear*, vol. 105, pp. 257–277, 1985.

[15] A. V Levy and W. Buqian, “Erosion of hard material coating systems,” *Wear*, vol. 121, no. 3, pp. 325–346, Feb. 1988.

[16] T. Foley and a. Levy, “The erosion of heat-treated steels,” *Wear*, vol. 91, no. 1, pp. 45–64, Oct. 1983.

[17] L. E. K. Hein and P. G. Shewmon, “Effects of hardness on the solid particle mechanisms in AISI 1060 steel,” *Wear*, vol. 89, pp. 291–302, 1983.

[18] G. Green, R. Taggart, and D. Polonis, “Influence of microstructure on the erosion of plain carbon steels,” *Metallography*, vol. 212, pp. 191–212, 1981.

[19] T. Singh, S. N. Tiwarib, and G. Sundararajan, “Room temperature stainless steels erosion behaviour of 304 ,” *Wear*, vol. 145, pp. 77–100, 1991.

[20] G. Sundararajan, “The solid particle erosion of metallic materials: the rationalization of the influence of material variables,” *Wear*, vol. 186187, pp. 129–144, 1995.

[21] A. Ninham, “The effect of mechanical properties on erosion,” *Wear*, vol. 121, no. 3, pp. 307–324, Feb. 1988.

[22] A. V Levy and P. Chik, “The effects of erodent composition and shape on the erosion of steel,” *Wear*, vol. 89, pp. 151–162, 1983.

[23] S. Srinivasan and R. Scattergood, “Effect of erodent hardness on erosion of brittle materials,” *Wear*, vol. 128, pp. 139–152, 1988.

[24] M. Vite-Torres, J. R. Laguna-Camacho, R. E. Baldenebro-Castillo, E. a. Gallardo-Hernández, E. E. Vera-Cárdenas, and J. Vite-Torres, “Study of solid particle erosion on AISI 420 stainless steel using angular silicon carbide and steel round grit particles,” *Wear*, Feb. 2013.

[25] Z. Feng and a. Ball, “The erosion of four materials using seven erodents — towards an understanding,” *Wear*, vol. 233–235, pp. 674–684, Dec. 1999.

[26] G. Sundararajan and P. G. Shewmon, “A new model for the erosion incidence of metals at normal,” *Wear*, vol. 84, pp. 237–258, 1983.

[27] G. Sundararajan, “A comprehensive model for the solid particle erosion of ductile materials,” *Wear*, vol. 149, pp. 111–127, 1991.

[28] I. M. Hutchings, “A model for the erosion of metals particles at normal incidence by spherical,” vol. 70, pp. 269–281, 1981.

[29] I. M. Hutchings, *Tribology: friction and wear of engineering materials SE - Metallurgy and materials science*. Edward Arnold, 1992.

[30] Y. I. Oka, K. Okamura, and T. Yoshida, “Practical estimation of erosion damage caused by solid particle impact,” *Wear*, vol. 259, no. 1–6, pp. 95–101, Jul. 2005.

[31] C.-K. Fang and T. . Chuang, “Surface morphologies and erosion rates of metallic building materials after sandblasting,” *Wear*, vol. 230, no. 2, pp. 156–164, May 1999.

[32] Y. I. Oka, H. Ohnogi, T. Hosokawa, and M. Matsumura, “The Impact Angle Dependence of Erosion Damage caused by Solid Particle Impact,” *Wear*, vol. 203–204, pp. 573–579, 1997.

[33] A. P. Harsha and D. K. Bhaskar, “Solid particle erosion behaviour of ferrous and non-ferrous materials and correlation of erosion data with erosion models,” *Mater. Des.*, vol. 29, no. 9, pp. 1745–1754, Oct. 2008.

[34] J. Laguna-Camacho, “Solid Particle Erosion on Different Metallic Materials,” in *Tribology in Engineering*, 2013, pp. 63–77.

[35] M. Matsumura, “Erosion–corrosion of metallic materials in slurries,” *Corros. Rev.*, vol. 12, no. 3–4, pp. 321–340, 1994.

[36] A. Neville, T. Hodgkiess, and H. Xu, “An electrochemical and microstructural assessment of erosion–corrosion of cast iron,” *Wear*, vol. 233–235, no. 0, pp. 523–534, Dec. 1999.

[37] R. C. Barik, J. A. Wharton, R. J. K. Wood, K. S. Tan, K. R. Stokes, and M. Planck, “Erosion and Erosion-Corrosion Performance of Cast and Thermally Sprayed Nickel-Aluminium Bronze,” no. June, pp. 7–9, 2003.

[38] R. J. K. Wood, “6.09 – Erosion/Corrosion,” *Compr. Struct. Integr.*, vol. 6, no. 12, p. pg. 395–427, Dec. 2007.

[39] E. J. Wright, K. D. Efrid, J. A. Boros, and T. G. Hailey, “Rotating cylinder electrode (RCE) simulation of corrosion in sweet production,” in *Nace Conference and Expo*, 2008, no. 08629.

[40] J. M. Maciel and S. M. L. Agostinho, “Use of a rotating cylinder electrode in corrosion studies of a 90/10 Cu-Ni alloy in 0.5 mol/L H2SO4 media,” *J. Appl. Electrochem.*, vol. 30, pp. 981–985, 2000.

[41] H. X. Guo, B. T. Lu, and J. L. Luo, “Interaction of mechanical and electrochemical factors in erosion–corrosion of carbon steel,” *Electrochim. Acta*, vol. 51, no. 2, pp. 315–323, Oct. 2005.

[42] P. Novak and A. Macenauer, “Erosion-corrosion of passive metals by solid particles,” *Corros. Sci.*, vol. 35, pp. 635–640, 1993.

[43] T. Hong and W. Jepson, “Corrosion inhibitor studies in large flow loop at high temperature and high pressure,” *Corros. Sci.*, vol. 43, pp. 1839–1849, 2001.

[44] K. P. Roberts, S. A. Shirazi, J. R. Shadley, E. F. Rybicki, and C. Joia, “Flow Loop Study of NaCl Concentration Effect on Erosion , Corrosion , and Erosion-Corrosion of Carbon Steel in CO 2 -Saturated Systems,” *Corros. Eng.*, vol. 68, no. 2, pp. 1–9, 2012.

[45] R. O. Rihan and S. Nešić, “Erosion–corrosion of mild steel in hot caustic. Part I: NaOH solution,” *Corros. Sci.*, vol. 48, no. 9, pp. 2633–2659, Sep. 2006.

[46] R. Malka, S Nesic, and D. A. Gulino, “Erosion corrosion and synergystic effecrs in disturbed liquid-particle flow,” *Nace Expo*, no. 06594, p. 22, 2006.

[47] M. H. Koike, “Erosion–corrosion of stainless steel pipes under two-phase flow with steam quality 26%,” *J. Nucl. Mater.*, vol. 342, no. 1–3, pp. 125–130, Jun. 2005.

[48] K. Sasaki and G. Burstein, “Erosion–corrosion of stainless steel under impingement by a fluid jet,” *Corros. Sci.*, vol. 49, pp. 92–102, 2007.

[49] A. Neville, M. Reyes, and H. Xu, “Examining corrosion effects and corrosion/erosion interactions on metallic materials in aqueous slurries,” *Tribol. Int.*, vol. 35, no. 10, pp. 643–650, Oct. 2002.

[50] H. H. and M. Y. Masanobu Matsumura, Yoshinori OKA, “The Role of Passivating Film in Austenitic Stainless Steel,” *ISIJ Int.*, vol. 31, no. 2, pp. 168–176, 1991.

[51] S. Aribo, R. Barker, X. Hu, and A. Neville, “Erosion–corrosion behaviour of lean duplex stainless steels in 3.5% NaCl solution,” *Wear*, vol. 302, no. 1–2, pp. 1602–1608, Apr. 2013.

[52] E. Hussain and M. Robinson, “Erosion–corrosion of 2205 duplex stainless steel in flowing seawater containing sand particles,” *Corros. Sci.*, vol. 49, pp. 1737–1754, 2007.

[53] M. Aminul Islam, Z. N. Farhat, E. M. Ahmed, and a. . Alfantazi, “Erosion enhanced corrosion and corrosion enhanced erosion of API X-70 pipeline steel,” *Wear*, vol. 302, no. 1–2, pp. 1592–1601, Apr. 2013.

[54] C. F. Dong, K. Xiao, X. G. Li, and Y. F. Cheng, “Erosion accelerated corrosion of a carbon steel–stainless steel galvanic couple in a chloride solution,” *Wear*, vol. 270, no. 1–2, pp. 39–45, Dec. 2010.

[55] a. Neville and X. Hu, “Mechanical and electrochemical interactions during liquid–solid impingement on high-alloy stainless steels,” *Wear*, vol. 251, no. 1–12, pp. 1284–1294, Oct. 2001.

[56] J. C. Nava, F. Stott, and M. Stack, “The effect of substrate hardness on the erosion-corrosion resistance of materials in low-velocity conditions,” *Corros. Sci.*, vol. 35, pp. 1045–1051, 1993.

[57] E. Heitz, “Chemo-Mechanical Effects of Flow on Corrosion,” *Corrosion*, vol. 47, no. 2, pp. 135–145, Feb. 1991.

[58] B. Chexal, J. Horowitz, B. Dooley, P. Millet, C. Wood, and R. Jones, “Flow-Acclerated Corrosion in Power Platns,” *EPRI TR-106611-R1 Palo Alto, CA Electr. Power Res. Inst.*, 1998.

[59] U. Lotz and J. Postlethwaite, “Erosion-Corrosion in Disturbed Liquid/Particle Flow,” *Corros. Sci.*, vol. 30, no. 1, pp. 95–106, 1990.

[60] “ASTM standard, G76-95 (1995), Standard practice for conducting erosion tests by solid particle impingement using gas jets, ASTM Standards.,” vol. 95, no. Reapproved, pp. 1–5, 2000.

[61] A. Ruff and L. Ives, “Measurement of solid particle velocity in erosive wear,” *Wear*, vol. 36, pp. 195–199, 1975.

[62] P. H. Shipway and I. M. Hutchings, “A method for optimizing the particle flux in erosion testing with a gas-blast apparatus,” *Wear*, vol. 174, no. 1–2, pp. 169–175, May 1994.

[63] C. Gomes-Ferreira, D. Ciampini, and M. Papini, “The effect of inter-particle collisions in erosive streams on the distribution of energy flux incident to a flat surface,” *Tribol. Int.*, vol. 37, no. 10, pp. 791–807, Oct. 2004.

[64] G. L. Sheldon and I. Finnie, “On the ductile behavior of nominally brittle materials during erosive cutting,” *J. Eng. Ind.*, vol. 88, no. 11, pp. 387–392, 1965.

[65] A. Levy and M. Liebhard, “The effect of erodent particle characteristics on the erosion of metals,” *Wear*, vol. 151, pp. 381–390, 1991.

[66] C. T. Morrison, R. O. Scattergood, and J. L. Routbort, “Erosion of 304 stainless steel,” *Wear*, vol. 111, no. 1, pp. 1–13, Aug. 1986.

[67] I. Hutchings, “A model for the erosion of metals by spherical particles at normal incidence,” *Wear*, vol. 70, pp. 269–281, 1981.

[68] K. C. Goretta and A. C. Thompson, “Erosion of heat-treated AISI 4140 steel,” *Mater. Sci. Eng.*, vol. 161, pp. 7–10, 1993.

[69] I. Finnie, “The mechanism of erosion of ductile metals,” *Wear*, vol. 3, no. 1, p. 76, Jan. 1960.

[70] K. E. García, a. L. Morales, C. a. Barrero, and J. M. Greneche, “New contributions to the understanding of rust layer formation in steels exposed to a total immersion test,” *Corros. Sci.*, vol. 48, no. 9, pp. 2813–2830, Sep. 2006.

[71] “ASTM G 119 - 04, Standard Guide for Determining Synergism Between Wear and Corrosion,” vol. 93, no. May 2004, pp. 1–7.

[72] C. P. Dillon, *Forms of corrosion*. MPE Engineers Inc., 2001.

[73] Y.-S. Choi and J.-G. Kim, “Aqueous Corrosion Behavior of Weathering Steel and Carbon Steel in Acid-Chloride Environments,” *Corrosion*, vol. 56, no. 12, pp. 1202–1210, Dec. 2000.

[74] J. Malik, I. H. Toor, W. H. Ahmed, Z. M. Gasem, M. a. Habib, R. Ben-Mansour, and H. M. Badr, “Evaluating the Effect of Hardness on Erosion Characteristics of Aluminum and Steels,” *J. Mater. Eng. Perform.*, Apr. 2014.

[75] S. A. Nelson, M. J. Baker, and W. F. Deans, “The Effect of Surface Roughness on the Erosion of Mild Steel,” in *2004 International Pipeline Conference*, 2004, pp. 803–810.

VITAE

Name	JAHANZAIB MALIK
Place and Date of Birth	11th August 1988, Pakistan
Email	jahanzaib_malik@hotmail.com

Academic Background

Master of Science in Materials Science & Engineering,
Jan 2012 – May 2014
King Fahd University of Petroleum and Minerals,
Dhahran, Saudi Arabia.

Bachelor of Science in Materials Engineering,
September 2007 – June 2011
Ghulam Ishaq Khan Institute of Engineering Sciences and Technology,
Topi, KP, Pakistan.

Publications and Conferences

1. **J. Malik**, I. H. Toor, W. H. Ahmed, Z. M. Gasem, M. a. Habib, R. Ben-Mansour, and H. M. Badr, Evaluating the Effect of Hardness on Erosion Characteristics of Aluminum and Steels. *Journal of Materials Engineering and Performance*, April, 2014.
2. B.S. Yilbas, Ihsan-ul-Haq Toor, **Jahanzaib Malik**, F. Patel, Laser gas assisted treatment of AISI H12 tool steel and corrosion properties, *Optics and Lasers in Engineering*, Volume 54, March 2014, Pages 8-13.
3. B.S. Yilbas, Ihsan-ul-Haq Toor, **Jahanzaib Malik**, F. Patel, C. Karatas, Electrochemical testing of laser treated bronze surface, *Journal of Alloys and Compounds*, Volume 563, 25 June 2013, Pages 180-185.
4. **J. Malik**, I.H. Toor, W.H. Ahmed, Z.M. Gasem, H.M. Badr, Corrosion-Enhanced Erosion Behavior of Carbon Steel AISI 1020 and Stainless Steel AISI 316. *NACE International Corrosion Conference*, Texas, United States, 9-13th March, 2014.
5. **Jahanzaib Malik**, Abdul Azeem, Ihsan-ul-Haq Toor, Effect of annealing temperature on corrosion behavior of two stainless steel alloys, *15th Middle East Corrosion Conference*, 2-5 Feb, 2014.